In Situ Microemulsion Formation in Enhanced Oil Recovery

Marc M.J. Broens

Technische Universiteit Delft

TU Delft Delft University of Technology

Challenge the future

In Situ Microemulsion Formation in Enhanced Oil Recovery

by

Marc M.J. Broens

in partial fulfillment of the requirements for the degree of

Master of Science
in Applied Earth Sciences

at the Delft University of Technology,
to be defended publicly on Monday December 7, 2015 at 15:00.

Professor:	Prof. ir. C. van Kruijsdijk	TU Delft - Shell
Supervisor:	Dr. E. Unsal	Shell
Thesis committee:	Prof. Dr. W. R. Rossen	TU Delft
	Prof. Dr. J. Bruining	TU Delft

TU Delft Delft University of Technology

ABSTRACT

The formation of microemulsions of an EOR surfactant with n-decane was studied in a microfluidic setup using fluorescence microscopy. Generally microemulsions are studied under static conditions by means of phase behavior tests. However, oil mobilization from reservoirs is a dynamic process and therefore it is important to understand how microemulsions form under dynamic conditions. The microemulsion was formed in situ in T-junctions and dead end channels which were etched in glass microchips. Using a solvatochromic fluorescent dye (Nile Red) real time visualization of the aqueous phase, oil phase and microemulsion was possible. The T-junction geometry was used to study initial mixing and consequential formation of microemulsion while both the aqueous phase and the oil phase were mobile. The dead end channel geometry allowed us to study the emulsification when only the aqueous phase was injected into an initially oil saturated microchip. The surfactant concentration and injection rates were found to have an effect on the emulsification rate and the flow dynamics in the T-junctions. In the dead end channels, the emulsification was mainly driven by diffusion and the gradients in the concenration of the chemicals. Some of the results of the dynamic experiments deviated from what would be expected from the phase behavior tests. Results of the experiments were reproduced where possible using commercial software (Comsol Multiphysics) which helped to get a qualitative understanding of the flow dynamics. An analytical model was implemented using the saturation profiles observed in the experiments. Possible emulsification mechanisms were identified.

PREFACE

Looking back on the previous 10 months I can truly say that I have learned a great deal while doing the research that lead to this report. Not only on a scientific level but also on a personal level, doing research is confronting. Although writing a thesis is very much a personal project, I am thankful that whenever I got stuck there was always someone around with either a helping hand or a friendly word of advise.

Special thanks goes out to my supervisor Evren who has guided, mentored and coached me throughout the project. It was good to have someone badgering me to start writing down my results throughout the project. This report would not have been otherwise.

Thanks also goes out to Cor who kept the academic focus in my project. It was beneficial to have a Professor who was available for help so often.

I would like to thank the microemulsion meeting for the critical feedback I received on my interpretations of the experiments. For help with either experimental matters or data interpretation I would like to thank Merit van der Lee, Steffen Berg, Willem Bart Bartels, Micheal Golombok, Winfried Theis, Jasper de Reus and Dierderik van Batenburg. A word of thanks also goes out to my fellow interns with whom I could discuss theis writing while playing pool. Finally, a warm thanks to my parents, family and friends for their willingness to hear me complain about my thesis. This is especially the case for Doris, who helped me to structure my work on a rainy sunday afternoon.

Marc M.J. Broens
Amsterdam, December 2015

CONTENTS

1

INTRODUCTION

The steady growth of the global population together with a worldwide growth of the middle-classes is putting pressure on the worlds' energy supplies. Even though climate change is now widely considered a serious problem, crude oil still made up 40% of the total energy consumption in 2012 [1]. Although the relative share of oil consumption is expected to decline in years to come, absolute crude oil consumption is expected to remain constant due to the growth in energy demand. To meet this demand, new and more challenging sources of oil will have to be explored and eventually exploited, which requires innovative technology and solutions. One of the solutions which has been under research since the early 1970's is enhanced oil recovery (EOR). After primary and secondary oil recovery (producing oil under natural reservoir pressure and injecting water to maintain reservoir pressure and mobilize oil respectively), an average oil reservoir will still contain approximately 60%-80% of its oil initially in place (OIIP) [2][3].

The remaining oil in the reservoir is trapped in the pores because of capillary forces which exceed the viscous forces of the flowing brine [4]. To overcome these capillary forces, the interfacial tension (IFT) between the injected brine and the trapped oil must be decreased to such a level that the capillary forces no longer dominate over the viscous forces. In conventional modelling of multiphase flow in porous media one of the important constitutive relations is the capillary desaturation curves (CDC, figure 1.1, which shows that the residual oil saturation decreases from a critical Nc onwards ([4] [5]). Fundamental mechanisms of chemical enhanced recovery (cEOR) are based on this relationship; by injecting surfactants into the reservoir, the IFT reduces at the oil/water interface. The common assumption is that the lower the IFT, the more effective the oil mobilization becomes due to the increased Nc. Therefore, the surfactant formulation is often optimized in a way that an in situ microemulsion phase forms generating ultra-low IFT values. However, the rheology of the microemulsions can be very unpredictable regardless of how ultra-low IFT they generate. A dramatically high viscosity may impair the oil recovery process by restraining the flow.

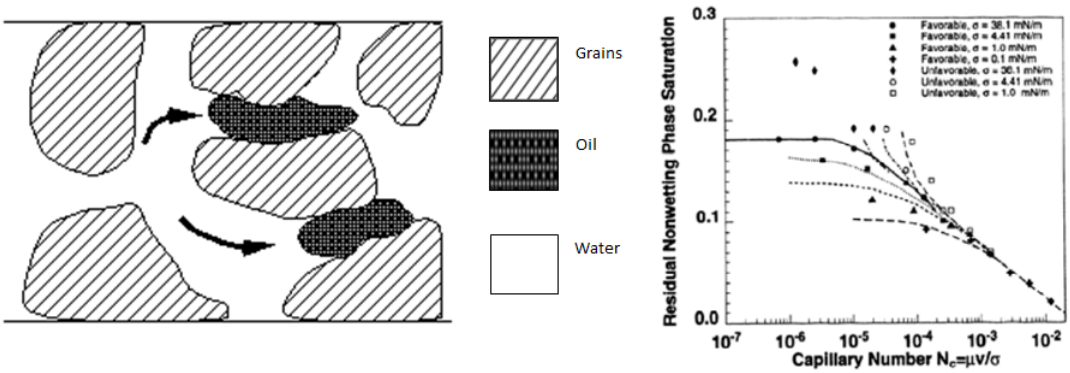

Figure 1.1: a) Schematic of trapped oil in pore space in immiscible two-phase flow, b) capillary desaturation curve [6]

Microemulsions are thermodynamically stable dispersions of an oil phase and a water phase, generally accompanied by a cosolvent and electrolytes (e.g. salt)[7][8][9][10]. The formation behavior of microemulsions has been characterized by phase behavior tests [11]. However, phase behavior tests require the mixture

of oil, water and surfactants to stabilize and are thus a characterization under equilibrium (static) conditions. Since chemical EOR is a dynamic process, the question remains whether microemulsions formed in a phase behavior test are representative for the microemulsions which are formed *in situ* (meaning in the pores under flowing conditions). Coreflood experiments are used to study surfactant solutions and their effect under flowing conditions, however these do not permit real time visualization of flow at the porescale. To investigate microemulsion formation at this scale it's necessary to get a feeling for which physcial mechanisms dominate the formation of microemulsions at the porescale (with typical pore diameters of order 10^{-6} m and typical reservoir flow rates of the order of 10^{-6} m/s). One method that allows us to investigate this is by visualizing porescale flow and mixing behaviour in micromodels. This report is the outcome of an experimental study about the in situ (pore-scale) formation of microemulsions. Experiments were conducted by injecting oil (n-decane) and different surfactants solutions into the micromodels to observe how microemulsion is formed. Different geometries were used to see how the mixing takes place at T-junctions after co-injection and in dead-end pores after saturation with oil.

2

BACKGROUND

Already in the 1970s it was demonstrated that microemulsions could form in situ during surfactant flooding in oil reservoirs [12][13][14]. The surfactant cocktails are optimized for each crude oil and reservoir conditions including temperature and salinity. The optimum phase behavior is generated, where the surfactant predominantly partitions into a middle microemulsion phase with ultra-low IFT [15] [16][11].

There has been significant development of microemulsion with specific properties, namely, high solubilizing ability and temperature insensitivity. Phase behaviour studies, also known as the solubility or salinity scan tests, have provided foundations for surfactant systems which can generate compatible microemulsions. For EOR related research, the microemulsion is created by mixing some crude oil from the reservoir, injection/formation water and the surfactant. This is done in test tubes and at reservoir temperature. Multiple test tubes are prepared with different salt concentration in order to form a salinity scan. The content of the tubes are shaken vigorously, and let to reach equilibrium. The formation and the stability of the microemulsion are observed over time, from hours to weeks. When the hydrophile-lipophile properties of the surfactant at the water/oil interface are balanced bi-continuous-type microemulsions are formed. When the surfactant is more hydrophilic or lipophilic, oil-in-water (O/W) or water-in-oil (W/O) microemulsions form [11][17]. Once at equilibrium the microemulsion phase may be collected from each tube for additional anlysis, i.e. IFT and rheology. Since the microemulsion phase is tested once it's formation is completed and it is in equilibrium with excess phases, these tests are referred to as static.

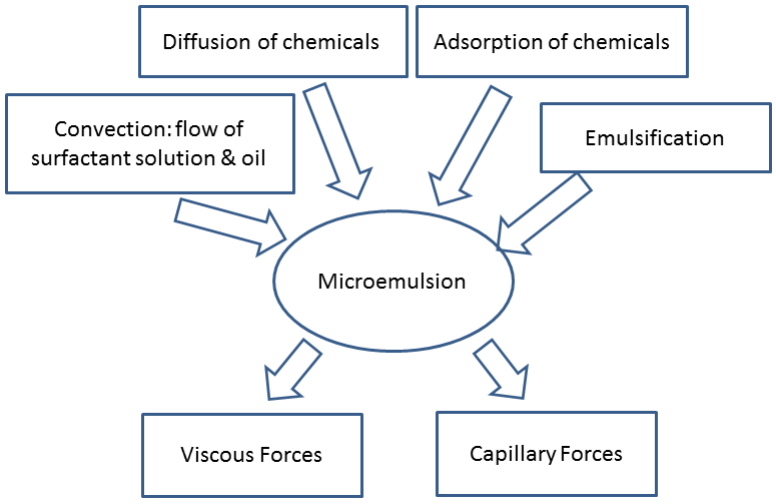

Figure 2.1: Diagram of effects which cause microemulsion to form in situ. The microemulsions cause viscous and capillary forces to take place which affects the mobilization of oil from the reservoir.

The measurement of non-equilibrium properties of microemulsions have received relatively less attention, even though they also have important scientific and industrial applications. Unlike simple fluids that

are composed of intact molecules, the structure a self-assembled fluid like microemulsion can change under small perturbations. During oil mobilization with surfactant flooding, the multi phase fluid system is dynamic; it may never reach equilibrium. While the microemulsion formation still occurs, it's properties may be different from an equilibrated microemulsion. The dynamic microemulsion laboratory studies are commonly performed in corefloods and granular packs, where a surfactant solution is injected into an oil saturated porous medium. Direct visualization of the displacement is not possible; the in situ properties of the fluids are interpreted from pressure readings and collected effluents. Glass and/or polymer microfluidic devices are commonly used to perform surfactant-based displacement as they allow the visualization of pore scale events. These studies mainly focus on the wettability modification and displacement efficiency during multiphase flow [18][19][20][21][22][23]. However, only few of them studied only the microemulsion systems.

The existence of microemulsion has to be considered at multiple stages during a surfactant injection. Understanding microemulsion formation is important, but not enough to design a successful operation. Once a microemulsion phase forms it becomes part of the flow system; it can impact the flow dynamics if it has a problematic rheology. It is important to keep a favourable viscosity ratio between the injected and in situ forming phases. With ultra-low IFT at the oil contact line the interface becomes very flexible and prone to viscous fingering. And once the oil mobilized, the microemulsion becomes part of the flow system, and it has to be recovered. In this study we did not study the microemulsion dynamics in terms of displacement of phases and viscosity ratio instability. The microefludic experiments focused more on the flow of the microemulsion phase once it is formed. Earlier studies report various flow immiscible, two-phase flow in the microchannels. Depending on the flow rate and volumetric flow ratio, the regimes can be slug, slug-annular, annular, parallel, or bubbly [24][25]. These studies mainly focus on fluid system with higher IFTs, i.e., oil-water or air-water where no surfactant is present. In an ultra-low IFT multiphase flow system, similar regimes still occur, however, the transition between them is not necessarily well defined as in the case of high IFT systems.

2.1. FLUID DYNAMICS AT THE PORESCALE

This study investigates how microemulsions form under in situ conditions as opposed to test tube conditons. In EOR, in situ conditions are characterized by a wide range of effects. This study focusses on the effect of two of these conditions:

- Fluid flow effects (flow rate order of magnitude $10^{-6} - 10^{-4}$ m/s)
- Pore sizes and geometry (diameter order of magnitude $10^{-5} - 10^{-4}$ m)

The field of microfluidics focusses on studying fluid flow at the microscale and nanoscale and therefore captures the above mentioned effects well [26]. The forces which play a role in microfluidic flow will be discussed below .

2.1.1. VISCOUS FORCES

An important characteristic of microscale flow is that inertial forces are negligible compared to viscous forces due to the small scale. The dynamic viscosity of a liquid is defined as its resistance to deformation by a shearing force (usually caused by flow). It's given by the constant μ in equation 2.1.

$$\tau = \mu \nabla u \tag{2.1}$$

The Reynolds number gives a measure of the ratio of inertial over viscous forces [27] and is given in equation 2.2.

$$Re = \frac{\rho u L}{\mu} \tag{2.2}$$

Where ρ is the density in kg/m^3 , u is the fluid velocity in m/s, L is the characteristic flow dimension in m and μ is the dynamic viscosity of the flowing medium in Pa.s. While at larger scale the inertial forces quickly dominate the flow regime causing the flow to become turbulent, at microscale the Reynolds number is generally too low [28][26]. In this report, all flow can be considered to be laminar unless specifically mentioned otherwise.

2.1.2. CAPILLARY FORCES

Capillary forces arise from the combination of cohesive forces within a fluid and adhesive forces between the fluid and the walls of its container. The forces are therefore driven by the interfacial tension between

the liquid phases and the wettability of the solid of the container relative to the two liquid phases. Capillary forces are static in the sense that they don't require flow or motion to take effect (as opposed to viscous forces, which only exist under shear stresses which arise when there is movement). The capillary pressure P_c across a meniscus separating two phases with interfacial tension γ in a capillary with radius r_c is given by equation 2.3 (figure 2.2).

$$P_c = \frac{2\gamma cos(\theta)}{r_c} \tag{2.3}$$

The contact angle between the two phases and the wall of the capillary is given by θ and depends on the wettability of the capillary material (figure (2.2). In this study the capillary walls can be considered water wet. The Capillary number N_c characterizes the ratio of viscous (dynamic) forces over capillary (static) forces in the medium [27].

$$N_c = \frac{u\mu}{\gamma} \tag{2.4}$$

In equation 2.4 u represents the velocity of the displacing fluid, μ represents the viscosity of the displacing fluid and γ represents the IFT between the displacing and the displaced fluid. A high capillary number means viscous forces dominate interfacial forces.

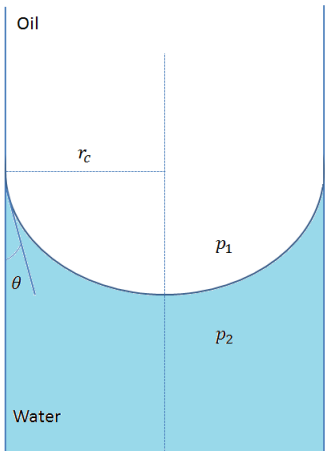

Figure 2.2: Diagram of a capillary with an interface between two liquids. The relation between the pressures and the contact angle is given by equation 2.3

2.2. TRANSPORT EQUATIONS

Mass transport (and consequently mixing of phases) in multiphase microfluidic flow is governed by the convection-diffusion equation. Convection and diffusion will first be introduced separately. The equation and its restructuring to Fick's laws of diffusion will then be discussed.

2.2.1. CONVECTION

Convection is the combined transport mechanism of molecules in a fluid by advection and diffusion. Advection is the transport mechanism by which the bulk of the fluid is transported through the system. This is usually caused by a macroscopic pressure gradient over the fluid and this is also the case for this study. Diffusion can take place within the bulk and is independent of the pressure gradient which causes the bulk of the fluid to be transported.

2.2.2. DIFFUSION

Diffusion of mass (usually molecules but larger particles can also be subject to diffusion) is a concentration gradient driven transport mechanism. Momentum, energy and mass can all be transported by means of diffusion if a gradient is present and hence they all have their own diffusion equations. The thermodynamic explanation for diffusion is that gradients (e.g. chemical, temperature or velocity) in a system cause the system to be in an unfavorable configuration from a free energy perspective. Diffusion is the mechanism by which such a system corrects its configuration so that it finds itself in its most favorable (thermodynamically

stable) configuration. In this study we are interested in the transport of mass by means of diffusion and so it is the chemical gradients that will be of interest.

2.2.3. THE CONVECTION DIFFUSION EQUATION

The convection diffusion equation is given in 2.5:

$$\frac{\partial c}{\partial t} = \nabla \cdot (D\nabla c) - \nabla \cdot (\vec{v}\, c) + R \tag{2.5}$$

The equation has four terms:

- $\frac{\partial c}{\partial t}$: the time derivative of the concentration, describing how the concentration in the system changes with time
- $\nabla \cdot (D\nabla c)$: the diffusion term which describes how the concentration changes due to mass transport by diffusion
- $\nabla \cdot (\vec{v}\, c)$: the convective term which describes how the concentration changes due to mass transport by convection
- R: a source or sink term which describes the production or consumption of a species in the system, usually through a chemical reaction

Depending on the assumptions made the equation can be rewritten and simplified so that analytical solutions to the problem may be found. In this study we will consider a closed system without a source or a sink term. This means that the last term drops out of the equation. Because we only work with incompressible fluids, the velocity term $\vec{v}$ can be taken out of the divergence.

2.2.4. FICKS'S LAWS OF DIFFUSION

Ignoring the convective term in the convection diffusion equation allows us to rewrite the equations to Fick's laws. If the system has not reached steady state and assuming the diffusion coefficient is independent of spatial variations it is descibed by Fick's second law 2.6:

$$\frac{\partial c}{\partial t} = D\nabla^2 c \tag{2.6}$$

In case the system has reached steady state, it is described by Fick's first law 2.7:

$$\vec{J} = -D\nabla c \tag{2.7}$$

Both equations desrcibe diffusion driven mass transport. Fick's first law of diffusion (2.7) describes the molecular flux of particles along a constant concentration gradient. The distance traveled by a particle over time as a result of diffusion (also called the diffusion length) is given by equation 2.8.

$$x_D = \sqrt{Dt} \tag{2.8}$$

Where x_D is the diffusion length (m), D is the diffusion coefficient ($\frac{m^2}{s}$) and t is time (s). The diffusion coefficient has several definitions depending on the system described. For a sphere of radius R diffusiong through a liqudi medium with viscosity μ the diffusion coefficient was given by Einstein in 1905 [29].

$$D = \frac{kT}{6\pi\mu R} \tag{2.9}$$

It can be used to calculate typical diffusion coefficients for micelles diffusing through a liquid.

If the concentration changes with time, Fick's second law can be used to track the propagation of the concentration distribution. The solution to equation 2.6 is given by equation 2.10:

$$c(x,t) = c_0(1 - erfc(\frac{x}{2\sqrt{Dt}})) \tag{2.10}$$

Diffusion is generally a much slower mixing mechanism than convective flow or turbulence. However, in microfluidics it is very often the dominant mixing mechanism and therefore important to understand.

Mixing of two liquid phases in macroscopic flow is generally dominated by convective flow and/or turbulence more than diffusion. This is captured by the Péclet number 2.11:

$$Pe = \frac{u_x L}{D_x} \tag{2.11}$$

In equation 2.11 u_x is the local flow velocity (m/s), L is the characteristic length (m) and D_x is the mass diffusion coëfficient (m^2/s). The Péclet number gives a measure of which type of mass transport plays a dominant role at the specified scale: convection or diffusion. It is defined as the ratio of convective transport rates over diffusive transport rates [27]. At the macroscale the characteristic length scales are generally too large for diffusion to play a significant role in mixing. The driving mixing mechanism at these scales is turbulence which reduces mixing path lengths and increases the contact surface between two phases. However, microfluidics takes place at a different scale where flow is generally laminar and the characteristic lengths become such that diffusion is not negligible any longer.

2.2.5. MARANGONI SPREADING

The marangoni effect is a surface tension gradient based transport mechanism. When a surfactant is present at the interface between two fluids it will decrease the interfacial tension locally. The higher interfacial tension surrounding this local dip will give rise to a force pulling the surfactant outwards to eliminate the gradient in surface tension, effectively creating a transport mechanism for surfactants across an interface. The oil trapped in the dead end pores is surrounded by a thin film of water assuming a water wet rock. Marangoni spreading may therefore be a mechanism that helps the surfactant to spread across the water film and reach the oil at the back of the dead ends. This would also be interesting because Marangoni spreading is faster than diffusion. An equation for Marangoni driven transport of surfactants across a water film inside the poresace has been derived and can be found in appendix B. It is a diffusion like transport mechanism driven by the surfactant concentration gradient (which causes a surface tensions gradient). The "Marangoni diffusion coefficient" depends on the viscosity of the liquid film μ, the film thickness H_0 and the IFT σ_0 between the two phases which form an interface without any surfactants present. The applicable equations can be found in equation 2.12 and 2.13 and a derivation can be found in appendix B.

$$\alpha \frac{d}{dx}(\Gamma \frac{d\Gamma}{dx}) = \frac{d\Gamma}{dt} \tag{2.12}$$

$$\alpha = \frac{H_0}{\mu}\sigma_0 \tag{2.13}$$

Because equation 2.12 behaves very much like the diffusion equation, the sollution to the diffusion equation will be used for modeling purposes.

2.3. MICROEMULSIONS

The most common definition of a microemulsion found in literature was first given by Danielson and Lindmann[15] [16][11]: "*a system of water, oil and an amphiphile which is a single optically isotropic and thermodynamically stable liquid solution*". The principal difference between regular (macro)emulsions and microemulsions is that a microemulsion is thermodynamically stable. The dispersed droplets in macroemulsions will grow over time which will lead to phase separation in the long run. This is not the case for microemulsions because of the ultralow interfacial tensions associated with microemulsions.

2.3.1. THERMODYNAMIC STABILITY

A thermodynamically stable system is a system which is in a state with minimum free energy. It won't spontaneously change its state unless energy is added to the system. Until a certain interfacial tension, emulsions are classified as macroemulsions. Macroemulsions are thermodynamically unstable which causes them to separate if left untouched. Microemulsions start to form when the interfacial tension is reduced to ultralow values (order of magnitude 10^{-6} N/m). They will form spontaneously (don't need any energy to be added to form) and won't separate over time because their emulsified state is energetically favorable to their separated state (lower free energy). This can be understood by considering the Gibbs free energy of the system (equation 2.14)

$$\Delta G_{form} = \Delta A_{form}\gamma - T\Delta S_{form} \tag{2.14}$$

ΔG_{form} is the free energy change associated with the formation of new surface ΔA_{form} with surface tension σ. This free energy consists of two parts: an increase due to the extra interfacial surface which is created ($\Delta A_{form}\sigma$) and a decrease due to an increase in the Entropy of the system ($T\Delta S_{form}$). When the interfacial tension is of a typical order of magnitude (10^{-2} N/m), the first term outweighs the second and the associated change in free energy is positive. Because a systems will always tend to be in the state with minimal free energy it will tend to decrease its interfacial surface instead (phase separation). However, when the interfacial tension decreases to ultralow values, the first term is outweighed by the second term (gain in Entropy). The free energy change will now be negative, and the system will tend to increase its interfacial surface. The lower the interfacial tension, the higher the amount of interfacial surface the system will want to gain.

2.3.2. WINSOR CLASSIFICATION

Winsor was the first to classify the types of microemulsions based on their phase behavior in 1948 [11]. His classification is still used today. According to Winsor, there are 3 different types of phase behaviour the microemulsion can exhibit: Winsor-I, Winsor-II and Winsor-III (figure 2.3). These phase behavior types cab be described as follows:

1. Winsor-I: a 2 phase mixture where the surfactants will prefer to reside in the aqueous phase causing an o/w microemulsion at the bottom and a (surfactant poor) excess oil phase on top.

2. Winsor-II: a 2 phase mixture where the surfactants will prefer to reside in the oleic phase causing a w/o microemulsion at the top and a (surfactant poor) excess water phase at the bottom .

3. Winsor-III: a 3 phase mixture where the microemulsion coexists with both an excess water and excess oil phase at respectively the bottom and on top.

The mixture will change from one phase into the other (from I to II via III) if the tuning parameter is changed. For anionic surfactants, the tuning parameter is the salinity. Figure 2.3 depicts the three types of microemulsion at the macroscale and at the molecular scale. Winsor-I systems are also referred to as systems which are at *under optimum salinity*. Winsor-III systems are at *optimum salinity* and Winsor-II systems are known as *over optimum salinity* systems.

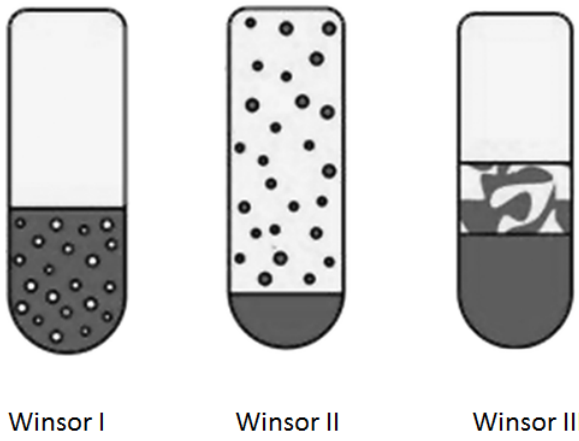

Figure 2.3: Diagram of the Winsor Classification in the test tube. Winsor I shows oil filled micelles in an external aqueous phase. Winsor II shows water filled inverted micelles in an oleic external phase. Winsor III has the lowest interfacial tension causing a bicontinuous thrid phase to form.[30]

2.3.3. MICROEMULSION STRUCTURES

The Winsor classification can also be understood from a microemulsion structure perspective. The relative area taken up by the surfactant tail versus that of the head is called the critical packing paramater (CPP) [8]. Increasing the salinity increases the amount of positively charged ions in the surfactant solution which alters the CPP. As the CPP changes, so does the preferred structure of the microemulsion. Figure 2.4 shows the

different types of structures that can form depending on the CPP. With the microemulsion structure, properties like the viscosity also change. It is also probable that the structure of the microemulsion is broken up if subjected to too much shear.

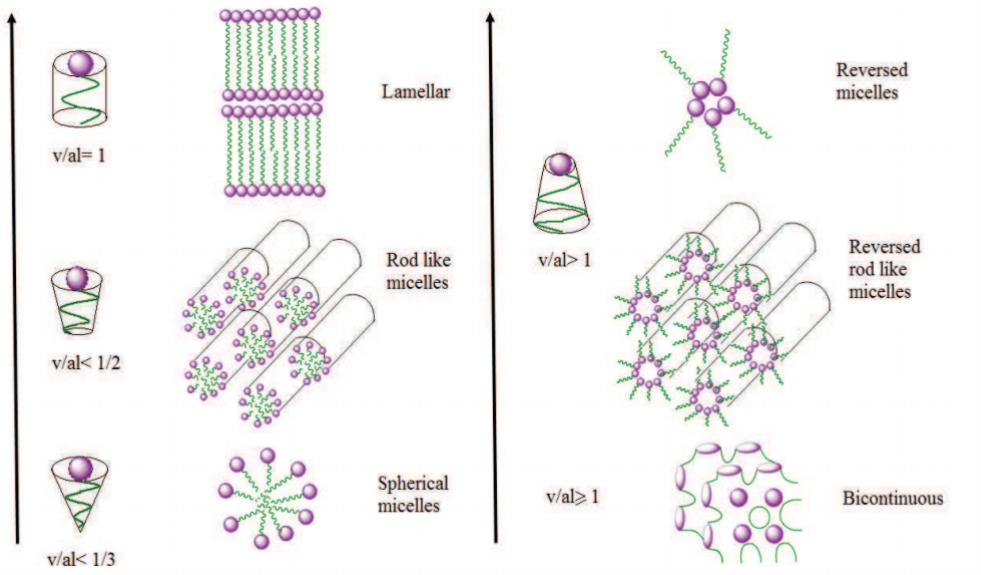

Figure 2.4: depiction of molecular microemulsion structures depending on the CPP. Optimum salinity systems which have a very low IFT will tend to form bicontinuous structures[8]

2.3.4. SPONTANEOUS EMULSIFICATION

Because microemulsions are thermodynamically stable they can form spontaneously when a surfactant solution comes into contact with an oil. This process has been described as spontaneous emulsification [31] [32] [33] and three different mechanisms have been proposed as reasons for its occurrence. The first two mechanisms are dispersive in nature, i.e. they will form an emulsion by breaking up the bulk phase. This can occur when interfacial tension gradients cause convective currents (which break up the interface) or when local instabilities break-up ultra low interfacial tensions interfaces (also referred to as negative interfacial tension driven emulsification) [32]. The third mechanisms is different because it is driven by a chemical instability instead of a mechanical instability. It is called diffusion and stranding and occurs when diffusion creates regions of supersaturation where consequently emulsification will take place [31]. A model for this mechanism was proposed by Ruschak and Miller in 1972 which was also experimentally validated using a mixture of water, AOT and Toluene. In this study, the model used by Ruschak and Miller will not be checked, however the relation for the displacement of the interface between two phases due to diffusion and stranding is used as a measure for the emulsification rate in the dead end pores (equation 2.15).

$$x = 2K\sqrt{Dt} \tag{2.15}$$

Where K is an unkwon constant and x is the position of the interface in 1-D.

3

MATERIALS & MEASUREMENTS

In this chapter, an overview of the materials used is given. First the chemicals and fluids will be described, followed by a detailed overview of the surfactant systems that were used in the experiments. The surfactants systems that were used in the experiments are aqueous solutions of Shell produced ENORDET O242 surfactant, 2-butanol and salt. They were tested on an oleic phase (n-decane). Several systems were used, varying surfactant concentration, cosolvent concentration and salinity. The properties of these systems have been listed in table 3.1. In the following subsections, the separate components will be discussed.

3.1. SURFACTANT

A model fluid system that is active and optimal at ambient conditions was selected for the microfluidic experiments. The surfactant, ENORDETTM O242, produced by Shell Chemicals, was used as it has practical relevance for field applications of enhanced oil recovery. Its active components include an internal olefin sulfonate (IOS) with a distribution of 20-24 carbon atoms. The sulfonate group can be attached anywhere on the carbon-backbone. There are two types of the molecule: one with a double bond and one with an OH group (figure D.1)[34].

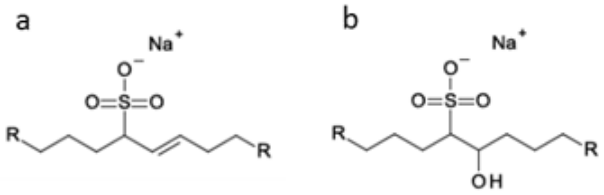

Figure 3.1: structure of Shell ENORDET O242. Two types of molecules can be observed: a) with double bond b) with OH-group [34]

3.2. COSOLVENT: 2-BUTANOL (SBA)

The effect of cosolvent on the phase behaviour is both an increase in the rate at which the microemulsion forms and an increase in the flexibilty of the interface [35]. This causes the microemulsion to form a structure with smaller pockets of oil and water and so a decrease in the solubilization of oil and water into the microemulsion. Tis can also be translated into an increase of microemulsion interface per microemulsion volume. Thisis visible in the phase behavior tests where we see that the amount of microemulsion in the phase behavior test tubes decreases with increasing cosolvent concentration. The cosolvent used in all surfactant systems is 2-Butanol (SBA).

3.3. SURFACTANT SYSTEMS

The aqueous solution was prepared by mixing the surfactant and the co-solvent in deionized water. Three surfactant solutions with different concentrations were prepared; the formulations are listed in Table 1. The

bulk surfactant solution of System I had a yellowish color with some turbidity due to higher surfactant concentration. System II and III solutions were clear. The oil phase was n-decane (C10) for all three systems.

Table 3.1: Surfactant solution formulations used. DI is de-ionised water.

Surfactant System	Surfactant Concentration (%)	Cosolvent Concentration (%)	Make-up water
I	4.00	5.00	DI-Water
II	2.00	5.00	DI-Water
III	0.50	5.00	DI-Water
IV	0.50	0.50	DI-Water

3.4. OIL

The oil used in the experiments was n-decane (C-10). Its properties can be found in table 3.2.

Table 3.2: oleic phases and their properties used in the experiments

Name	Formula	Density	Viscosity
n-decane	$C_{10}H_{22}$	720 kg/m3	0.001 mPa.s

3.5. NILE RED DYE

Nile red dye (9-diethylamino-5H-benzo[α]phenoxazine-5-one) is a fluorescent, solvachromatic dye wich is most notably used to dye lipid molecules due to its hydrophobicity [36]. Its structure (3.3) is similar to that of a surfactant in that its amphiphilic because of the polarity induced by its electron conjugation. Fluorescence is the emission of light by a material when excited by light which has a wavelength whithin a certain range (the excitation spectrum). Solvatochromism is the change of color of a material depending on its chemical environment. In the case of Nile Red the emitted light shows a red shift with increasing polarity. This means that it can be used to identify between different phases depending on their polarity. The absorption and emission spectra of Nile Red can vary greatly with the polarity of the solvent. The research which is discussed in this report uses n-decane as organic solvent, which emits a green-yellow light (pure n-decane). When the microemulsion forms, the dye in the oil will move towards the interface between the oil and the water just like the surfactants. In the microemulsion phase, the dye will emit a light which varies from orange to bright red which can be clearly distinguished from the green to yellow colour emitted by the dye in pure n-decane. [37][38][39][40][41]. The cell-based assay Nile Red solution was diluted with n-decane (x500 dilution by volume).

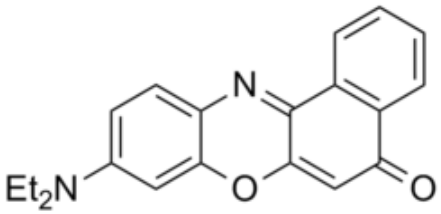

Figure 3.2: structure of Nile Red dye [42]

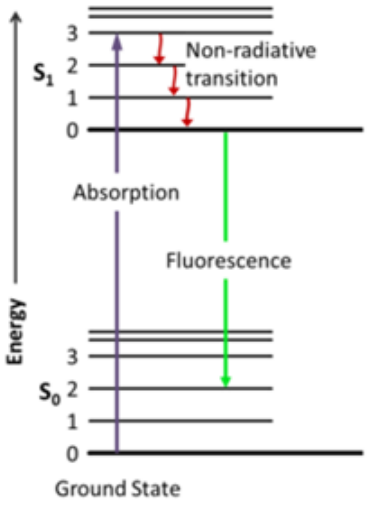

Figure 3.3: principle behind fluorescence. Light of a certain wavelength will excite electrons in the fluorescent material to a higher energy level. When they relax back to their ground state they emit light of a different (known) wavelength, making it an ideal property to tag material with for detection (Wikipedia)

3.6. MEASUREMENTS

3.6.1. INTERFACIAL TENSION (IFT)

A spinning drop tensiometer (SVT 20, DataPhysics, Germany) was used for the IFT measurements. The manufacturer defined the measuring range of the tensiometer between 1E-6 to 2E3 mN/m. The sample holder was filled with the excess aqueous phase; a drop of microemulsion was placed at the top. The holder was then rotated at various rates, causing a pressure to be exerted on the interface between the microemulsion and the excess phase. The software the determined the two radii of curvature R_1 and R_2 and the IFT was calculated according to the Young-Laplace Equation 2.3.

3.6.2. RHEOLOGY MEASUREMENTS

The rheology measurements were performed with a shear rheometer (ProRheo LS300). The viscosity was measured as a function of shear using a program that ran from a shear of 100/s to 1/s and then back to 100/s again. The representative field flow rate is typically 1 ft/day which corresponds to the shear rate of 7/s. The viscosities reported in this study were measured at a shear rate of 7/s at room temperature (25^oC). The samples were prepared as follows: the phase is extracted from a pase behavior test tube using a fine metal syringe (ca. 1 ml). The liquid is injected into a holder and placed in the rheometer. A metal rod (D = 1 cm) is then lowered into the liquid holder to form an evenly distributed liquid annulus around the rod. When the shear rheometer is turned on the rod spins at the desired rate and the rehometer measures the torque exerted on the rod as a result of the viscous forces. The torque as a function of shear rate is used to calculate the viscosity 2.1.

4

Analysis

In this section the experimental setups and methodology will be described for all of the experiments that were performed as part of this study: the phase behavior tests (static) and the microfluidic experiments (dynamic).

4.1. Phase Behavior Tests (Static Method)

The surfactant solutions listed in 3.1 were prepared. They were then subjected to a phase behavior tests. This is done by mixing the surfactant solution with the oil in several test tubes, each with a different salinity. The test tubes are then shaken vigorously and left to stabilize and form microemulsions. In this study, the surfactant solutions were prepared in de-ionised water with the surfactants discussed in the Materials section. The salinity varied by adding sodium chloride (NaCl). The oil phase was n-decane. 7.5 mL surfactant solution and 7.5mL n-decane was added in 15 mL graduated test tubes (mixing ratio of 1:1). One tube per salinity was prepared. The content of the tubes were shaken vigorously. The tubes were then left for their contents to reach equilibrium. The phase behaviour was observed over time, until no more change was observed. The required time could be from a few hours to a few days. The salinities at which a third microemulsion phase formed were identified for further testing. All tests were done at room temperature.

4.2. Microfluidic Experiments (Dynamic Method)

4.2.1. Setup

The setup used for the microfluidic experiments can be found in figure 4.1. The syringes used are Hamilton 50 μl of the type "Gastight 1705". The syringes are used in combination with the syringe pump to achieve the steady, low injection rates necessary in microfluidic experiments.The syringe pump used in the experiments is a Harvard Apparatus PHD Ultra syringe pump. It can generate injection rates of between pL/min and ml/min. It holds two injection needles at the same time so that co-injection at the same injection rate can accurately be achieved. The pump works with a piston which is connected to a screw thread. The microscope used to visualize the experiments is a Leica DMI6000B. It has a regular transmission light source as well as a fluorescent light for which the source is situated next to it on top of the table. The software used to set up the microscope as well as the camera is Leica Qwin. This software is also used to process the images captured by the camera.

4.2.2. Micromodel Geometries & Experimental Procedure

In this study microfluidic chips were used to simulate pore scale geometries. The micromodels are etched in glass and produced by Micronit (The Netherlands). They were designed in-house at Shell Rijswijk and were customised so that they could be used to test specific fluid flow mechanisms. The geometries of the micromodels used in the experiments discussed in this report are described below.

T-Junction

The T-Junction is used to simulate mixing behavior of two separate phase flows merging at a porethroat. The design and dimensions of the micromodel used are given in fig 4.2. A T-junction micromixer consists of two capillaries which meet at a 90^o angle. The n-decane and the surfactant solution are injected into different

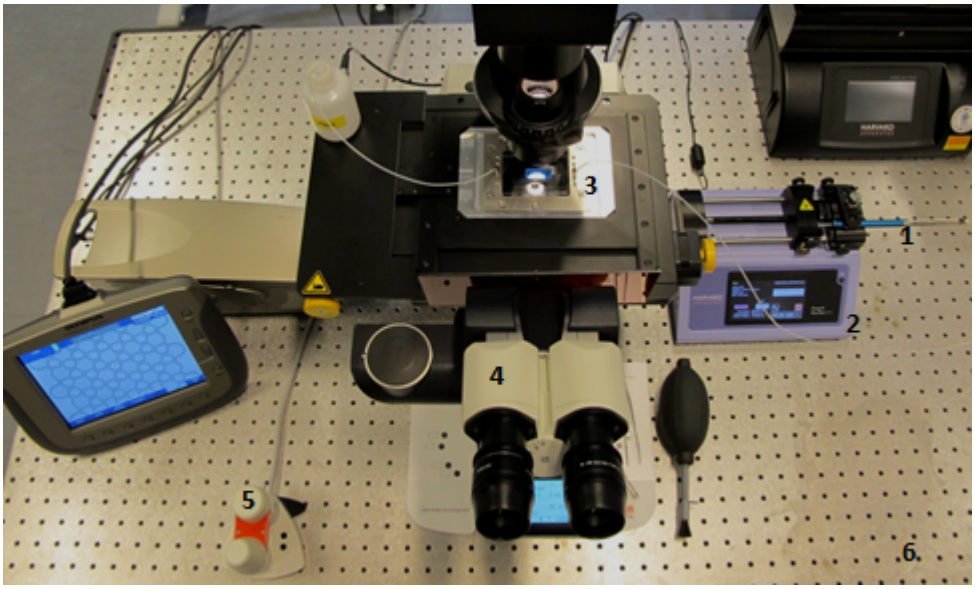

Figure 4.1: The experimental setup used to conduct the experiments 1) Syringe 2) Syringe Pump 3) Micromodel 4) Inverted Transmission Microscope 5) Smart move control unit 6) Optic Table

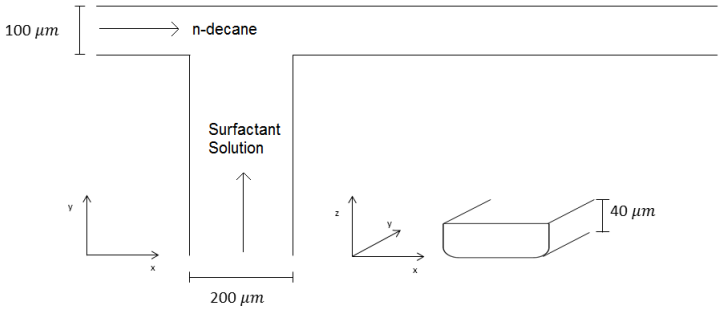

Figure 4.2: the geometry of the T-Junction in the micromodel used in the first set of experiments

channels and meet at the t-junction. Assuming the flow is laminar, mixing of the two phases solely depends on diffusion perpendicular to the flow direction at the interface ([43]). Because of this, mixing is generally slow and depends on the following factors:

- the Diffusion coefficient D(mixing rate)
- the capilary diameter h (mixing length)
- the length of the channel L (mixing time)
- the (convective) flow rate u (mixing time)

These four paramaters can be combined into a dimensionless number which predicts the mixing efficiency for the considered system: θ_{mix}.

$$\theta_{mix} = \sqrt{\frac{DL}{uh^2}} \tag{4.1}$$

The mixing efficiency parameter given in equation 4.1 quantifies the mixing efficiency for two phase parallel laminar flow where diffusion perpendicular to the direction of flow is the sole mixing mechanism. Mixing is effective when $\theta_{mix} >> 1$. In the experiments conducted as part of this study the injection rate and the diffusion coefficient are variables. The diffusion coefficient will be the main focus because it quantifies the rate of emulsification. Two types of data were recorded from the experiments with the T-Junctions:

- Images of the flow regime at the T-Junction
- Images of the phase saturations up to 1 mm downstream of the T-Junction

The experimental procedure for the T-Junction experiments is as follows. Before every experiment the micromodels are cleaned using (in that order) dry cleaning naphta, propanol and water. Due to the order in which the model is cleaned, it can initially be considered water wet. Two syringes are filled with the surfactant solution and the n-decane respectively. They are screwed on to the micromodel inlets with two small tubes of equal length (length 20 cm, diameter 0.5 mm) and placed in the syringe pump. The micromodel is placed under the transmission microscope and the pump is turned on at the desired volumetric injection rate. Because the same pump is used for the two syringes the volumetric flow rate is equal at both inlets ($Q_1 = Q_2$). When the flows reach the T-Junction the system is allowed to reach steady state. Images are then recorded of the T-Junction. After the images of the T-Junction have been recorded, an elongated image of the section downstream of the T-Junction needs to be recorded. This can be done by using the "Record Mosaic" function in Leica Qwin. This function allows the used to consecutively record a predesignated amount of images at predescribed positions on the image frame. These images can then be "stitched" together using the image analysis software to create one continuous image of the downstream saturation. 8 images are recorded at 0,5 second intervals to create a complete image of the downstream section of the capillary (10 mm). The delay between the recording of the images starts to be significant at an injection rate of 100 nl/min when it takes approximately 20 seconds for the fluid to travel the complete distance. However, because the systems show steady state behavior at these flow rates the errors in the recorded images due to the recording delay is disregarded.

DEAD END PORES

The dead end channel design is used to study microemulsion formation in dead end porespace. The design and dimensions of the micromodel used are given in fig 4.3. Dead end pores are unconductive to flow and

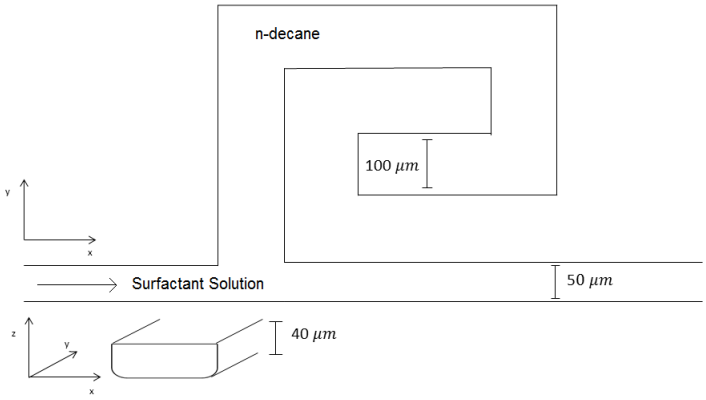

Figure 4.3: the geometry of the dead end pore in the micromodel used in the second set of experiments

mixing of two phases in a dead end is therefore not dominated by the macroscopic pressure gradient which drives the flow in the main channel. Two other physical phenomena have been proposed to enable transport of the miscible phases into the unconductive porespace:

- Diffusion
- Marangoni Spreading

These mechanisms were both discussed in chapter 2.

Before every experiment the micromodels are cleaned using (in that order) dry cleaning naphta, water and propanol. This is the only way to completely clean the dead ends of any remaining oil, water or air. This means that the dead end pores are filled with Propanol before the n-decane is injected to saturate the pores with. As n-decane is injected into the dead ends the propanol dissolves into the n-decane. After injecting n-decane for a minimum of 10 characteristic diffusion times into the micromodel, the propanol is considered to have been sufficiently diluted for the experiment to take place. The characteristic diffusion time was based

on the length of a dead end pore (1.2 mm) with a self diffusion coefficients of $10^{-9} m/s^2$. The initial wettability of the micromodels varies due to the complicated cleaning and saturation process. However, because a water film quickly (almost instantaneously) forms around the oil as soon as the surfactant solution is injected, the micromodels in the dead end pore experiments are also considered to be water wet. A syringe (similar as for the previous experiments) is filled with the surfactant solution and connected to the inlet of the micromodel with a small tube. The pump is turned on at the desired injection rate so that the surfactant solution flows into the main capillary where emulsification is initiated. By focussing the microscope on one of the pores and using the time lapse function of Leica Qwin, the microscope can record an image of the experiment at pre set intervals. These images can then be used in image analysis to deduce the typical time scales and length scales at which emulsification take place.

4.3. IMAGE ANALYSIS

The outcome of the experiments are images which are analysed using Leica Qwin. Two types of images are recorded: colored images with the flurorescent light and grayscale images with the regular transmitted light. The images recorded using the fluorescent light contain information which enables differentiation between the phases due to the solvachromatic dye. The image analysis software can be used to diferentiate between the phases quantitatively. The color of the light emitted by a microemulsion should theoretically reflect the solubilization ratios of oil and water in the emulsion, allowing to identify between certain types of microemulsion. To capture the relationship between the colour emitted by the emulsion and the solubilization ratios a phase behavior test was performed using dyed n-decane. The solubilization ratios of oil and water in the microemulsion were calculated from the phase behavior tests. The microemulsion was then extracted from the test tube and directly injected into the micromodel. Images were then recorded and anlysed.

5

RESULTS: SURFACTANT SYSTEMS

The surfactant systems used in the microfluidic experiments were first studied under static conditions. This was done by means of phase behavior tests, rheology measurements and interfacial tension measurements. The results for the optimum salinity systems can be found in table 5.1.

5.1. PHASE BEHAVIOR TESTS

Phase behaviour tests were performed with the four surfactant systems using NaCl to characterize their behavior under static conditions. The results of the phase behaviour tests were photographed and have been added to appendix D. An example of such a phase behavior test can be found in figure 5.1. The volume fractions of oil and water in the microemulsions can be calculated from the phase behavior tests. We observe an

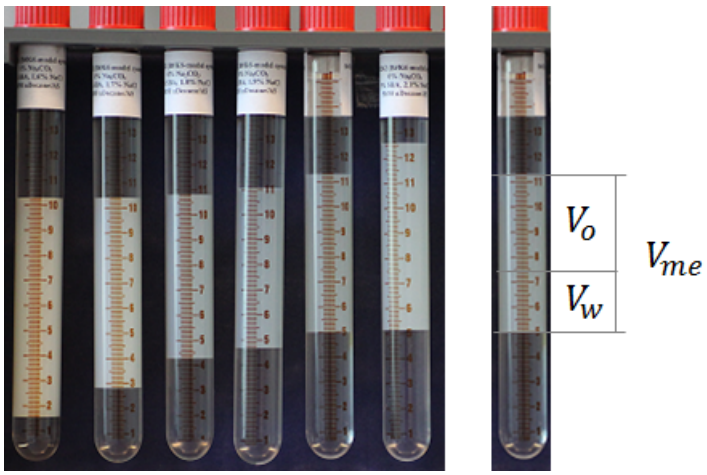

Figure 5.1: Example of a phase behavior test (4% O242 5% SBA) using NaCl. The test tube on the right shows how the volume fractions of oil and water in the microemulsion can be calculated from the test tube.

increase in the volume of microemulsion that forms with an increase of surfactant in the surfactant solution. The optimum salinity decreases with an increase in surfactant concentration because the surfactant adds

Table 5.1: table with the summary of the viscosities for the surfactant systems, viscosities for the corresponding microemulsions at optimum salinity and interfacial tension for the corresponding microemulsions at optimum salinity.

Surfactant System	μ_{ss}	μ_{me} **(mPa.s)**	γ_{me} **(mN/m)**
I	6	4.3	0.002
II	0.9	4.1	0.003
III	0.9	3.6	0.005
IV	0.9	1.1	0.001

positively charged ions to the solution. At 5% SBA concentration the microemulsion that forms is relatively clear because the cosolvent causes the interface in the microemulsion to increase, making the separate pockets of oil and water in the emulsion relatively small. When these pockets are smaller than the wavelength of light, it doesn't reflect and goes trough the emulsion causing it to look clear. When the cosolvent concentration decreases to 0.5%, the interface between oil and water in the microemulsion becomes less flexible and the separate pockets in the emulsion increase in size. This means that for an equal amount of surfactant a larger volume of microemulsion forms because more oil and water can solubilize in the microemulsion. Due to the larger size of the pockets, the microemulsions becomes a milky-white phase instead of clear (figure D.4).

5.2. RHEOLOGY

The viscosity of the middle phase was measured using a shear rheometer in each of the test tubes which showed a middle phase in the phase behavior tests. A plot of the viscosity of the middle phase as a function of salinity for each of the surfactant systems can be be found in figure 5.2. The viscosities depicted in the figure were all measured at a shear rate of 7 s^{-1}.

The viscosities show a clear salinity dependence which can be understood when taking into account that the structure of the microemulsion changes with the intefacial tension. The minimum viscosity lies around the optimum salinity. It then increases symetrically as the salinity increases or decreases due to the symmetry in the phase behavior. Oil in water emulsions form at under optimum salinities and water in oil emulsions form at over optimum salinity. Only three measurements could be performed for system IV (0.5% surfactant concentration 0.5% SBA) because the phase behavior test only formed a third phase in three of the test tubes (figure D.4). The viscosity shows a small increase with an increase in surfactant concentration. This could indicate that adding surfactant can further decrease the IFT in the microemulsion, making the pockets of oil and water slightly smaller and increasing the amount of surfactant per volume of microemulsion which in turn increases the viscosity. This is also the reason why there is such a large difference between the viscosities of the 5% SBA systems and the 0.5% SBA system. The added cosolvent decreases the size of the pockets, increasing the amount of surfactant per volume of microemulsion which increases the viscosity.

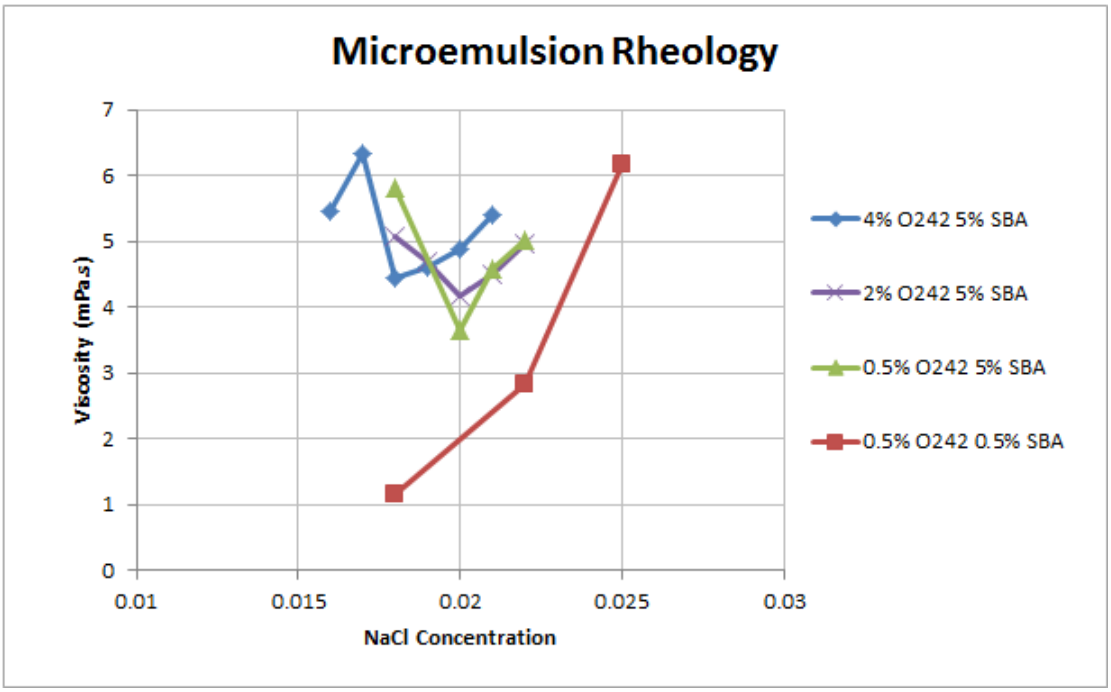

Figure 5.2: Rheology as a function of salinity for the 4 surfactant systems used in the microfluidic experiments. The viscosity was measured at a shear of 7 s-1 which corresponds to reservoir flow rates of 1 ft/day

5.3. INTERFACIAL TENSION

The interfacial tension between the microemulsion and the brine was measured using the spinning drop technique for each of the systems which showed a middle phase. A plot of the IFT as a function of the salinity of the brine can be found in figure 5.3. The plot shows that the IFT depends on the salinity and that it reaches a minimum around the optimum salinity. Surfactant system III shows an extra minimum at under optimum salinity which can't be explained within the experimental error. This is probably an erroneous measurement which should be repeated. System I doesn't show a pronounced minimum around the optimum salinity. A possible explanation for this is that the spinning drop technique is not an accurate enough technique to measure the ultralow interfacial tensions observed in these conditions.

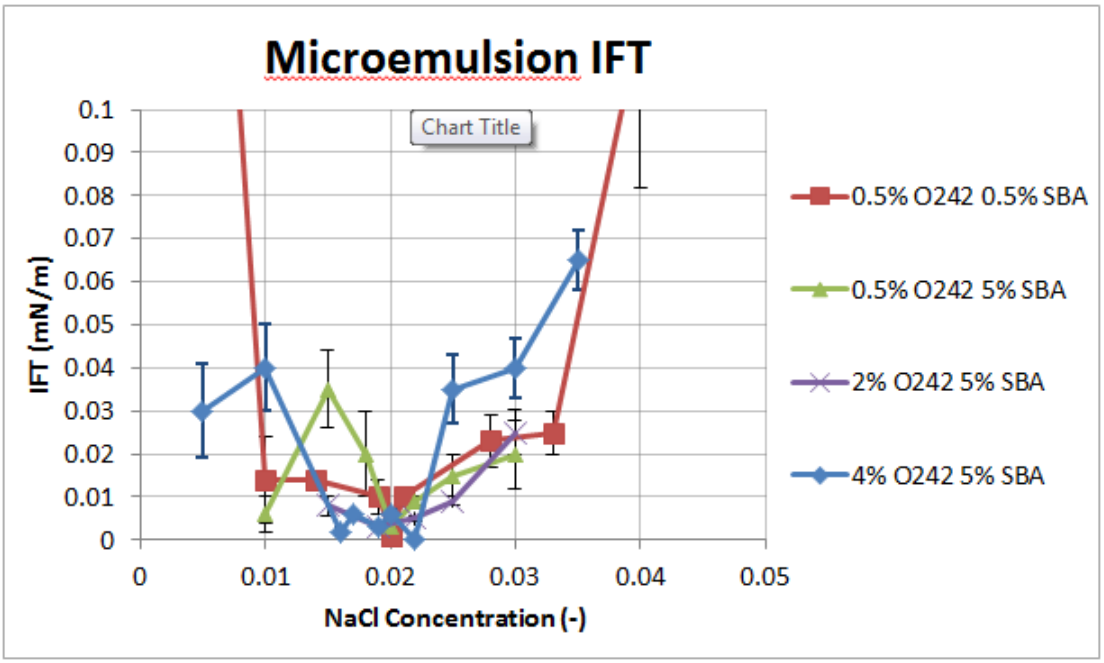

Figure 5.3: Interfacial tension as a function of salinity for the 4 surfactant systems used in the microfluidic experiments. The interfacial tension was measured using the spinning drop technique.

6

RESULTS: COLOR CALIBRATION

The behavior of Nile Red in combination with the surfactant system and the model oil was studied. Because the dye is known to show a blue shift in its emission spectrum with decreasing polarity it is thought that it should do so in a microemulsion with increasing oil solubilization (and consequently increasing salinity). This will allow the measurement of oil and water solubilization in the microemulsion from the recorded images of the microfluidic experiments. In this chapter the results of such a color calibration is discussed.

6.1. PHASE BEHAVIOR TEST (STATIC)

To quantify the oil solubilization in the microemulsion a phase behavior test using dyed n-decane (500 x dilution by volume) was performed. The resulting phase behavior is found in figure 6.1. From the phase

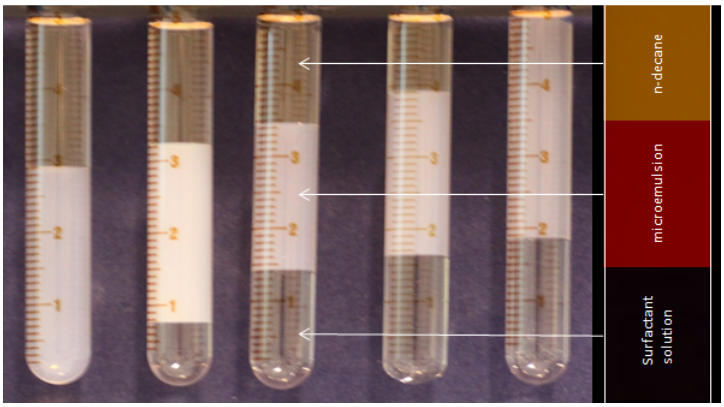

Figure 6.1: phase behavior tests for a 4% O242 5% SBA surfactant solution mixed with n-decane and Nile Red dye. From left to right: 1.2% NaCl to 2.4% NaCl with 0.3% NaCl increments. The colors on the right are the color of the light emitted by the dye in different phases under a fluorescent lamp.

behavior tests the volume fractions of oil and water in the microemulsion can be calculated. The results can be found in table 6.1. The comparison was made with the phase behavior test of system I without the dye D.1 to see if the dye influences the phase behavior. It was shown that the dye doesn't affect the optimum salinity of the microemulsion. However, the solubilization of oil and water in the microemulsion with the dye was approximately 10% lower compared to the microemulsions which formed without the dye. Since the dye is also a surface active agent it is possible that it has an effect on the interface, further increasing its flexibility and hence creating smaller pockets of oil and water which have smaller solubilization capacity.

6.2. MICROFLUIDIC EXPERIMENT (DYNAMIC)

The microemulsions were then injected into the micromodel and illuminated with the fluorescent lamp. Figure 6.2 shows the under optimum (1.5% NaCl, bottom) and the over optimum (2.1% NaCl, top) solution under

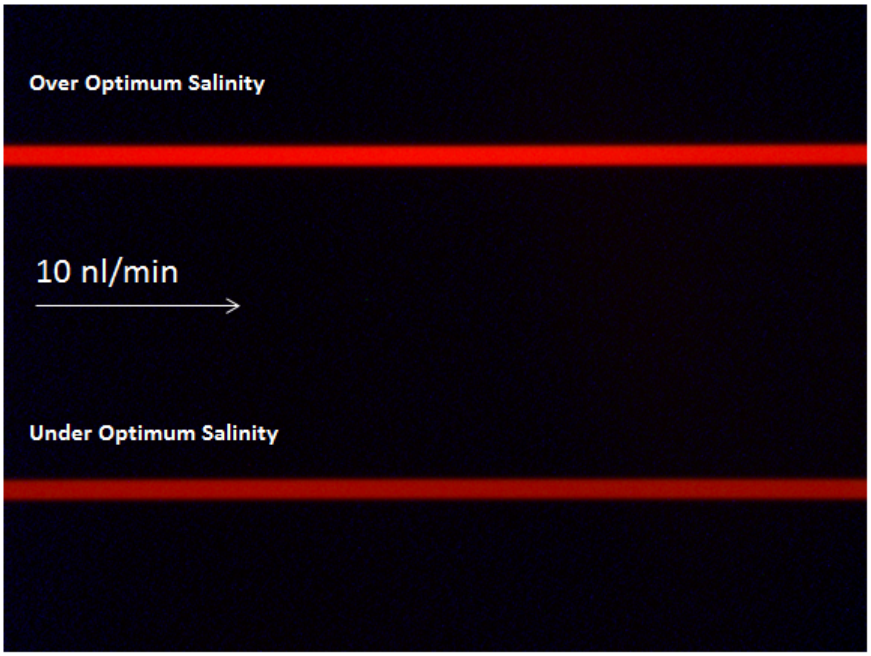

Figure 6.2: Top capillary: over optimum microemulsion (2.4% NaCl) flowing at 10 nl/min. Bottom capillary: under optimum microemulsion (1.2% NaCl) flowing at 10 nl/min.

flowing conditions (10 nl/min). After the image of the microemulsions was recorded under flowing conditions the pump was turned off and the emulsions were allowed to come to a halt in the micromodel. Figure 6.3 shows the same over optimum and under optimum solution after they have settled (no flow). The images were analysed using the image analysis software and the results of the RGB measurements can be found in table 6.1.

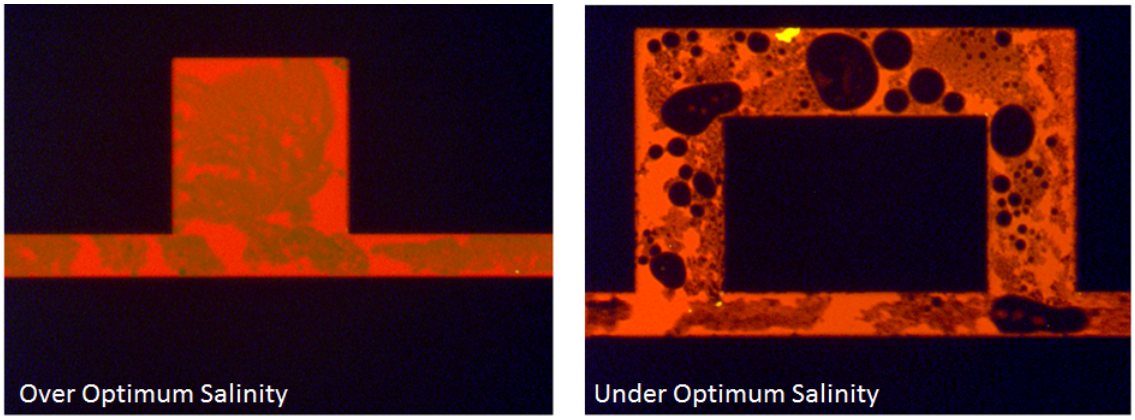

Figure 6.3: Left: Over optimum salinity (2.4% NaCl) microemulsion which has settled after flowing in figure 6.2. Right: Under optimum salinity (1.2% NaCl) which has settled after flowing in figure 6.2

6.3. DISCUSSION

From table 6.1 and the images we can conclude the following about the color of the microemulsion in the recorded images:

- Under **flowing conditions**, the dye in the (micro)emulsion will emit a dark red light. Since the emission spectrum of the dye emits a red shift with increasing polarity of the solvent, we can conclude that the dye will solubilize in a more polar structure when the microemulsion is subjected to flow.
- Under **flowing conditions**, an increase in the amount of oil solubilized in the (micro)emulsion will lead to an increase in the measured red value . This can be explained by the presence of more dye in the emulsion because of the fact that there is more oil.
- The (micro)emulsion will separate from the phase which has the highest solubilization in the (micro)emulsion **after flow**. The result is a continuous phase in which the dye emits an orange light which contains droplets of the excess phase. The orange light indicates that the dye is solubilized in a structure which is less polar than under flowing conditions.
- The difference in oil and water solubilization ratios in the (micro) emulsion under **static conditions** and after separating translated into a small difference in measured RGB values. Specifically, the over optimum salinity (micro)emulsion showed a stronger red value (indicating more water) than the under optimum salinity (micro)emulsion. This can possibly be explained by the fact that the excess phase has separated from the microemulsion, causing the continuous phase to contain less of the separated excess phase. However, it makes it difficult to quantify how much of each phase is actually solubilized in the continuous phase.

A probable cause for the strong effect of flow on the light emitted by the microemulsion is that the structure of the microemulsion changes under flowing conditions. Because the dye is surface active, the structure of the (micro)emulsion may have a strong effect on its fluorescent properties as has been noted in [37]. Under static conditions a microemulsion might find it energeticaly more favorable to form a different structure than under flowing conditions. Under flowing conditions, droplet like structures (micelles) may form which would also explain the strong red shift in the emission spectrum when the microemulsion is flowing [41]. Another factor which has not been shown in this chapter but which also has a strong effect on the color values measured by the software is the amount of time the dye has been exposed to the fluorescent light. Because of this, the decision was made to differentiate between the phases qualitatively and not quantitatively. This method will allow to differentiate between the separate phases and also between static and flowing (micro)emulsions. It will however not be possible to quantify the oil and water solubilization in the microemulsions.

Table 6.1: Measured RGB values for for the microemulsions from the PB tests in figure 6.1 under flowing and non flowing conditions for several recorded images. Figure 6.2 and figure 6.3 are represented by file 2 & 4 and 6 & 7.

File	Flow?	Salinity	V_o	V_w	Mean Red	Mean Grn	Mean Blu	σ_r	σ_g	σ_b
1	Yes	2.1	0.61	0.39	254.2	0.2	0.0	1.126657	0.004714	0
2	Yes	2.4	0.78	0.22	243.1	11.1	0.0	1.347887	1.902285	0
3	Yes	1.5	0.32	0.68	143.3	6.6	0.5	0.948203	0.902146	0.043205
4	Yes	1.2	0.14	0.86	159.3	8.0	0.0	0.748435	0.676314	0
5	Yes	1.2	0.14	0.86	185.4	21.1	0.0	2.08631	0.342929	0
6	No	1.2	0.14	0.86	250.2	77.4	0.0	1.378413	3.81927	0
7	No	2.4	0.78	0.22	243.1	53.2	0.0	5.215338	7.456059	0

7

RESULTS: T-JUNCTION EXPERIMENTS

The t-junction micromodel experiments are not intended to study the liquid-liquid flow patterns in micro-capillaries but rather to investigate the microemulsion formation and how it is affected by the flow regimes. The aqueous phase and the (colored) n-decane were co-injected through separate channels into the glass micromodel and the two capillaries merged at the t-junction (figure 4.2 where the two fluids mix for the first time. The microscope was focused on the junction to study the mixing behavior of the injected fluids and the microemulsion formation. As the microemulsion formed, the flow changed from two phase to quasi-miscible three phase flow. The flow of the phases continued into the downstream capillary.

The results of the T-junction experiments have been divided into two parts. Part one focuses on the flow regime at the T-Junction. Part two discusses how the flow regime and the varied parameters affect microemulsion in the downstream capillary. First a reference case experiment with water & oil will be discussed. This will be followed by a series of experiments where the surfactant solutions (systems I-III, table 3.1) are co-injected with the oil. The influence of the flow rate, the surfactant concentration and the salinity will be discussed.

7.1. REFERENCE CASE

Co-injection of DI water and n-decane was performed to define a reference case that helps to identify the effect of IFT between oil and water on the flow regime. No surfactants were used in the reference case experiment. The result of the reference experiment for the T-Junction (100 nl/min, $Q_{oil} = Q_{water}$) is shown in figure 7.1. It produced alternating flow patterns immediately after the t-junction due to the high interfacial tension. This prohibits the oil and the water from flowing in the downstream capillary simultaneously. The experiment was repeated at an injection rate of 1 nl/min and 10 nl/min which also resulted in alternating flow as can be expected from the capillary number (decrease in viscous forces). The snap-off of the phases are shown in figure 7.1.

- a) The continuous phase (water) is flowing uninterrupted while the n-decane is building up pressure
- b) the pressure build up causes the meniscus between water and n-decane to move downstream which forces the connection between the water in the inlet and the water downstream to be squeezed against the corner
- c) the water phase snaps at the corner when a critical pressure is reached, breaking the water phase (breaking point marked by x)

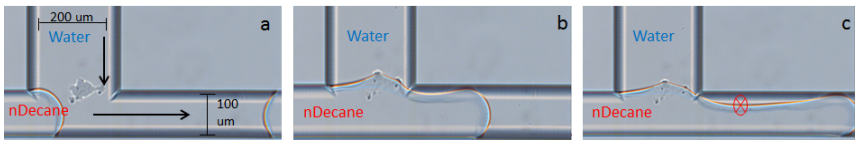

Figure 7.1: Reference case experiment for the T-Junction. Water and n-decane were coinjected at equal rates (Q = 100 nl/min) to meet at the T-Juntion. a-c show consecutive time steps.

7.2. SYSTEM I & N-DECANE CO-INJECTION

Co-injection of system I and n-decane was performed. Three different salinities of system I was prepared in order to study the effect of phase behavior on the microemulsion formation under flow (Appendix D): 1.6% Nacl (under optimum) 1.8% (optimum) and 2.0% (over optimum). The phases were injected at 1, 10 and 100 nl/min.

7.2.1. FLOW REGIME

1.6% NACL

The flow regimes at the t-junction for system-I at under optimum salinity is shown in figure 9.2. At 1 nl/min the interface fluctuates resulting in snap-offs where microemulsion has formed locally (red patches in image 1). As the rate increaes to 10 nl/min we still see fluctuations at the interface but less. A red strip of microemulsion is formed as the two phases flow downstream (image 4). At 100 nl/min we hardly see any microemulsion formation at the proximity of the t-junction and no snap-offs (image 7).

1.8% NACL

The mixing and flow behavior at the t-junction was very similar with the behavior witnessed at 1.6% NaCl. The only exception was that snap-offs were still observed at 10 nl/min injection rate (image 5).

2.0% NACL

At 1 nl/min injection rate there were continuous but small fluctuations at the interface. They facilitated the microemulsion formation (image 3) but seldomly resulted in snap-offs. At higher rates no snap off occurred and the microemulsion formation was minimal in the proximity of the t-junction.

7.2.2. DOWNSTREAM SATURATION

The recorded images and plots of the ME saturation profiles downstream of the t-junction for system-I are shown in figure 7.3 and 7.4. Figure 7.4 shows two plots: the top plot shows the saturation downstream as a function of distance (spatial distribution) and the bottom figure shows the saturation as a function of time. The time steps were acquired by dividing the distance by the (constant) flow rate. The results will be discussed separately for each of the salinities.

1.6% NACL

At 1 nl/min injection rate we observe full emulsification downstream of the t-junction (red) with patches of unemulsified oil (yellow). As the injection rate increases, we see parallel flow where red (micro)emulsion forms at the interface between the two fluids. If we increase the injection rate further, the amount of (micro)emulsion which forms at the interface decreases. This is because there is less time to form emulsion in the capillary as the two fluids flow downstream. Under parallel flowing conditions the emulsification rate is linear with time at 100 nl/min injection rate. At 10 nl/min injection rate the emulsification shows square root of time dependence.

1.8% NACL

At 1.8% NaCl we observe similar behavior as at 1.6% NaCl. At 1 nl/min injection rate the fluctuating interface at the t-junction causes snap-offs to occur resulting in full emulsification downstream (again with pathces of oil). As the injection rate increases to 10 nl/min injection rate the n-decane and the emulsion begin to mix and form an orange fase. At 100 nl/min injection rate the same behavior as at 1.6% NaCl is observed. Under parallel flowing conditions the emulsification rate is linear at 100 nl/min injection rate.

2.0% NACL

At 2.0% NaCl similar behavior is observed as with the previous salinities. At 1 nl/min the low injection rate causes a fluctuating interface resulting in full emulsification downstream with patches of unemulsified oil due to snap offs. As the injection rate increases to 10 nl/min the interface stabilizes more and due to the shorter time range, full emulsification is only achieved at the end of the capillary (as in the 1.6% NaCl experiment). At 100 nl/min injection rate the same profile as at 10 nl/min is observed but with only 1/10th of the time to emulsify (as in the 1.6% NaCl experiment). Under parallel flowing conditions the emulsification rate is linear with time at both 100 nl/min and 10 nl/min injection rates.

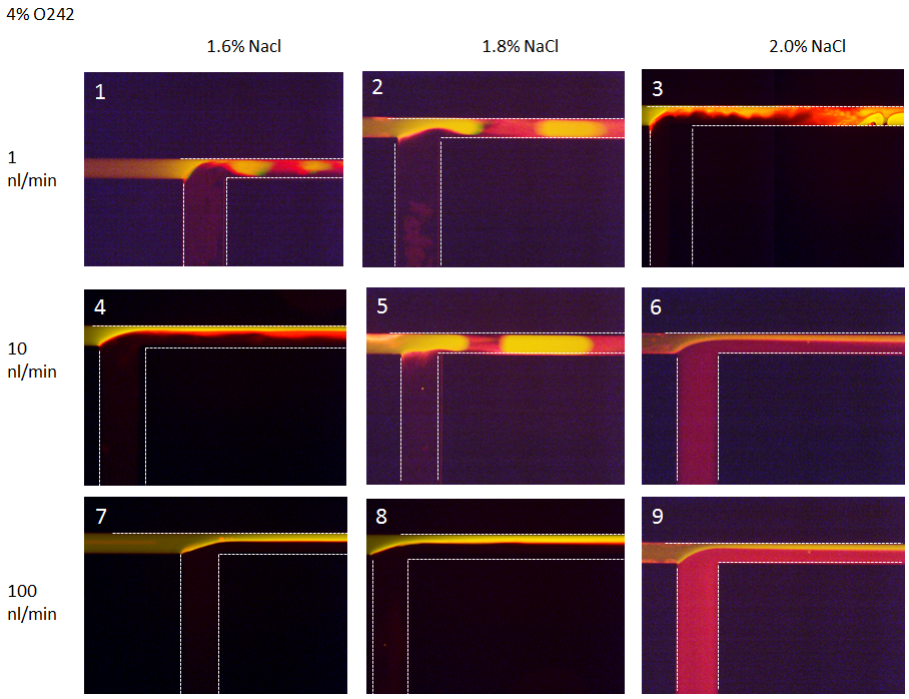

Figure 7.2: Flow regime at the T-Junction for the 4% surfactant concentration solution. The surfactant solution (black) is injected from the bottom and the decane (yellow) is injected from the right. The salinity was varied between 1.6% NaCl (under optimum salinity), 1.8% NaCl (optimum salinity) and 2.0% NaCl (over optimum salinity). The volumetric flow rates Qo and Qs were varied between 1, 10 and 100 nl/min. Qo=Qs for all experiments.

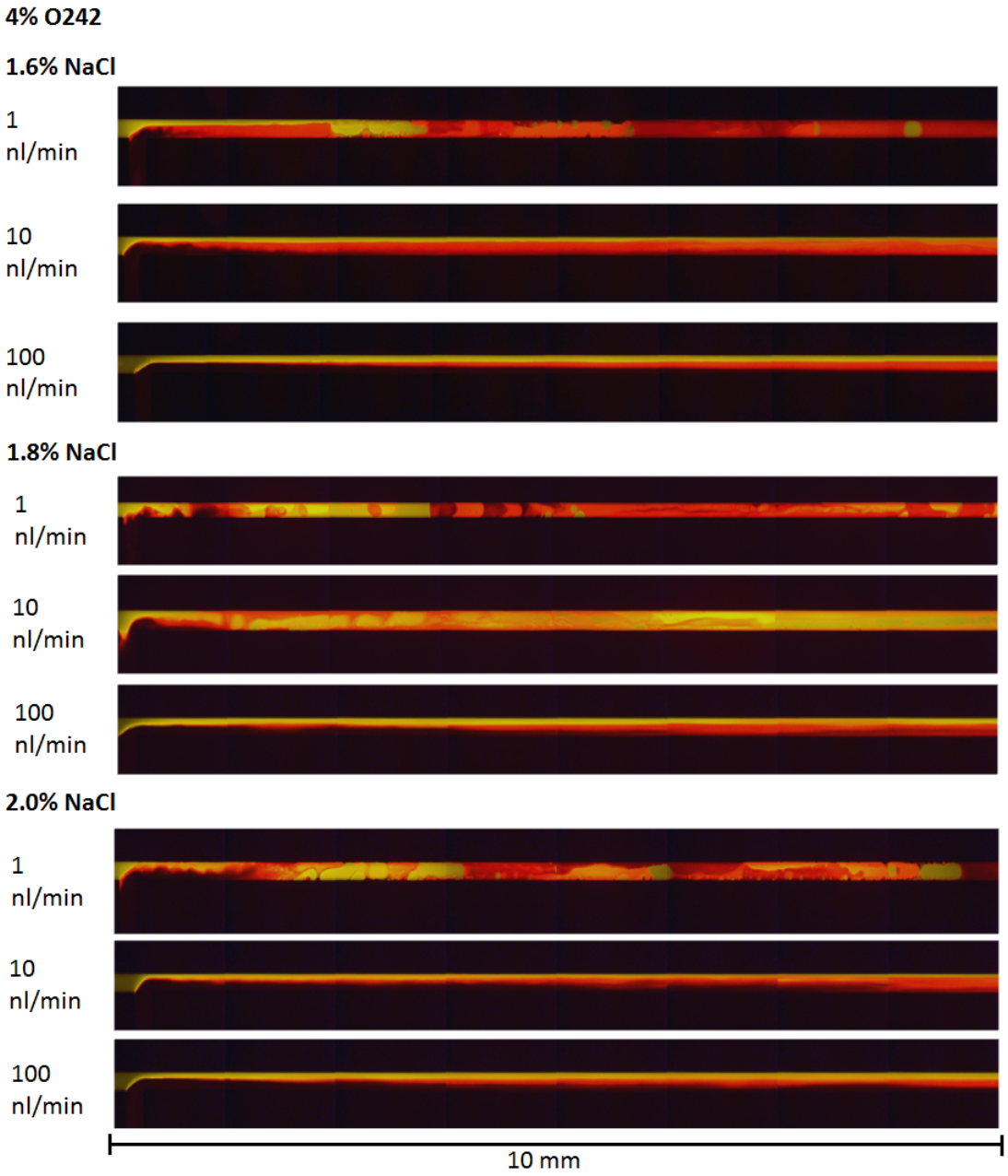

Figure 7.3: ME saturation profiles for the 4% surfactant concentration solution. The surfactant solution (dark) flows in from the bottom left and the decane (yellow) flows in from the left. The two phases then meet at the T-junction and mix to form microemulsion (red)

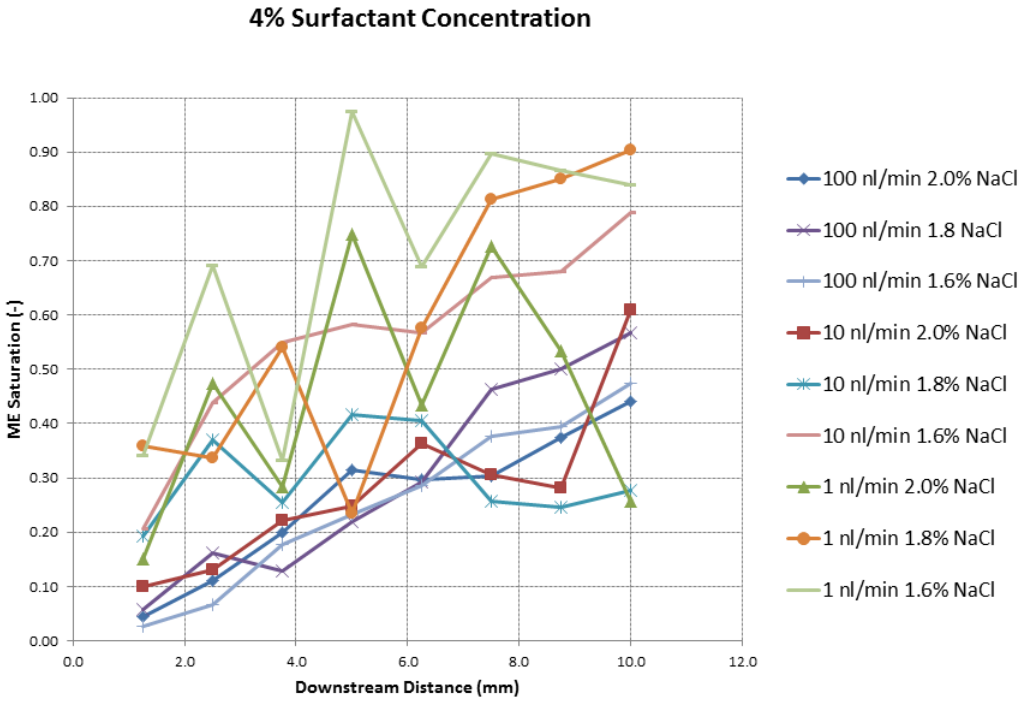

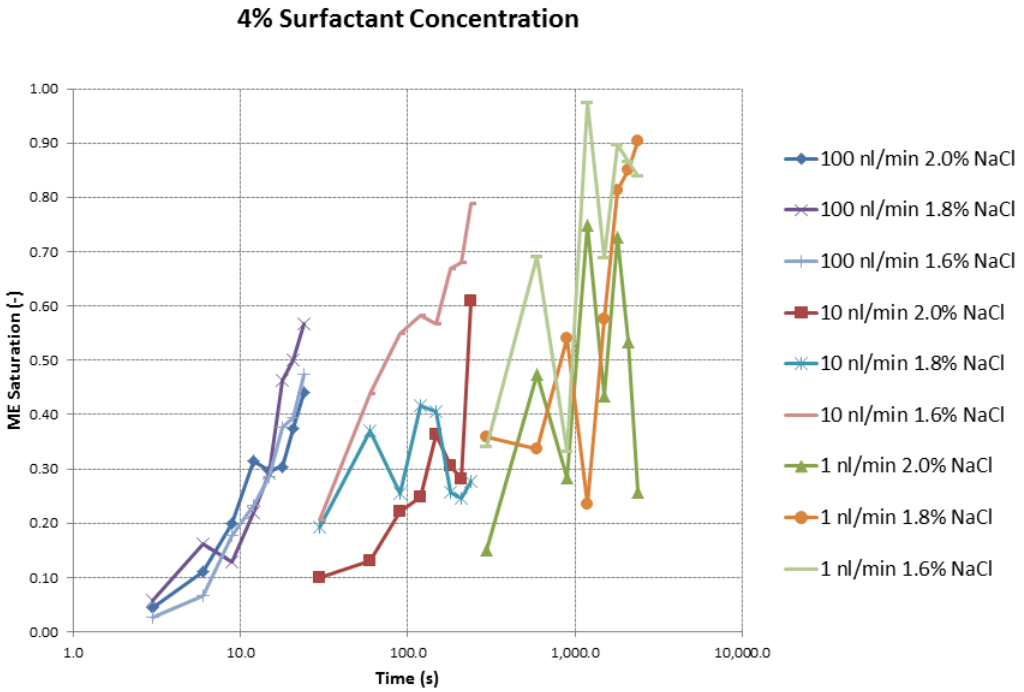

Figure 7.4: Top: microemulsion saturation downstream of the t-junction as a function of distance (mm). Bottom: microemulsion saturation downstream of the t-junction as a function of time (s). The time steps are acquired by dividing the distance by the (constant) flow rate (m/s)

7.3. SYSTEM II & N-DECANE CO-INJECTION

Co-injection of system II and n-decane was performed. Three different salinities of system II were prepared in order to study the effect of phase behavior on the microemulsion formation under flow (Appendix D): 1.6% Nacl (under optimum) 1.8% (optimum) and 2.0% (over optimum). The phases were injected at 1, 10 and 100 nl/min.

7.3.1. FLOW REGIME

1.6% NACL

At 1.6% NaCl parallel flow is observed at the t-junction for all injection rates. Emulsion (bright red) forms at the interface between the surfactant solution and the oil. The interface is straight at all flow rates (no fluctuations).

1.8% NACL

At 1.8% NaCl the exact same behavior as at 1.6% NaCl is observed for all injection rates. At 10 nl/min the pressure in the surfactant solution capillary seems to have fallen away which explains why oil has entered the capillary upstream.

2.0% NACL

At 2.0% NaCl parallel flow is observed for all systems at all injection rates. The only difference is that relatively less emulsion forms at 1 nl/min injection rate than is the case with the other two salinities.

7.3.2. DOWNSTREAM SATURATION

The recorded images and plots of the ME saturation profiles downstream of the t-junction for system-II are shown in figure 7.6 and 7.7. The saturations have been plotted against both the downstream capillary length and the time it takes for the fluids to travel that distance (assuming a constant flow rate). Plotting the saturations against logarithmic time allows to separate the three different injection rates in the time domain. The results will be discussed separately for each of the salinities.

1.6% NACL

At all injection rates the experiments show parallel flow. The emulsion that forms is bright red and forms as a continuous phase. Under these conditions we observe a linear emulsification rate at 100 nl/min injection rate and square root of time dependence at 10 nl/min injection rate. An emulsification cap is reached at a saturation of approximately 0.5.

1.8% NACL

At all injection rates the experiments show parallel flow. At 1 and 10 nl/min injection rate the emulsion no longer forms as a continuous phase which remains at the interface but as seperate emulsion flecks suspended in the surfactant solution. At 100 nl/min injection rate the emulsion forms as a continuous phase remaining at the interface between the oil and the surfactant solution. In this case the emulsification shows linear time dependence. The same emulsification cap is reached as at 1.6% NaCl at a saturation of 0.5.

2.0% NACL

At all injection rates the experiments show parallel flow. Specks of emulsion form at the interface between the oil and the surfactant solution at 1 and 10 nl/min injection rates. A continuous (red) emulsion forms at the interface between the surfactant solution and the oil at 100 nl/min injection rate. The emulsification rate is linear with time at 10 and 100 nl/min injection rates.

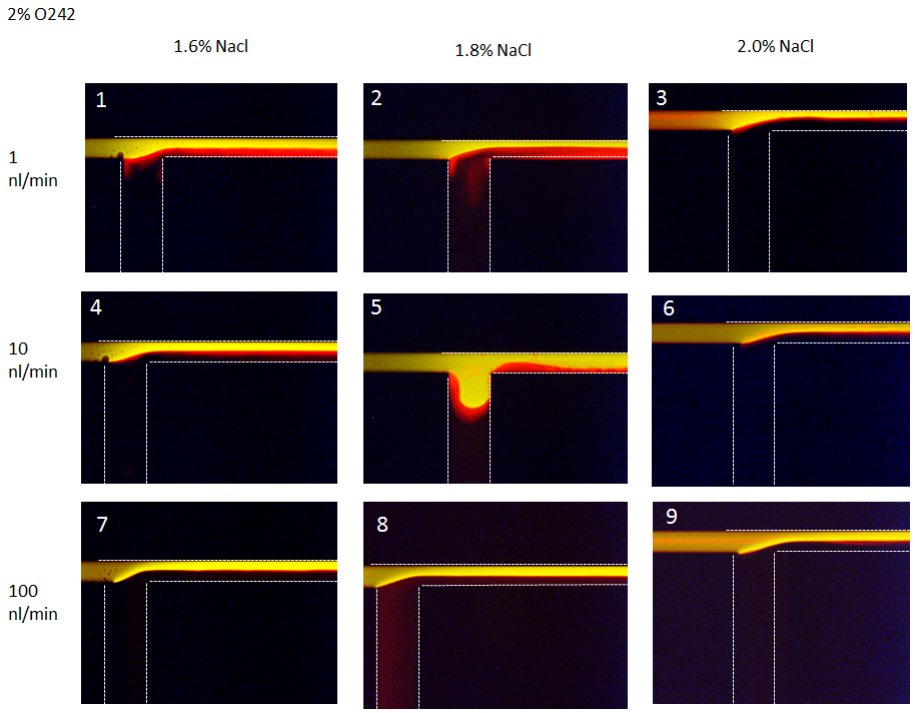

Figure 7.5: Flow regime at the T-Junction for the 2% surfactant concentration solution. The surfactant solution (black) is injected from the bottom and the decane (yellow) is injected from the right. The salinity was varied between 1.6% NaCl (under optimum salinity), 1.8% NaCl (under optimum salinity) and 2.0% NaCl (optimum salinity). The volumetric flow rates Qo and Qs were varied between 1, 10 and 100 nl/min. Qo=Qs for all experiments

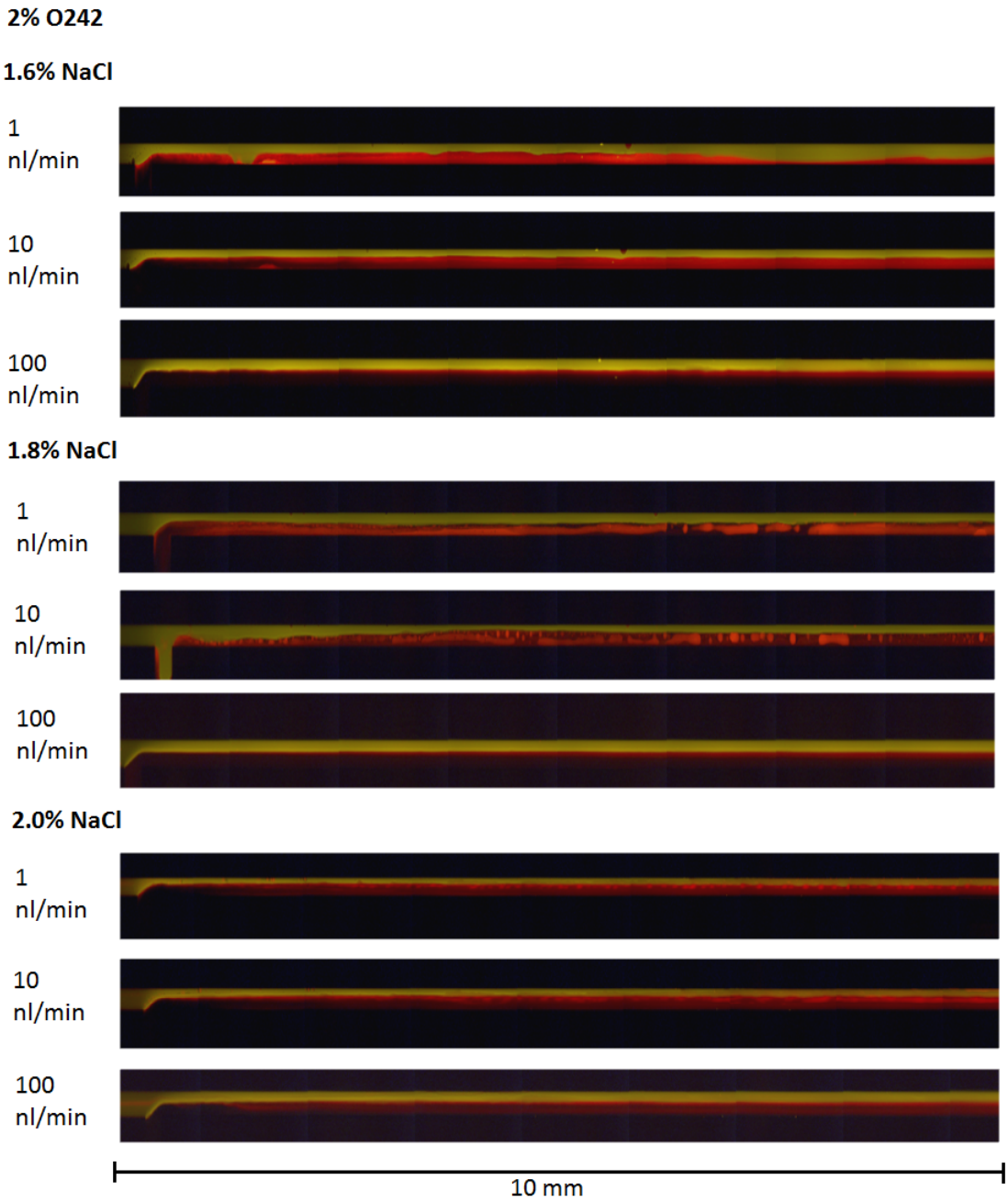

Figure 7.6: ME saturation profiles for the 2% surfactant concentration solution. The surfactant solution (dark) flows in from the bottom left and the decane (yellow) flows in from the left. The two phases then meet at the T-junction and mix to form microemulsion (red)

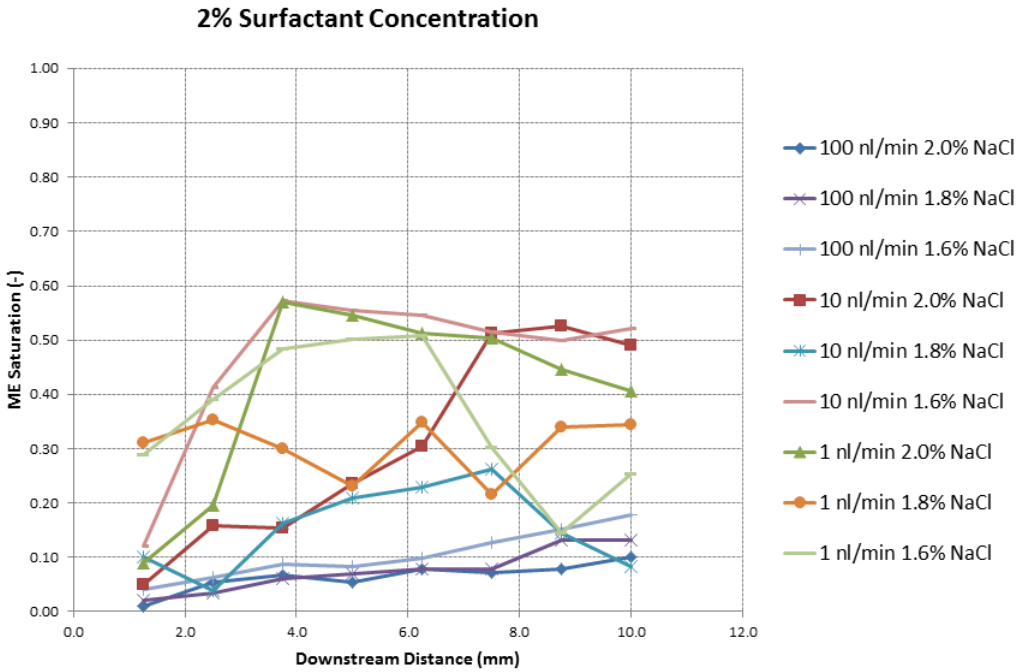

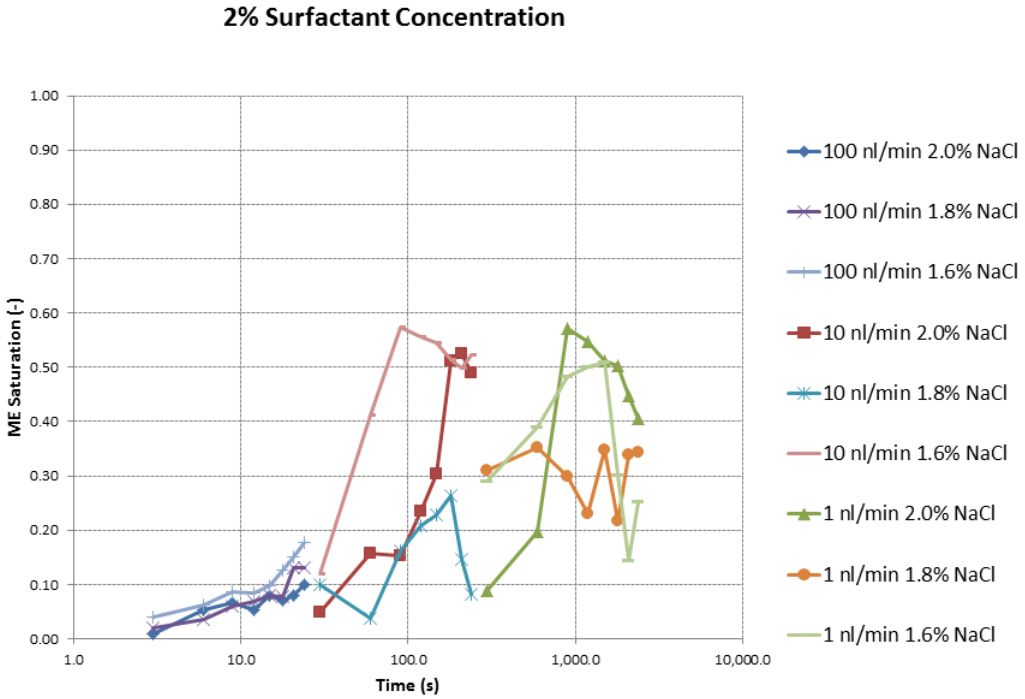

Figure 7.7: Top: microemulsion saturation downstream of the t-junction as a function of distance (mm). Bottom: microemulsion saturation downstream of the t-junction as a function of time (s). The time steps are acquired by dividing the distance by the (constant) flow rate (m/s)

7.4. SYSTEM III & N-DECANE CO-INJECTION

Co-injection of system III and n-decane was performed. Three different salinities of system III were prepared in order to study the effect of phase behavior on the microemulsion formation under flow (Appendix D): 1.6% Nacl (under optimum) 1.8% (optimum) and 2.0% (over optimum). The phases were injected at 1, 10 and 100 nl/min.

7.4.1. FLOW REGIME

At 0.5% surfactant solution the system shows parallel flow at all salinities and all flow rates. In two cases (image 2 & 3) emulsion forms at the interface in the shape of bright red specks which then flow downstream suspended in the surfactant solution.

7.4.2. DOWNSTREAM SATURATION

The images and plots of the ME saturation profiles for the 0.5% surfactant concentration solution are shown in figure (7.9 and 7.10). Because very little microemulsion is formed figure 7.11 shows the same results but on a smaller y-axis. At 0.5% surfactant concentration it seems there is not enough surfactant to form a continuous microemulsion phase at any injection rate. The experiments which do show some emulsification form small droplets of emulsion which flow downstream suspended in the surfactant solution. This happens in cases close to the optimum salinity (2.0%) and at low flow rates giving the phases time to "mix".

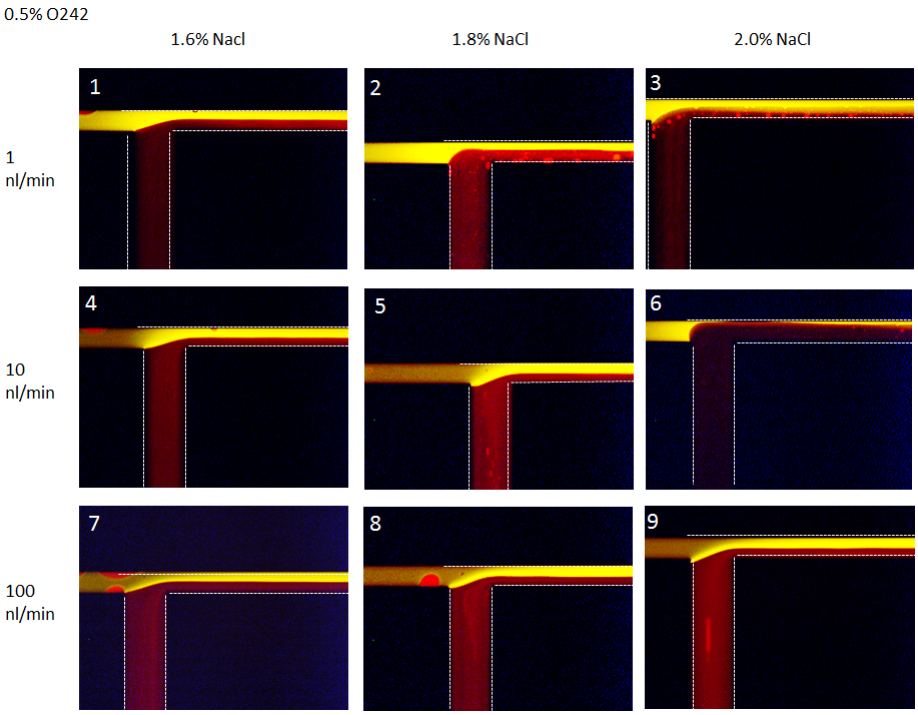

Figure 7.8: Flow regime at the T-Junction for the 0.5% surfactant concentration solution. The surfactant solution (black) is injected from the bottom and the decane (yellow) is injected from the right. The salinity was varied between 1.6% NaCl (under optimum salinity), 1.8% NaCl (under optimum salinity) and 2.0% NaCl (optimum salinity). The volumetric flow rates Qo and Qs were varied between 1, 10 and 100 nl/min. Qo=Qs for all experiments.

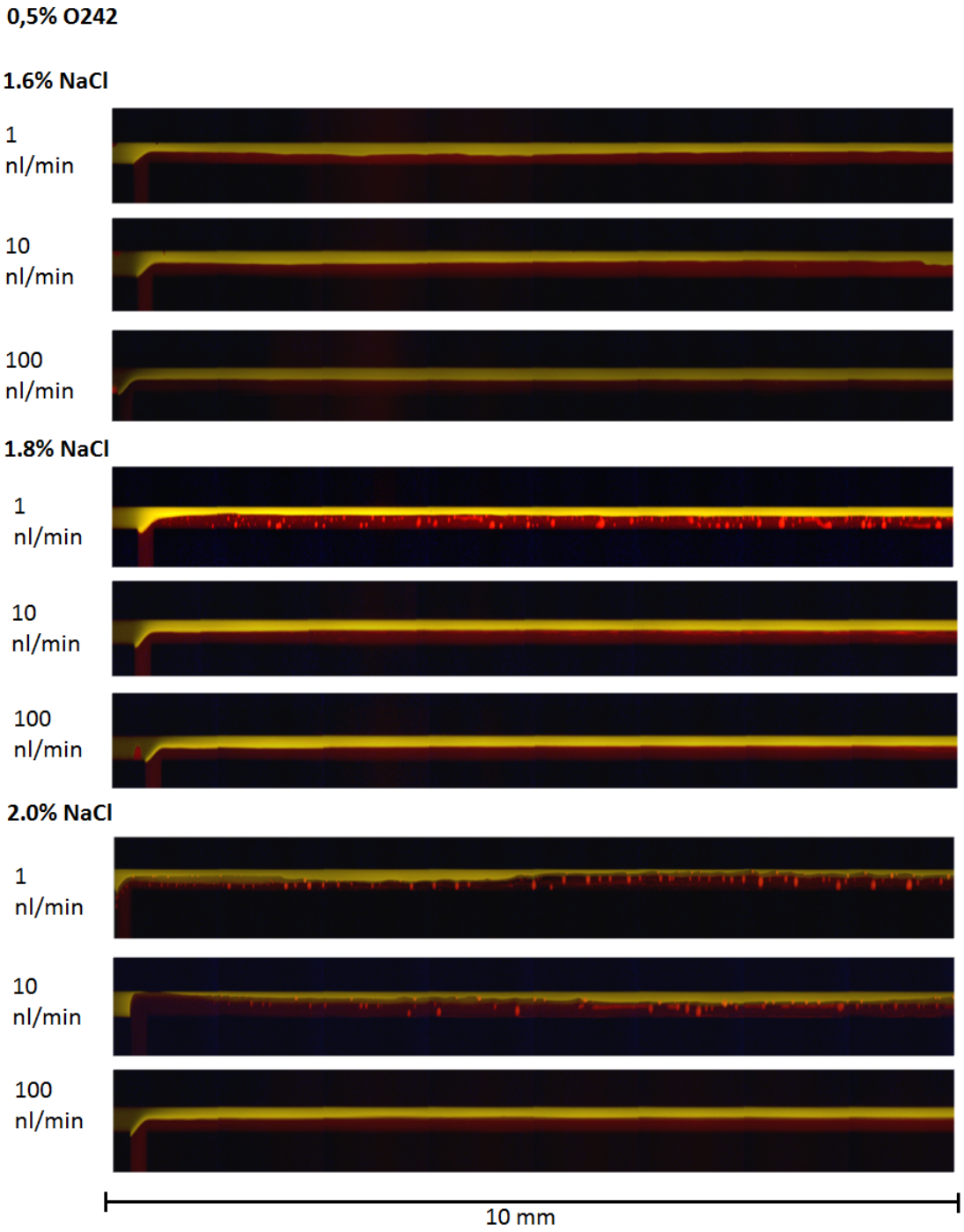

Figure 7.9: ME saturation profiles for the 0.5% surfactant concentration solution. The surfactant solution (dark) flows in from the bottom left and the decane (yellow) flows in from the left. The two phases then meet at the T-junction and mix to form microemulsion (red).

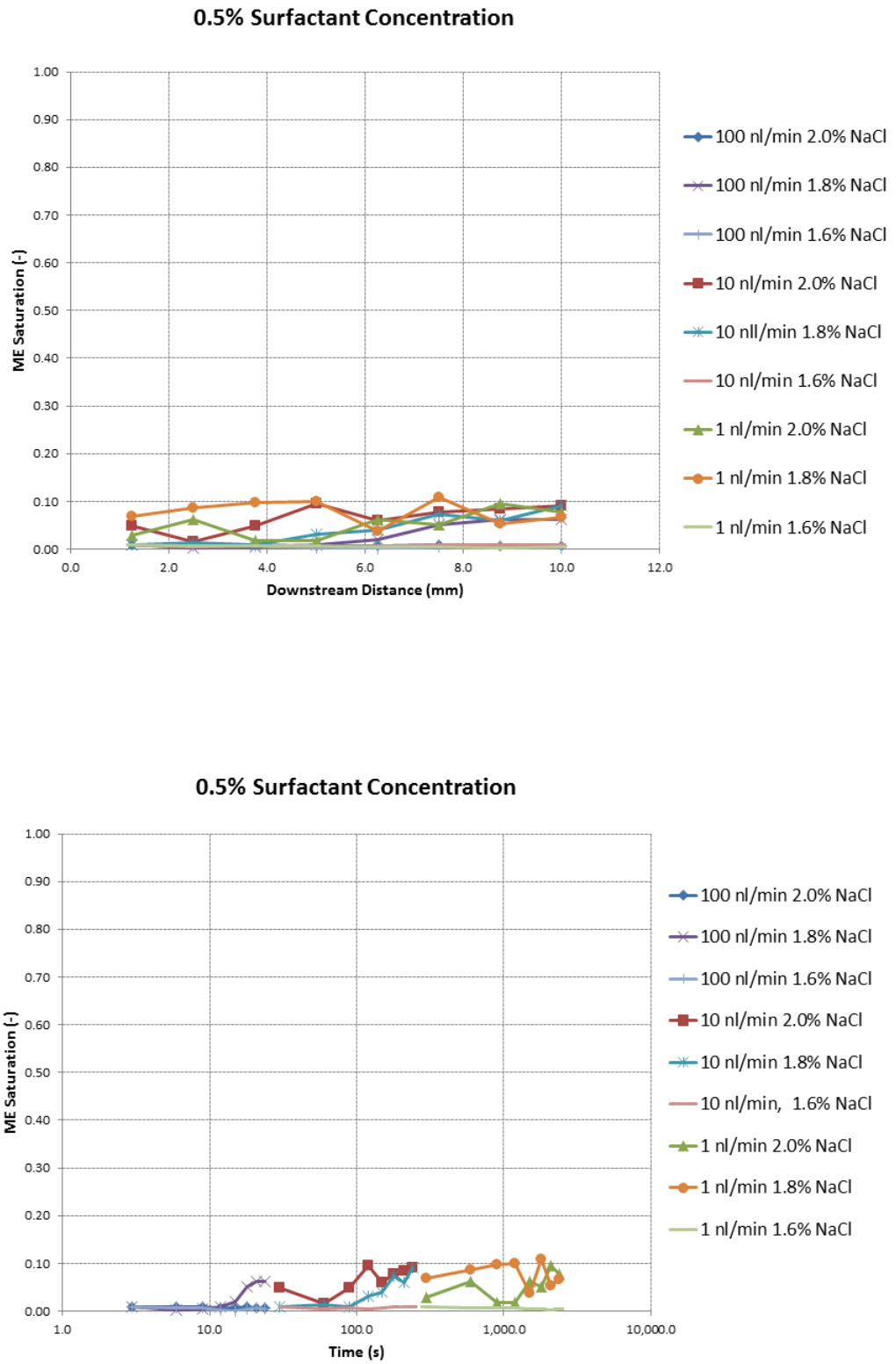

Figure 7.10: Top: microemulsion saturation downstream of the t-junction as a function of distance (mm). Bottom: microemulsion saturation downstream of the t-junction as a function of time (s). The time steps are acquired by dividing the distance by the (constant) flow rate (m/s)

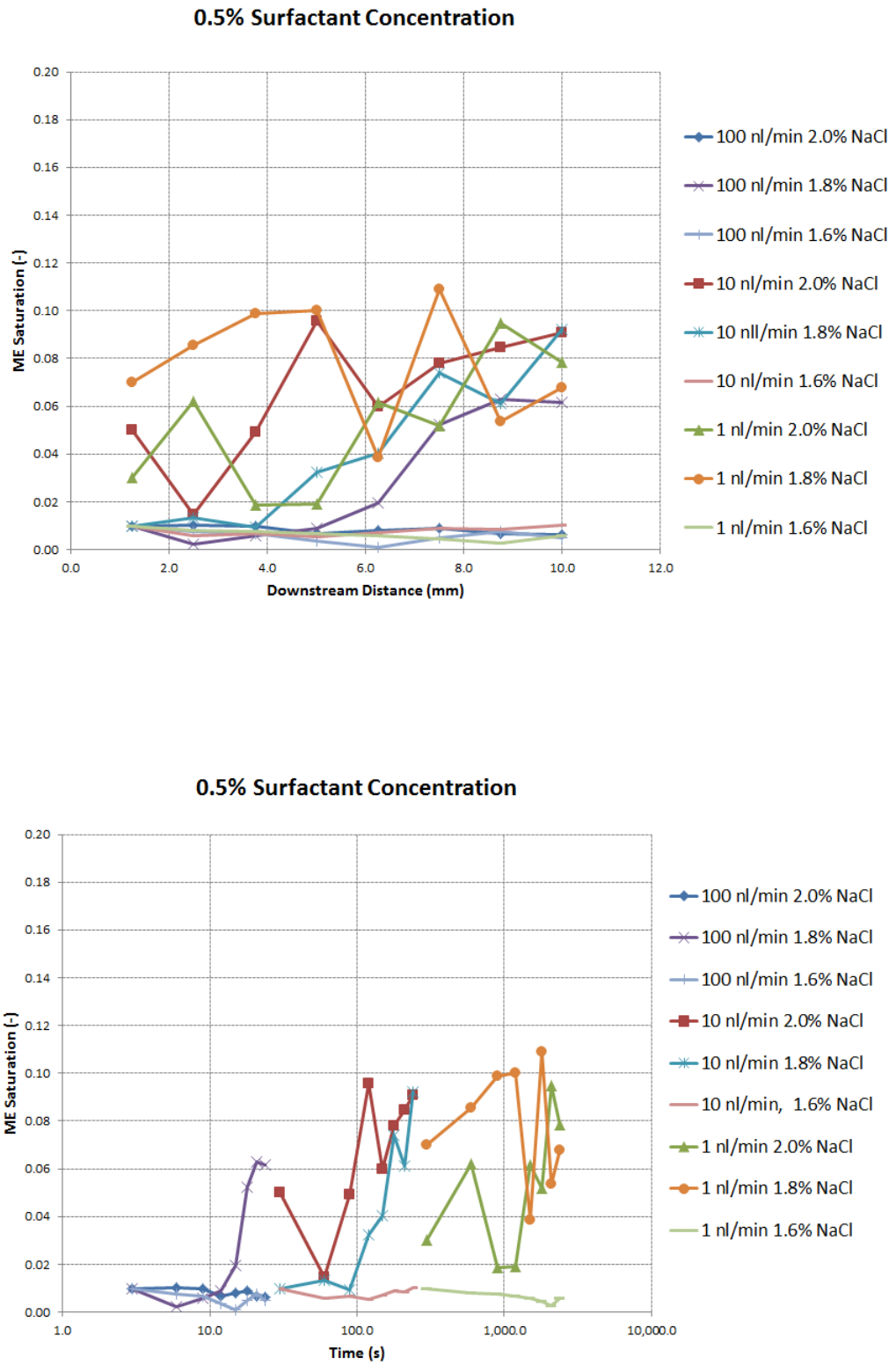

Figure 7.11: Top: microemulsion saturation downstream of the t-junction as a function of distance (mm). Bottom: microemulsion saturation downstream of the t-junction as a function of time (s). The time steps are acquired by dividing the distance by the (constant) flow rate (m/s)

7.5. LINEAR REGRESSION ANALYSIS: EMULSIFICATION RATES

The results of these experiments show that microemulsion formation in parallel flow depends on time linearly in the short time regime over short distances. Fitting the saturation values per timestep with a linear fit gives emulsification rates for the experiments which vary with injection rate, surfactant concentration and salinity. The emulsification rates are given in table 7.1. Using these rates, a linear least squares regression was performed on the emulsification rates of which the results can be found in appendix C. Salinity was translated to microemulsion volume per surfactant amount (in moles) and oil vs. water volume fraction ratio in the microemulsion, both calculated from phase behavior tests. Due to the sparse data set only first order dependencies are considered in this analysis to distinguish trends.

The first thing that should be noted is that the parameters which represent the influence of the salinity (V_{me}/N_{surf} and V_o/V_w) are statistically insignificant in their effect on the model (table 7.1). A possible explanation for this is that the variations in salinity between the experiments were not large enough. Only the injection rate and the surfactant concentration showed statistically significant effects on the emulsification rate. Both paramaters showed a positive correlation with the emulsification rate. For the surfactant concentration this can be explained by the fact that more surfactants do not only increase the amount of emulsification that can take place but will also cause an increase in surfactant solution viscosity. This viscosity causes a velocity profile to form with a stronger velocity gradient at the interface between the surfactant solution and the water which causes extra mixing through dispersion. This also explains the velocity dependence because dispersion is a flow rate dependent phenomenon.

C_s(%)	Salinity (%)	Q_{in} (nl/min)	E-Rate (m/s)	E-Rate (m3/s)	R^2
4	1.6	100	2.16E-06	1.08E-13	0.98
4	1.8	100	2.50E-06	1.25E-13	0.94
4	2	100	1.70E-06	8.5E-14	0.9
4	1.6	10	5.70E-07	2.85E-14	0.92
4	2	10	2.40E-07	1.2E-14	0.97
2	1.6	100	6.00E-07	3E-14	0.95
2	1.8	100	5.30E-07	2.65E-14	0.92
2	2	100	4.08E-07	2.04E-14	0.72
2	1.6	10	7.00E-07	3.5E-14	0.95
2	1.8	10	1.10E-07	5.5E-15	0.99
2	2	10	2.70E-07	1.35E-14	0.86
2	1.6	1	8.00E-08	4E-15	0.81
2	2	1	3.20E-08	1.6E-15	0.99
0.5	1.8	100	4.30E-07	2.15E-14	0.84
0.5	2	100	0	0	0
0.5	1.8	10	4.00E-08	2E-15	0.86
0.5	2	10	3.90E-08	1.95E-15	0.9
0.5	1.8	1	0	0	0
0.5	2	1	2.59E-09	1.29E-16	0.37

Table 7.1: Emulsification rates acquired from a linear fit of the microemulsion saturation as a function of position y (distance along the capillary) for the experiments which show steady state parallel flow.

7.6. UNCERTAINTY & EXPERIMENTAL ERROR

Finally a note should be made about the uncertainty in the emulsification rates. This stems from two sources:

1. The statistical uncertainty from the linear fit to the saturation measurements
2. The experimental error in the saturation measurements

Both have been quantified so that an idea of the accuracy of the emulsification rates can be given. The experimental error has been measured by performing a repeat experiment at 1 nl/min, 10 nl/min and 100 nl/min injection rate and measuring the standard deviation between the microemulsion saturations recorded. These errors were considered to be the experimental error for all T-junction experiments at the same injection rates. The plots for the error can be found in apendix E. The average experimental errors at 1 nl/min, 10 nl/min and 100 nl/min were respectively 35%, 23% and 5%. The statistical uncertainty in the linear fits quantified by the R^2 parameter in table 7.1. We can conclude from this that the experimental error grows with decreasing injection rate and that the linear fits are reasonably accurate approximations for the emulsification rates.

7.7. DISCUSSION

In this section the experimental results presented in this chapter will be discussed. The section will be divided into two parts: one about the fow regime at the t-junction and one about the downstream saturations. The effect of the surfactant concentration, flow rate and salinity on these results will be commented on.

7.7.1. FLOW REGIME

Two flow regimes are distinghuished in the t-junction experiments:

- Parallel Flow
- Alternating Flow (snap off of oil droplets at the t-junction)

The capillary number is a parameter which can ususally help explain the flow regimes of two liquid phases observed at a t-junction. Figure 7.12 shows the capilary number for the 27 experiments that were performed. What should be noticed is that the snap offs happen in a capillary number regime which occurs with all three surfactant systems (order 10^{-2}). The capillary number alone is therefore not sufficient to explain the snapping. The major difference between surfactant system-I (for which snap offs occur at low flow rates)

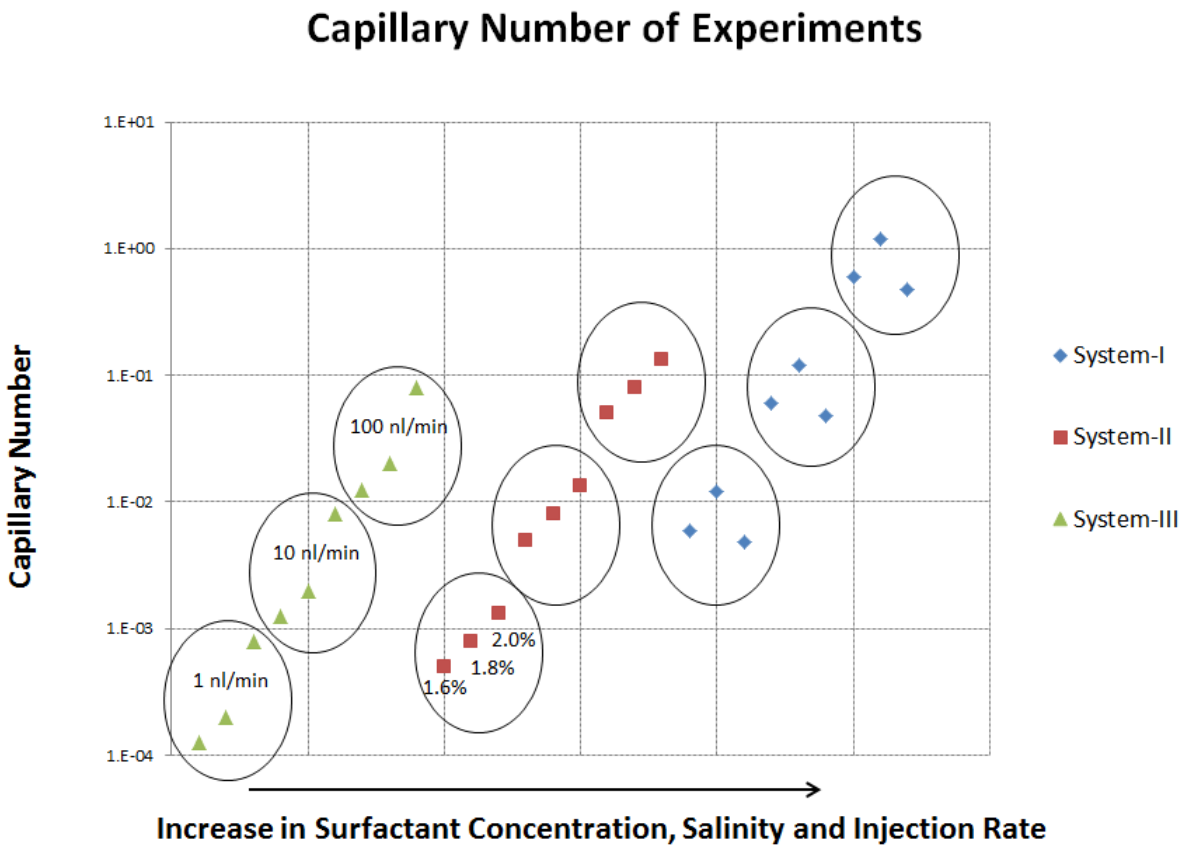

Figure 7.12: Capillary number for the t-junction experiments. The x-axis has no units but point in the direction of increase for all three variables from the experiments: surfactant concentration, injection rate and salinity

and the other two systems is the viscosity ratio. The continuous phase (surfactant solution) has a higher viscosity in those experiments and so it will exert a higher shear force on the oil phase, causing it to snap off [44]. Combining this with the effect of the emulsification which "eats" the oil this seems like a plausible explanation for the observed snapping of the oil phase.

Another phenomenon which is observed is the formation of microemulsion specks which are carried by the surfactant solution. This occurs in the low capillary number regime of figure 7.12 ($10^{-4} to 10^{-3}$). It can be explained by the relatively higher interfacial tensions that arise in the experiments with surfactant system 3. A low capillary number indicates a relatively higher importance of interfacial forces compared to viscous forces in the system. Combining this with the fact that only little emulsification can take place due to the limited amount of surfactants in the solution explains why only small specks of separate emulsion form instead of a continuous phase.

7.7.2. DOWNSTREAM SATURATIONS

The microemulsion saturation downstream of the t-junction was used to quantify the emulsification rate in the experiments. In case of laminar, parallel flow the emulsification rate is driven by diffusion of water, oil and surfactants across the interface. This causes microemulsion to form at the interface between the oil and the surfactant solution. In the case of high flow rates and low interfacial tension (high capillary number) the microemulsion forms a continuous phase at the interface. A low capillary number combined with low surfactant concentration causes the microemulsion to form as separate specks which flow downstream suspended in the surfactant solution. The emulsification rate shows square root of time dependence at low flow

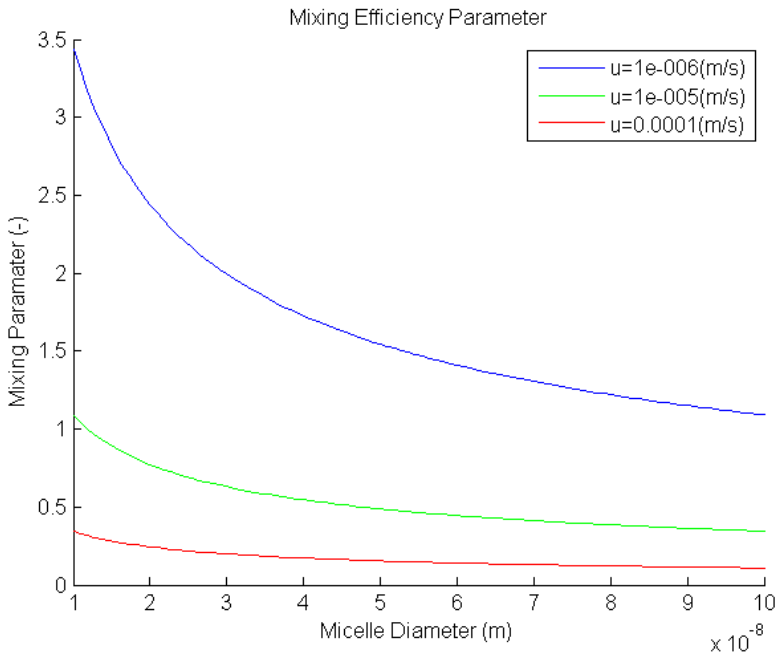

Figure 7.13: Mixing efficiency parameter θ_{mix} as a function of the "micelle diameter" if the mixing is approximated as the diffusion of oil in water micelles diffusing from the interface into the oil and the surfactant solution. The three flow rates correspond to the 100, 10 and 1 nl/min injection rates.

rates and linear time dependence at higher flow rates. This effect is more pronounced in the experiment with surfactant system-I. Because this system has a higher viscosity this is an indication that a dispersive mixing component also plays a role due to a velocity gradient perpendicular to the flow direction. The experiments that showed steady state parallel flow can be characterized by the mixing efficiency parameter which was discussed in chapter 2. A plot of this parameter for the three injection rates (1, 10 and 100 nl/min) as a function of the microemulsion droplet/micelle diameter (diffusion coefficient based on the stokes einstein equation) can be found in figure 7.13. It shows that as the diameter of the micelle increases (diffusion coefficient decreases) the mixing efficiency quickly decreases. The behavior of the curves as a function of the flow rate agree with the experimental results: full scale mixing is only achieved at low flow rates (in case there is an unlimited supply of surfactant, oil and water).

8

RESULTS: DEAD END PORES

The results of the microfluidic experiments with the dead end pore geometry will be discussed in this chapter. The porespace was initially saturated with n-decane. The aqueous phase was injected from the inlet side and mobilization of the oil trapped in dead end pores was studied. This was done by recording images of the experiment at regular time intervals. These images were then analysed using Leica Qwin.

First a reference case with water and oil will be discussed. This will be followed by an example of a typical result of an experiment with a surfactant system. A qualitative analysis of the images recorded from the example experiment will be given. Based on this qualitative analysis two mechanisms are investigated further. One of the mechanisms was quantified for each of the experiments with the surfactant systems. The resulting plots from these experiments will be discussed for each of the surfactant systems.

8.1. REFERENCE CASE: OIL & WATER

Figure 8.1 shows the experiment where DI water was injected into the n-decane saturated micromodel. Figure 8.1 a shows that the trapped n-decane phase while the water is flowing in the main channel. The n-decane at the pore throat is mobilized by the convection and replaced by brine. Figure 8.1 b shows the same pore after 12 hours. Thin water films can be seen behind the oil in the corners of the dead end. No further oil is mobilized.

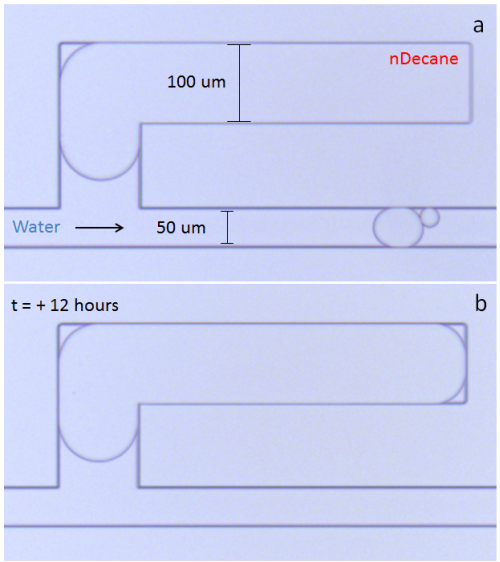

Figure 8.1: Water is injected into a micromodel which is saturated with n-decane from the left at 100 nl/min. a) after the injection has started, the oil is pushed out of the main channel by the water and some of the oil at the pore throat is mobilized due to the convection from the main channel. b) water seeps into the corners due to the water wetness of the micromodel, filling the space behind the oil in the corners.

8.2. QUALITATIVE ANALYSIS

Figure 8.2, 8.3 and 8.4 show three images which were recorded consecutively during an experiment over the period of an hour. Based on these images several physical mechanisms can be identified which may cause oil mobilization from dead end porespace. All figures show that there is brine in some of the corners of the pores. Because the model is water wet this is an indication of corner-and film flow around the oil. A second phenomenon that can be observed in figure 8.4 is that microemulsion forms in some of the corners of the dead end before the bulk has been emulsified. This indicates that surfactants are able to move around the bulk of the oil. From this qualitative analysis two transport/emulsification mechanisms are identified which will be further investigated:

- Marangoni Spreading of surfactants over the water film surrounding the oil
- Diffusive emulsification through the bulk of the oil

The (mirco)emulsion saturation in the dead end channel was measured using image analysis software. 9 experiments were performed with 3 different surfactant systems in total to investigate the effect of the surfactant concentration, the injection rate, the cosolvent concentration and the salinity.

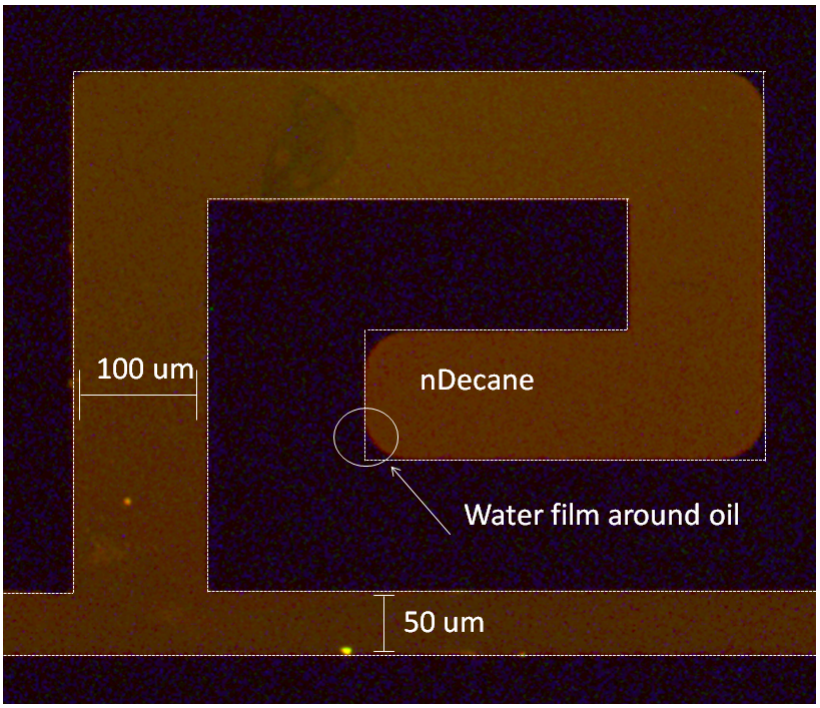

Figure 8.2: A dead end saturated with n-decane (green) before the experiment. The depth of the capillary is 40 microns. Some of the corners of the capillary show an interface which indicates that another phase which doesn't mix with n-decane fills the corners of the pores. This is probably water.

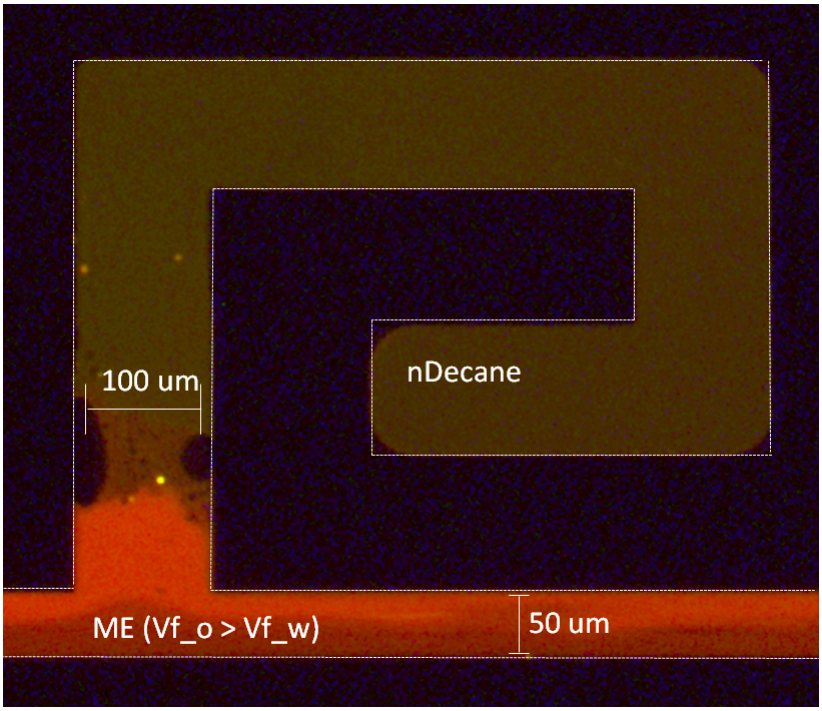

Figure 8.3: shortly after the injected surfactant solution (system-I, 2% NaCl) has arrived at the pore throat an emulsion begins to form. The low interfacial tension causes the interface between the oil and the surfactant solution to change and pockets of water form in the oil which coagulate and move to the walls due to the water wetness of the channel.

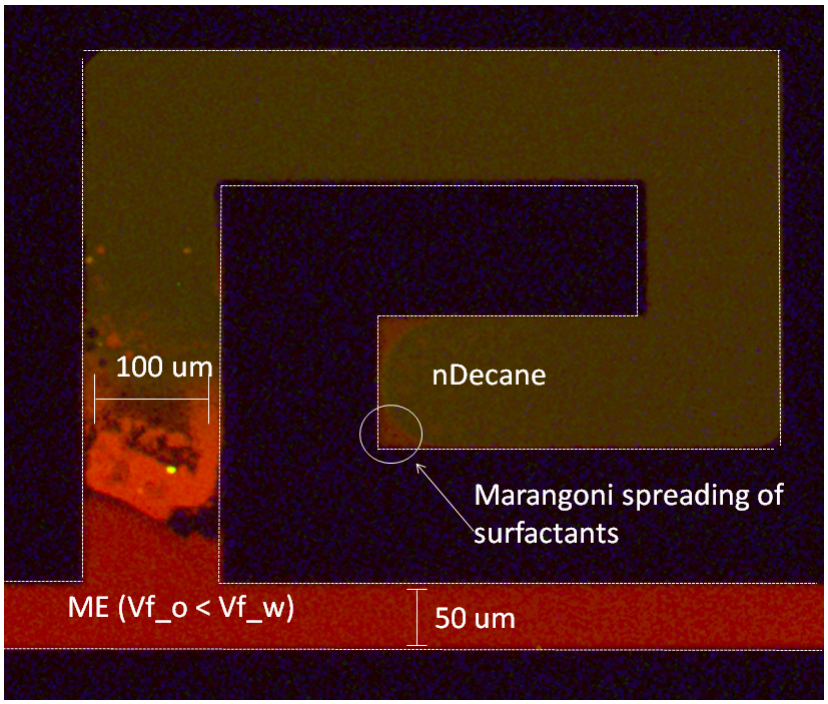

Figure 8.4: After a while the system reaches a state where (micro)emulsion flows in the main capillary and emulsion forms inside the dead end channel. There is a clear difference between the types of emulsion which is indicated by the difference in color emitted by the dye. There is a new "interface" between the two emulsion types (one static and one moving) which consists of water. Meanwhile emulsion droplets form in the oil and the emulsification front slowly moves into the pore. (Micro)emulsion has also started to form behind the oil in the corners where water was present. This confirms that there is an interconnected film around the oil phase. The surfactants move over this film through either diffusion or Marangoni spreading

Table 8.1: Overview of experiments conducted in the dead end pores . The emulsification rates are based on a linear fit of the experimental curves which doesn't.

Experiment #	C_s (%)	C_{SBA} (%)	Salinity (%)	Q_{in} (nl/min)	Rate (-/s)	Rate (m3/s)
1	4.00	5.00	1.60	100	6.00E-05	2.88E-16
2	4.00	5.00	2.00	100	3.00E-05	1.44E-16
3	4.00	5.00	1.60	1	2.00E-06	9.60E-18
4	4.00	5.00	2.00	1	1.00E-05	4.80E-17
5	0.50	5.00	1.80	1	1.00E-06	4.80E-18
6	0.50	5.00	2.20	1	8.00E-06	3.84E-17
7	0.50	0.50	2.20	100	7.00E-06	3.36E-17
8	0.50	0.50	1.80	1	8.00E-06	3.84E-17
9	5.00	0.50	2.20	1	1.00E-05	4.80E-17

8.3. SYSTEM-I AND N-DECANE

The images recorded from the experiments with system I can be seen in figure 8.5. They give a qualitative impression of the emulsification process that took place for each of the experiments. The corresponding plots of the microemulsion saturation evolution with time can be found in figure 8.6. The following observations were made:

- The systems form a third phase orange (micro)emulsion in all experiments.
- The emulsion flowing in the main channel generally has a darker color than the emulsion forming in the dead end. This could indicate that the (micro)emulsion that forms in the dead end has a higher oil solubilization than the emulsion/surfactant system flowing in the main capillary which makes sense intuitively. However, we can't conclude this for certain since the color calibration was inconclusive.
- In case there is a water film around the oil initially, surfactants are transported around the oil through this film and cause emulsification in the corners (experiment 2)
- The emulsification shows square root of time dependence
- An increase in the injection rate and consequently the flow rate at the pore throat causes an increase in the emulsification rate for system I
- The small changes in salinity studied have limited influence on the emulsification rate

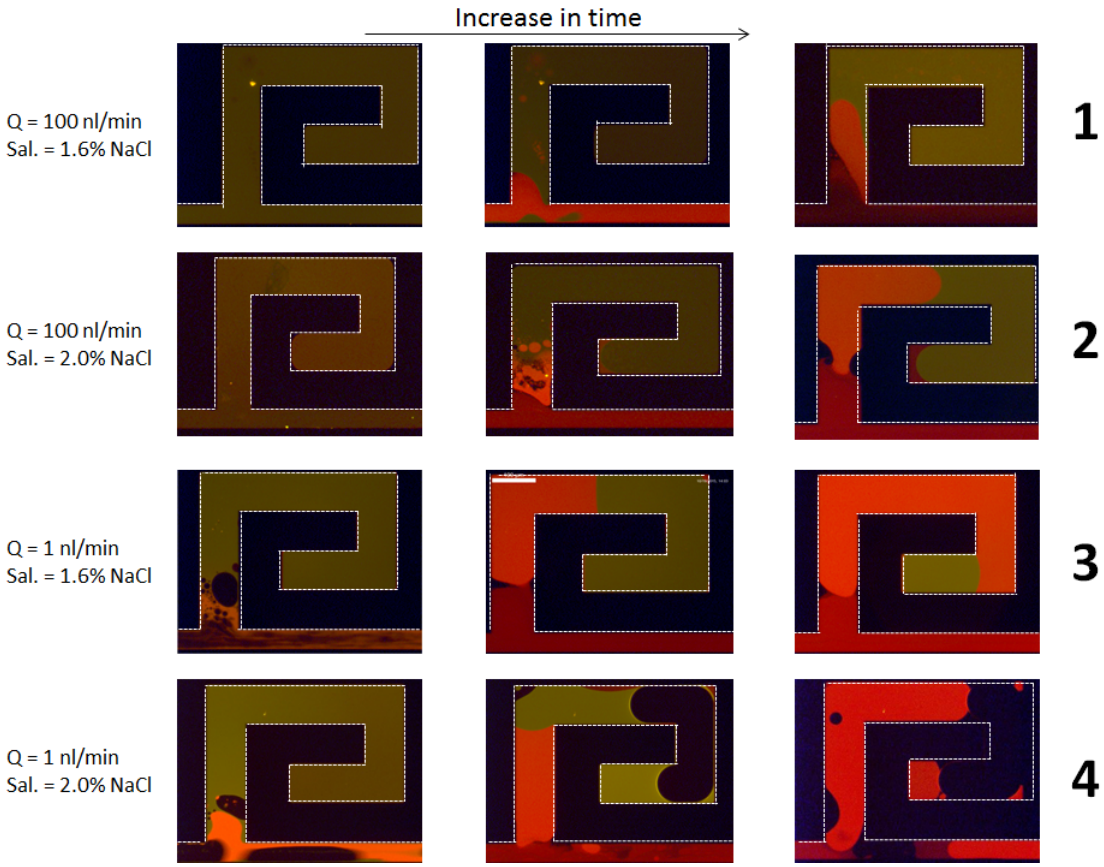

Figure 8.5: Images recorded from the dead end pore experiments with surfactant system I. For each experiment three images were selected which qualitatively show how the emulsification process evolved with time. **The time steps are arbitrary and can't be used to make a comparison between the different experiments quantitatively.**

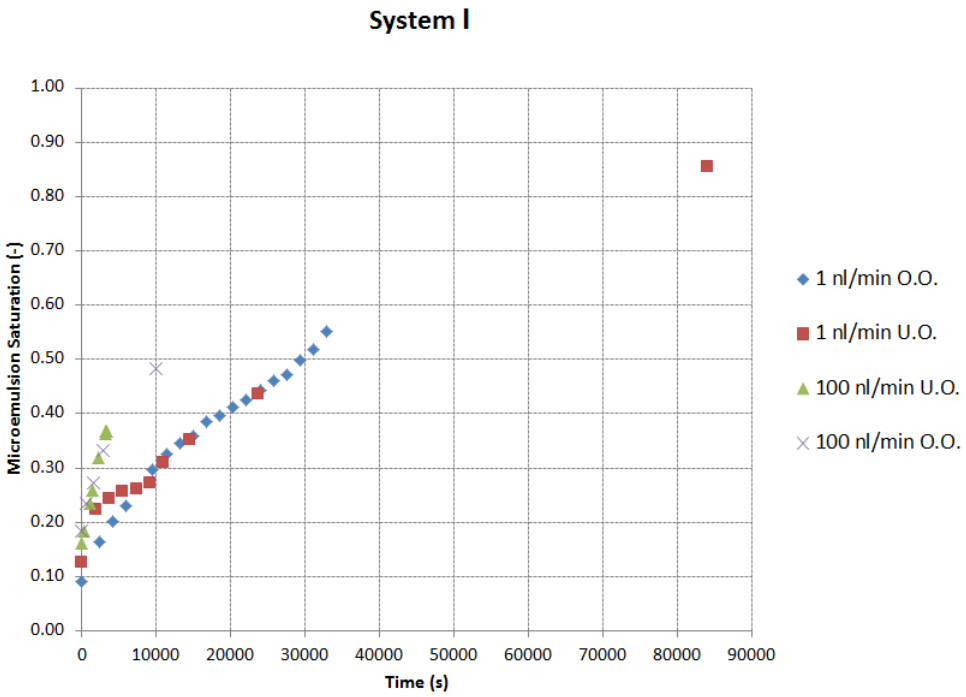

Figure 8.6: Microemulsion saturation evolution with time for the experiments conducted with surfactant system I.

8.4. SYSTEM-III AND N-DECANE

The results of the experiment with system-III can be found in figures 8.7 and 8.8. The following observations were made:

- The system forms a third phase orange (micro)emulsion in both experiments
- The (micro)emulsion forms looks similar to the (micro)emulsion that forms with system I
- (Micro)emulsion forms in the corners behind the oil in experiment 5
- (Micro)emulsion forms in the bulk of the oil away from the interface in experiment 5. This indicates such a strong
- The emulsification shows square root of time dependence
- The small change in salinity had a significant impact on the emulsification rate
- The emulsification rate for experiment 6 is similar to the emulsification rate of experiments 3 and 4 (surfactant system I)

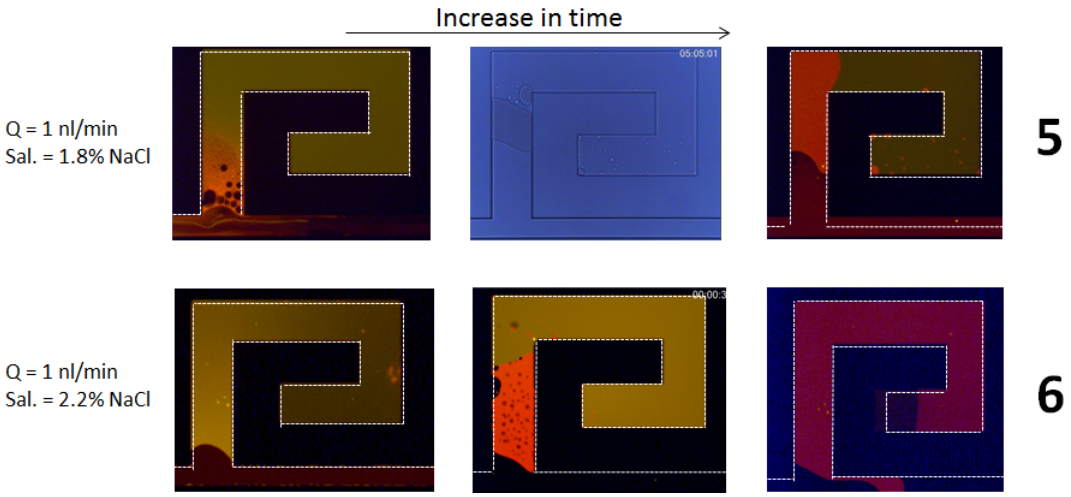

Figure 8.7: Images recorded from the dead end pore experiments with surfactant system II. For each experiment three images were selected which qualitatively show how the emulsification process evolved with time. **The time steps are arbitrary and can't be used to make a comparison between the different experiments quantitatively.**

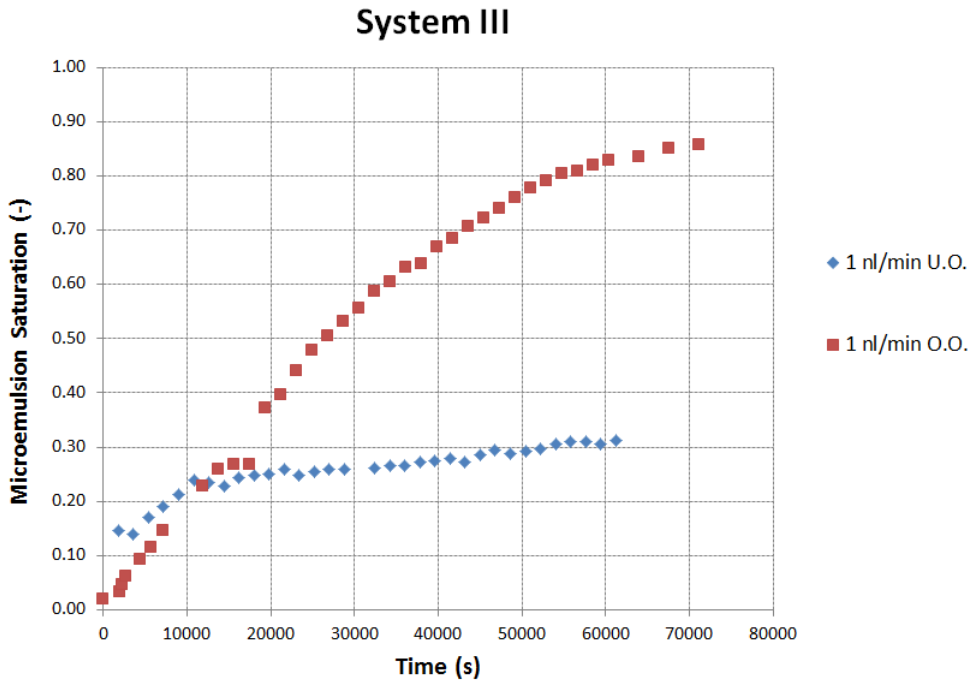

Figure 8.8: Microemulsion saturation evolution with time for the experiments conducted with surfactant system III.

8.5. SYSTEM-IV AND N-DECANE

The results of the experiment with system-III can be found in figures 8.9 and 8.10. The following observations were made:

- The system causes large pockets of water to form in the pore in experiment 8. No clear emulsification took place.
- The system forms orange (micro)emulsion in experiments 7 and 9.
- The (micro)emulsion that forms is different from the third phase (micro)emulsion which forms in the experiments with systems I and III. It is not clearly a separate phase (except in the last image of experiment 7) and shows a color gradient which indicates a chemical gradient in the emulsion.
- In case there is a water film around the oil initially, surfactants are transported around the oil through this film and cause emulsification in some of the corners (experiment 7).
- The emulsification shows square root of time dependence
- An increase in the injection rate and consequently the flow rate at the pore throat caused a small decrease in the emulsification rate at the pore throat for system IV.

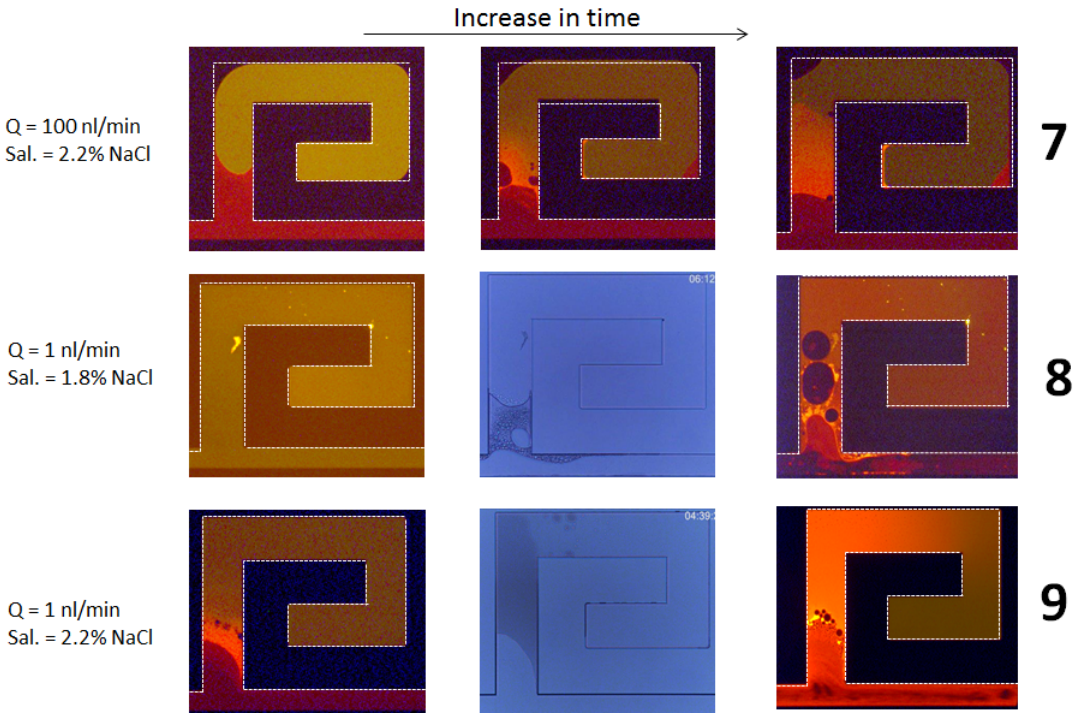

Figure 8.9: Images recorded from the dead end pore experiments with surfactant system IV. For each experiment three images were selected which qualitatively show how the emulsification process evolved with time. **The time steps are arbitrary and can't be used to make a comparison between the different experiments quantitatively.**

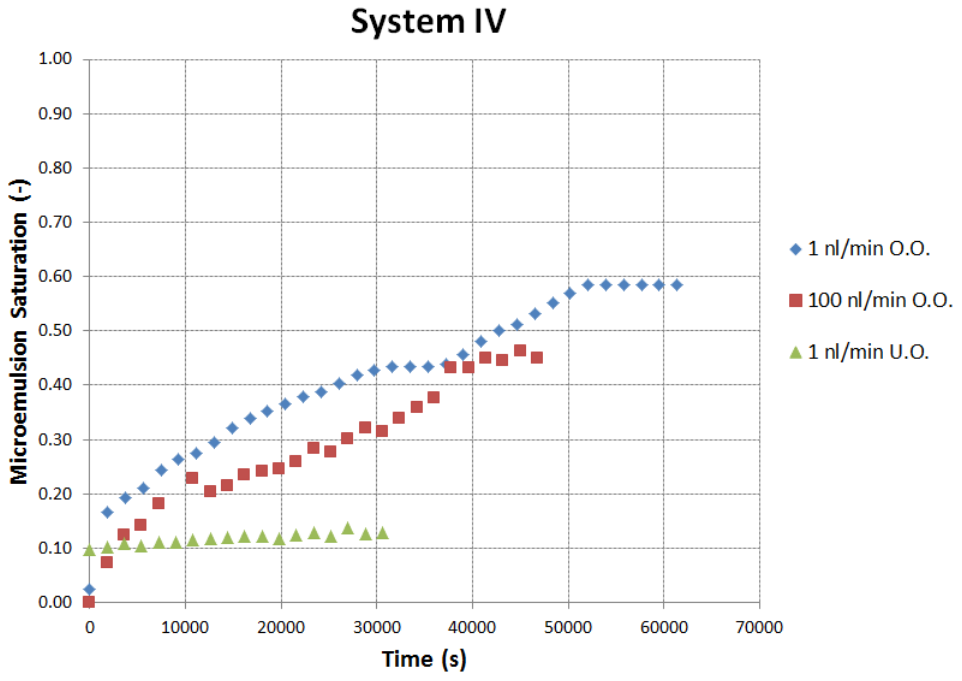

Figure 8.10: Microemulsion saturation evolution with time for the experiments conducted with surfactant system IV.

8.6. MARANGONI SPREADING

Figure 8.11 shows that emulsion forms in the corners behind the oil in case they are filled with water initially. A proposed mechanism for this emulsification is Marangoni spreading over the water film. To test this suggestion the time between first contact of the oil and the surfactant solution at the inlet of the pore and the first

observation of emulsification behind the oil was measured. After 720 seconds no observation of emulsification behind the oil in the corners was made. After 1020 seconds the interface between the oil and the water in the bottom right corner changed shape and the water started emitting a dark reddish light, indicating that oil has solubilized in the water and consequently the presence of surfactants. The process doesn't continue

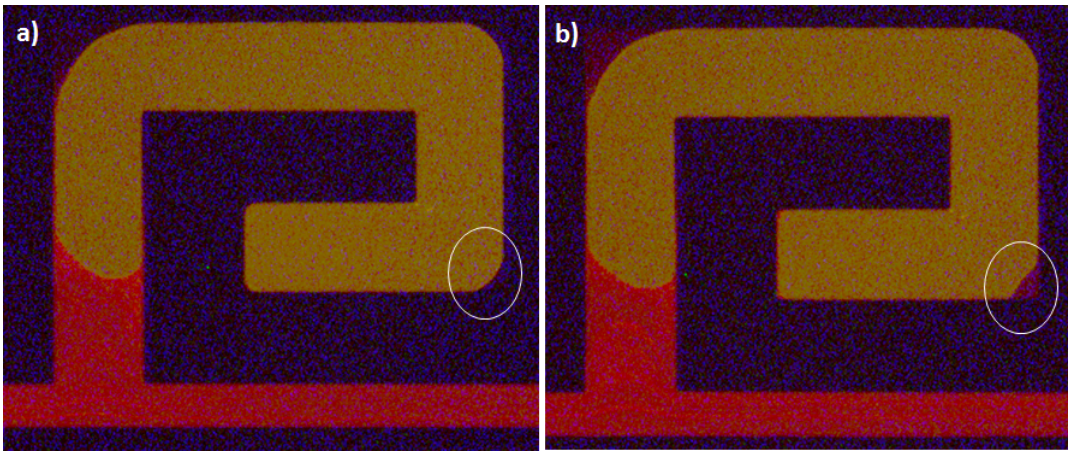

Figure 8.11: a) dead end pore experiment with system I (1.6% NaCl) 720 seconds after first contact between surfactant system and oil at pore throat. b) same experiment after 1020 seconds.

with time but stops after certain equilibrium has been attained. It is therefore a secondary mechanism in the recovery of oil from dead ends.

8.7. DISCUSSION

From the experiments we can conclude that the main emulsification mechanisms in the dead end pores is driven by diffusion. It is likely the emulsification process that is observed is spontaneous emulsification [31] [32] [33] which was introduced in the background of this report. The convective forces from the flow in the main channel only affect a small portion of the oil at the pore throat. The injection rate then serves as a boundary condition for the supply of water and surfactants to the system and the mobilization of oil out of the pore in the bottom right corner of the pore throat in the form of (micro)emulsion. Diffusion of water and surfactants into the oil is driven by a water/surfactant concentration gradient while oil diffuses into the opposite direction driven by an opposite concentration gradient. This gradient is best observed in the experiments with surfactant system IV. When this diffusive process leads to the formation of a region of supersaturation, a third phase microemulsion forms. The rate of this emulsification process is influenced by the boundary condition (supply of water and surfactant) and by the salinity and cosolvent concentration. A secondary emulsification mechanism takes place if the oil is initially surrounded by a water film (which may be the case after a water flood). It was observed that surfactants are transported over this film causing emulsification to take place in the back of the pore as well. This process does not continue with time but stops after an equilibrium has been reached. The influence of the surfactant formulations on this process was not studied.

8.7.1. SURFACTANT CONCENTRATION

Based on the results from the experiments it seems like the surfactant concentration has an influence on the emulsification rate. Diffusion is a chemical concentration gradient process and so it would make sense if an increase in emulsification rate was observed with an increase in surfactant concentration. This is observed when we compare experiment 1 and 2 to experiment 3. However, experiment 1 and 2 have a similar emulsification rate as experiment 4. The reason for this is that the surfactant concentration is not the only factor that influences the emulsification rate. The supply of water and surfactant at the boundary needs to keep up with diffusion of water and surfactant into the emulsion and the oil diffusing out of the pore needs to be carried off fast enough to keep the concentration gradient intact (which drives the emulsification).

8.7.2. INJECTION RATE

The results from the experiments with surfactant system I show that an increase in the flow rate does increase the emulsification rate. Because experiment 3 and 4 were not maintained long enough it is unclear whether this higher emulsification rate is sustained for longer times. Experiments 7 and 9 do not show an effect of the injection rate on the emulsification rate. The difference can possibly be explained by the surfactant concentration; a higher surfactant concentration can only maintain a higher emulsification rate as long as the supply of surfactant is sufficient. Because at 0.5% surfactant concentration the supply of surfactants is not high enough to increase the emulsification rate anyway, the flow rate (and consequently the supply of surfactants) will not have a an effect on the emulsification rate.

8.7.3. SALINITY

The effect of salinity on the emulsification rate was not felt in system I. A possible explanation for this is the high surfactant and cosolvent concentration in this system. Their effect dominates the emulsification process which causes the effects of the (small) salinity differences to be negligible. An effect of salinity on the emulsification rate is observed in the experiments with system III. Experiment 5 (under optimum salinity) shows a slower emulsification rate than experiment 6. This make sense because the emulsion forms in the oil, which is generally something one would expect from surfactant systems at over optimum salinity. However, no difference in either the color of the (micro)emulsion that forms or between the intefaces. These variations are expected based on phase behavior tests (differen volume fractions of oil and water) but were not observed. An effect of the salinity is also witnessed in the experiments conducted with system IV. Experiment 8 (under optimum salinity) doesn't form an emulsion in the same way as is observed in the other experiments. The emulsification is also slower.

8.7.4. COSOLVENT CONCENTRATION

The effect of the cosolvent concentration on the emulsification rate can be observed when comparing the experiments conducted with system III to the experiments conducted with system IV. Two observations can be made:

- a clear third phase (micro)emulsion doesn't form
- the emulsification rate is slower with lower cosolvent concentrations

These results are in agreement with what we know from phase behavior tests. Cosolvent increases the packing of the microemulsion, making it more pronounced separate phase. Microemulsions in phase behavior tests also form much quicker at high cosolvent concentrations.

9

MODELING

9.1. T-JUNCTION

This part of the study assesses the feasibility of modeling the observed phenomena at the t-junction using Comsol 5.0. Comsol Multiphysics is a finite-element solver (FEM) which can model coupled physical phenomena (multiphysics). It allows the user to couple the partial differential equations (PDE's) for different physical phenomena after which the system of PDE's is solved using the finite element method. The laminar two-phase flow module (phase field method) was used to solve a momentum transport and continuity equation. A two dimensional model of the t-junction was used to simulate the co-injection of an aqueous and oil phase. This module couples the convection-diffusion equation to the Cahn-Hilliard equation for phase separation. Because it is not straightforward to include in situ formation of a third phase in Comsol this was not attempted. However, ultralow interfacial tension and its effects on the flow regime at the t-junction could be studied. A 2-dimensional T-Junction geometry was used for the simulations. The setting for the model can be found in table 9.1.

Table 9.1: Settings used in the T-Junctions simulation

Parameter	**Symbol**	**System-I**	**System-II**	**System-III**
Contact Angle	Theta	5	5	5
Oil Density	ρ_o	720 kg/m^3	720 kg/m^3	720 kg/m^3
Surfactant Solution Density	ρ_s	1000 kg/m^3	720 kg/m^3	720 kg/m^3
Oil Viscosity	μ_o	0.85 mPa.s	0.85 mPa.s	0.85 mPa.s
Surfactant Solution Density	μ_s	6 mPa.s	1 mPa.s	1 mPa.s

9.1.1. REFERENCE CASE: OIL & WATER

The reference case experiment with oil and water was reproduced in Comsol. The result can be observed in figure 9.1. It shows that the high IFT prohibits the two phases from flowing together in the downstream capillary as expected.

9.1.2. SYSTEM-I

The results for the simulations with surfactant system-I can be found in figure 9.2. The flow regime at the T-Junction can be observed at 1, 10 and 100 nl/min injection rates ($Q_s = Q_o$) for three different salinities (1.6% NaCl, 1.8% NaCl and 2.0% NaCl).

The main observations are listed below:

- no snap offs are witnessed at the low flow rates
- a fluctuating interface between the oil and the surfactant system is observed at low flow rates
- the fluctuations seem to increase with a decrease in flow rate

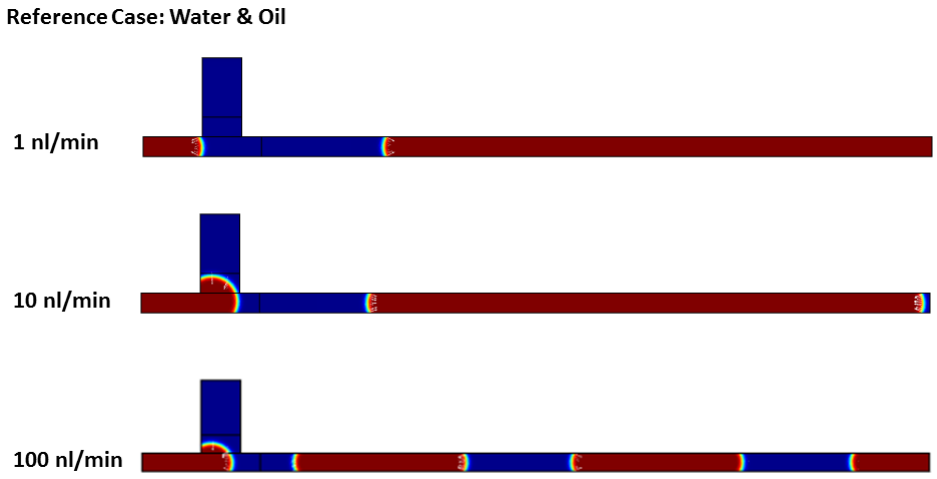

Figure 9.1: Flow regime at the T-Junction for reference case with oil and water. The water is represented by the blue phase and the oil by the red phase. The volumetric flow rates Qo and Qs were varied between 1, 10 and 100 nl/min. Qo=Qw for all experiments.

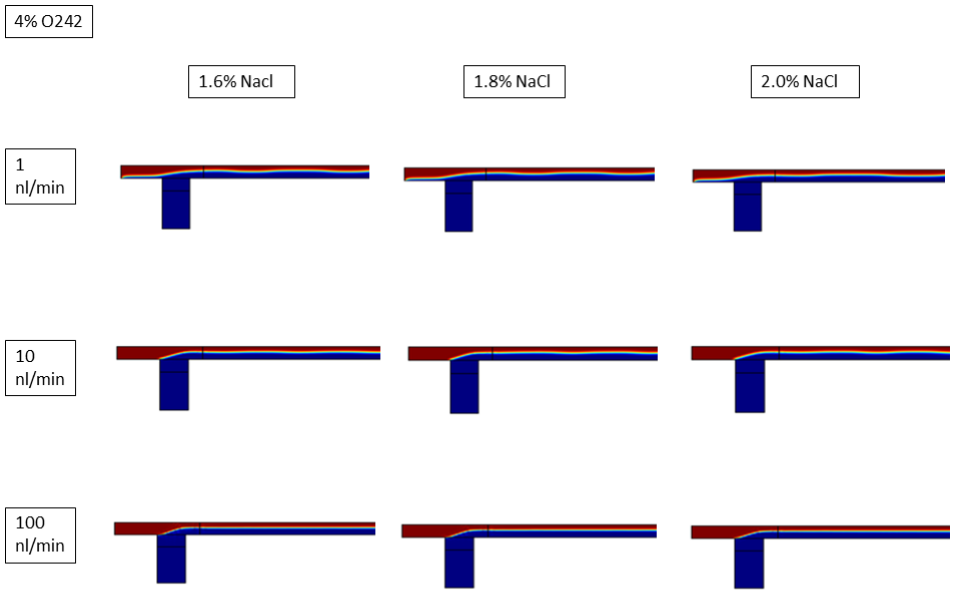

Figure 9.2: Flow regime at the T-Junction for the 4% surfactant concentration solution. The surfactant solution is represented by the blue phase and the oil by the red phase. The volumetric flow rates Qo and Qs were varied between 1, 10 and 100 nl/min. Qo=Qs for all experiments. The effect of the salinity is only reflected by a varying interfacial tension between the two phases.

To check whether injection rate instabilities could be a cause for the "snap-off" effect at low flow rates (1 nl/min) the ratio of Q_s/Q_o was varied. At ultralow interfacial tensions (order of magnitude of 10^{-6} N/m) the first snapping was witnessed at $Q_s/Q_o = 4$. Increasing the interfacial tension decreases the necessary flow rate difference to achieve snapping. An example can be found in figure 9.3. Because the snapping regime can occur with small variation in injection rate, this can be an explanation for incidental snapping. Another explanation for the snap-offs observed in the experiments is the fluctuating interface combined with the formation of the microemulsion. The fluctuations increase the surface area of the interface increasing emulsification. They also make the oil fraction in the capillary thinner locally which might cause snapping off of the phase.

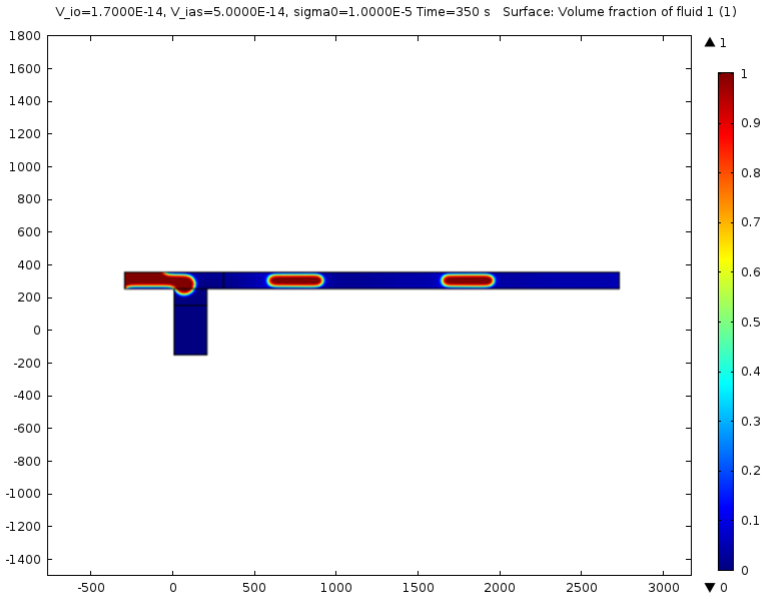

Figure 9.3: Snap off flow regime witnessed at $Q_s/Q_o = 3$ for an interfacial tension of 10^{-5}.

9.1.3. SYSTEM-II

The results for the simulations with surfactant system-II can be found in figure 9.4. The flow regime at the T-Junction can be observed at 1, 10 and 100 nl/min injection rates ($Q_s = Q_o$) for three different salinities (1.6% NaCl, 1.8% NaCl and 2.0% NaCl).

For the simulation with surfactant system-II parallel flow is observed for all flow rates and salinities which matches the results from the experiments.

9.1.4. SYSTEM-III

The results for the simulations with the 0.5% surfactant concentration solution can be found in figure 9.5. The flow regime at the T-Junction can be observed at 1, 10 and 100 nl/min injection rates ($Q_s = Q_o$) for three different salinities (1.6% NaCl, 1.8% NaCl and 2.0% NaCl).

For the experiments with surfactant system-III parallel flow is observed for all flow rates and salinities which matches the results from the experiments.

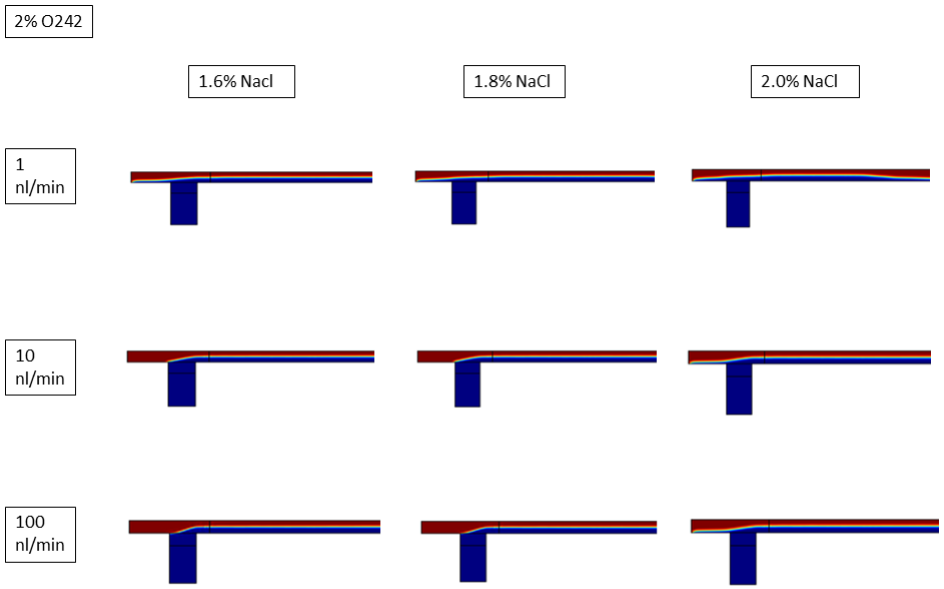

Figure 9.4: Flow regime at the T-Junction for the 2% surfactant concentration solution. The surfactant solution is represented by the blue phase and the oil by the red phase. The volumetric flow rates Qo and Qs were varied between 1, 10 and 100 nl/min. Qo=Qs for all experiments. The effect of the salinity is only reflected by a varying interfacial tension between the two phases.

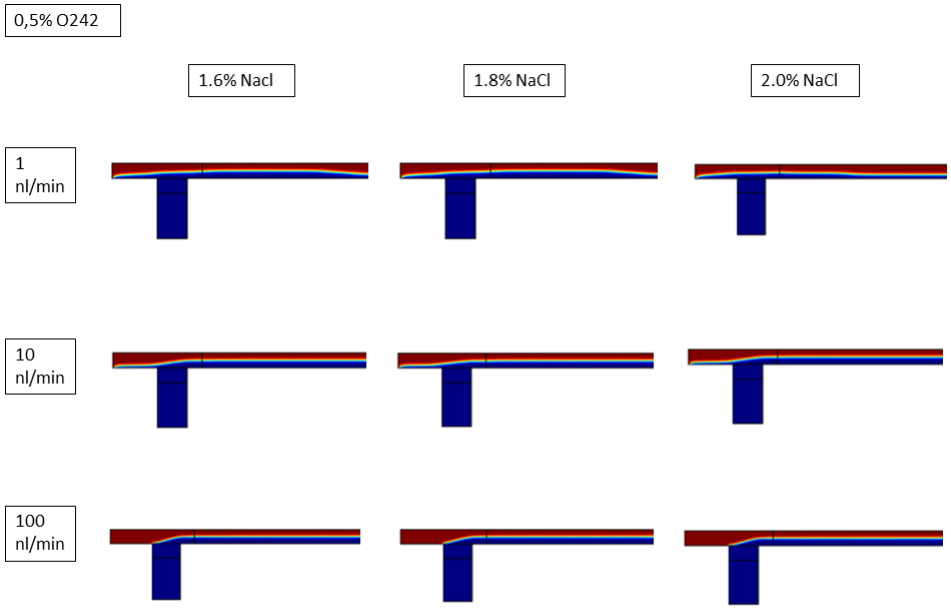

Figure 9.5: Flow regime at the T-Junction for the 05% surfactant concentration solution. The surfactant solution is represented by the blue phase and the oil by the red phase. The volumetric flow rates Qo and Qs were varied between 1, 10 and 100 nl/min. Qo=Qs for all experiments. The effect of the salinity is only reflected by a varying interfacial tension between the two phases.

9.2. DOWNSTREAM SATURATIONS

In this section the results of the modeling work for the downstream saturations is discussed. The objective is to check whether the microemulsion forms as expected from the phase behavior tests. The model and the assumptions will first be described followed by the results.

9.2.1. MODEL DESCRIPTION

A figure of the model and the derivation for the equations used can be found in appenix A. A steady state situation is assumed downstream of the t-junction as the two phases flow downstream. Microemulsion starts to form as soon as the surfactant solution and the oil come into contact. Emulsification of the two phases at the interface takes place at the linear rates which were observed in the experiments. The volumes of oil and water and the amount of surfactant are tracked as (micro)emulsion forms. The ratio of microemulsion volume vs. surfactant amount, water volume and oil volume is based on the phase behavior tests. Only system I and system II were modeled at 10 and 100 nl/min injection rates because these were the only systems which showed steady state emulsification of microemulsion at the interface. An overview of the model and its derivation can be found in appendix A.

9.2.2. SYSTEM I

The modeled results for surfactant system-I are shown in figure 9.6 and 9.7. The experimental values have been plotted as dots and the model results are plotted as lines.

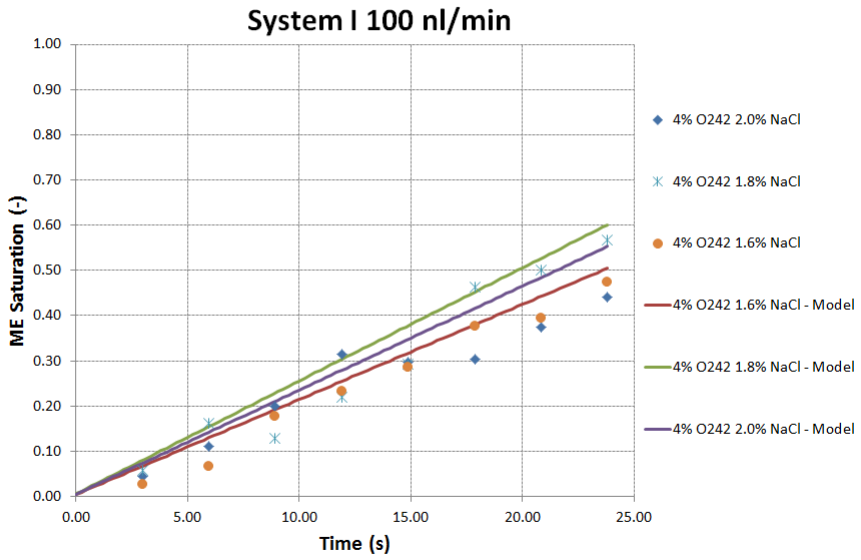

Figure 9.6

9.2.3. SYSTEM II

The modeled results for surfactant system-II are shown in figure 9.8 and 9.9. The experimental values have been plotted as dots and the model results are plotted as lines.

9.2.4. DISCUSSION

Since the model uses the experimental values for the emulsification rate they are a fit to the experimental values. The result that is of most interest is that the surfactant concentration runs out sooner in the model than observed in the experiments. This is best observed in figure 9.9. The solubilization ratios of oil, water and surfactant in the microemulsion from the phase behavior tests is used to calculate how much surfacant has

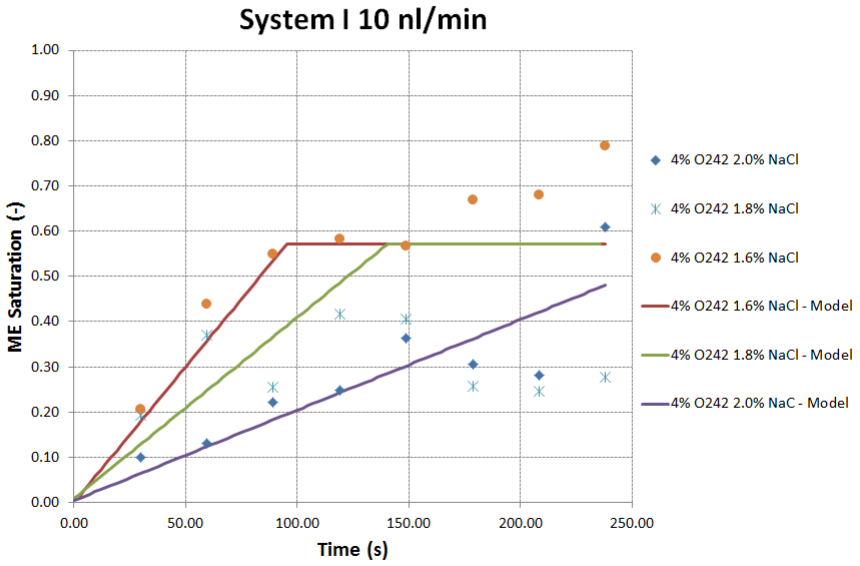

Figure 9.7

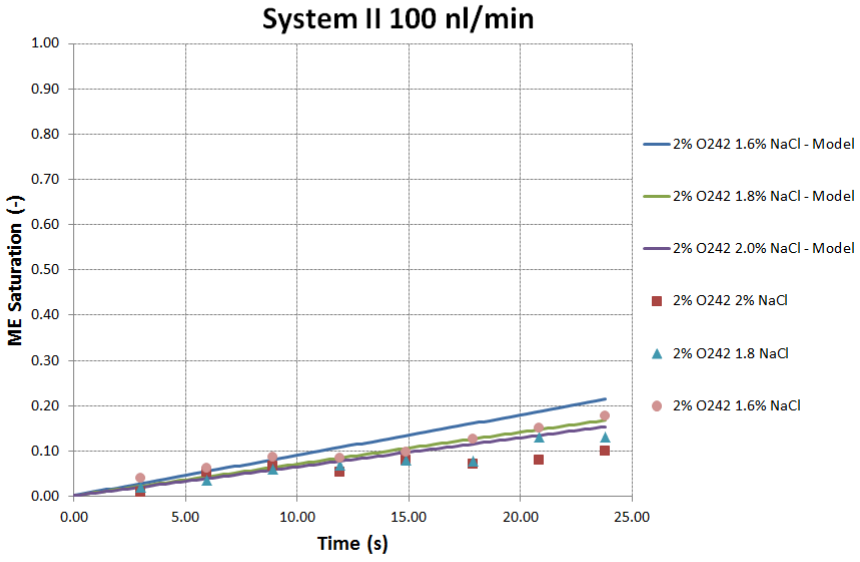

Figure 9.8

been solubilized. What can be seen is that the model runs out of surfactants much earlier than observed in the experiments. This is an indication that the microemulsion that forms under flowing conditions is different from the microemulsion in the test tubes. It forms larger volumes with the same amount of surfactants.

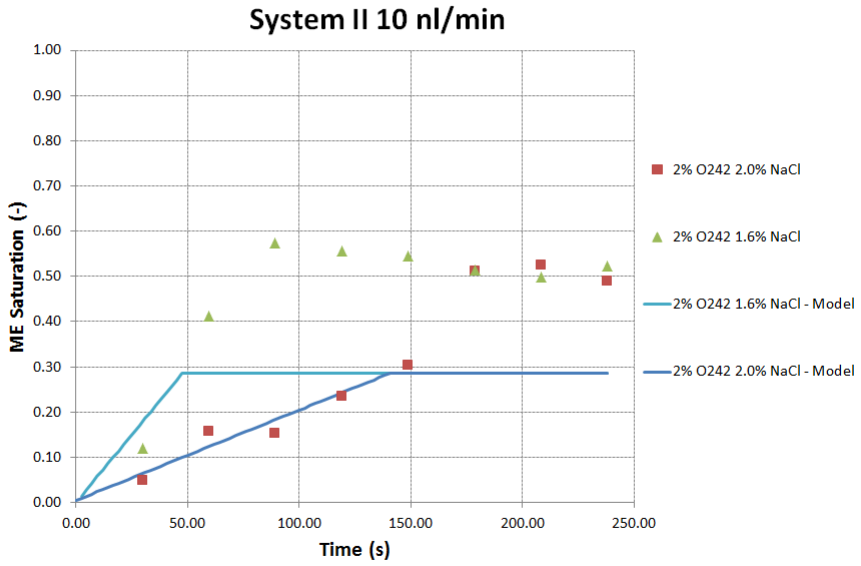

Figure 9.9

9.3. DEAD END PORES

In this section a model for the dead end pore geometry will be explored. From the experimental results we know the emulsification in the dead end pores shows square root of time dependence. This suggests tha diffusion is the main driver for the emulsification in the dead end pores. However, sometimes the formation of a separate third phase is clearly observed in the dead ends (figure8.5) and sometimes this isn't the case (figure 8.9, specifically at low cosolvent concentrations).

The distribution of a diluted species in space by means of diffusion is understood. However, when a third phase (microemulsion) forms another mechanism play a role. Spontaneous emulsification (which was propsed by Ruschak and Miller in 1972 [33]) is a possible mechanism by which the oil in the pores is emulsified. Diffusion creates local regions of supersaturation near the interface after which spontaneous emulsification occurs. The interface between the newly formed emulsion and the receding phase displaces itself with a square root of time dependence. If local super saturation doesn't occur the formation of a third phase does not happen. Instead, regular diffusion causes the water and surfactants to spread through the dead end pores.

9.3.1. 1D DIFFUSION OF MICELLES

The diffusion of water and surfactants into the oil causes a water in oil emulsion to form. This was modeled in 1 dimension using the analytical solution to Fick's second law (equation 2.10). The following assumptions were made:

- the effect of the corners in the dead end channel is assumed to be negligible (the channel is approximated as a straight channel)
- the surfactant solution flows through the main channel and deposits surfactants at the inlet of the dead end
- the surfactants form water in oil micelles at interface between the surfactant solution and the oil
- the micelles diffuse into the oil according to Fick's second law with a Diffusion coefficient given by the Einstein-Stokes relation

Table 9.2: Modeled systems with fitting parameter K and diffiusion coefficient D.

Experiment #	C_s **(%)**	C_{SBA} **(%)**	**Salinity (%)**	Q_{in} **(nl/min)**	**K (-)**	**D** (m^2/s)
1	4.00	5.00	1.60	100	10.00	1.284E-11
2	4.00	5.00	2.00	100	8.00	1.284E-11
3	4.00	5.00	1.60	1	3.00	1.284E-11
4	4.00	5.00	2.00	1	5.50	1.284E-11
5	0.50	5.00	1.80	1	3.50	1.284E-11
6	0.50	5.00	2.20	1	0.30	1.284E-11
7	0.50	0.50	2.20	100	-	1.284E-11
8	0.50	0.50	1.80	1	4.90	1.284E-11
9	5.00	0.50	2.20	1	5.00	1.284E-11

- no third phase microemulsion forms - the water is distributed through the channel according to the analytical solution of Fick's second law forming one continuous phase with the oil

Two plots of the time evolution of the water concentration distribution in the dead end channel can be seen in figure 9.10. The first plot shows the concentration distribution for spherical micelles with a radius of 200 nm. The second plot shows the concentration distribution for micelles with a radius of 20 nm. Figure 9.11 shows how the 20% water concentration front penetrates into the pore with time. From the plot we can see that the curves closely resemble the curve that was experimentally determined for system-III at 2.2% NaCl concentration. Assuming that the front that was tracked in the image analysis corresponds to a 20% water concentration the plot suggests that the micelles have a 30 nm radius. This is a realistic size.

9.3.2. SPONTANEOUS EMULSIFICATION

In the experiments where a third phase was clearly formed the mechanism proposed by Ruschak and Miller can be used to describe the movement of the interface between the microemulsion and the oil into the dead end channel. The position of the interface as a function of time is given by equation 2.15. The constant K has been used to fit the modeled curves to the curves which were acquired experimentally. The diffusion coefficient is determined by the Einstein-Stokes relation assuming the diffusion of spherical micelles with a radius of 20 nm (which is in the order of magnitude of the estimated pocket sizes of a bicontinuous microemulsion structure). The resulting plots can be found in figures 9.12, 9.13 and 9.14. The value for K increased with surfactant concentration, cosolvent concentration and injection rate. The fits show a good match with the experimental results.

9.3.3. MARANGONI SPREADING

The order of magnitude of the rate of Marangoni spreading across the brine film in the dead end channels has been calculated using equation 2.13. The results for two different film thicknesses can be found in figure 9.15. What can be observed is that the surfactant concentration across the film reaches an equilibrium after very short times (60 seconds). Consumption of the surfactants by emulsification along the way and in the back of the pore has not been taken into account. If we compare the results from this analytical model to the observations in the experiments (where emulsification in the back of the pore is first observed after 1000 s) we can conclude that there are more mechanisms that play a role. Emulsification along the way is probably consuming surfactants. Also, it might take some time before surfactants start emulsifiying the oil and actually become visible in the experiments.

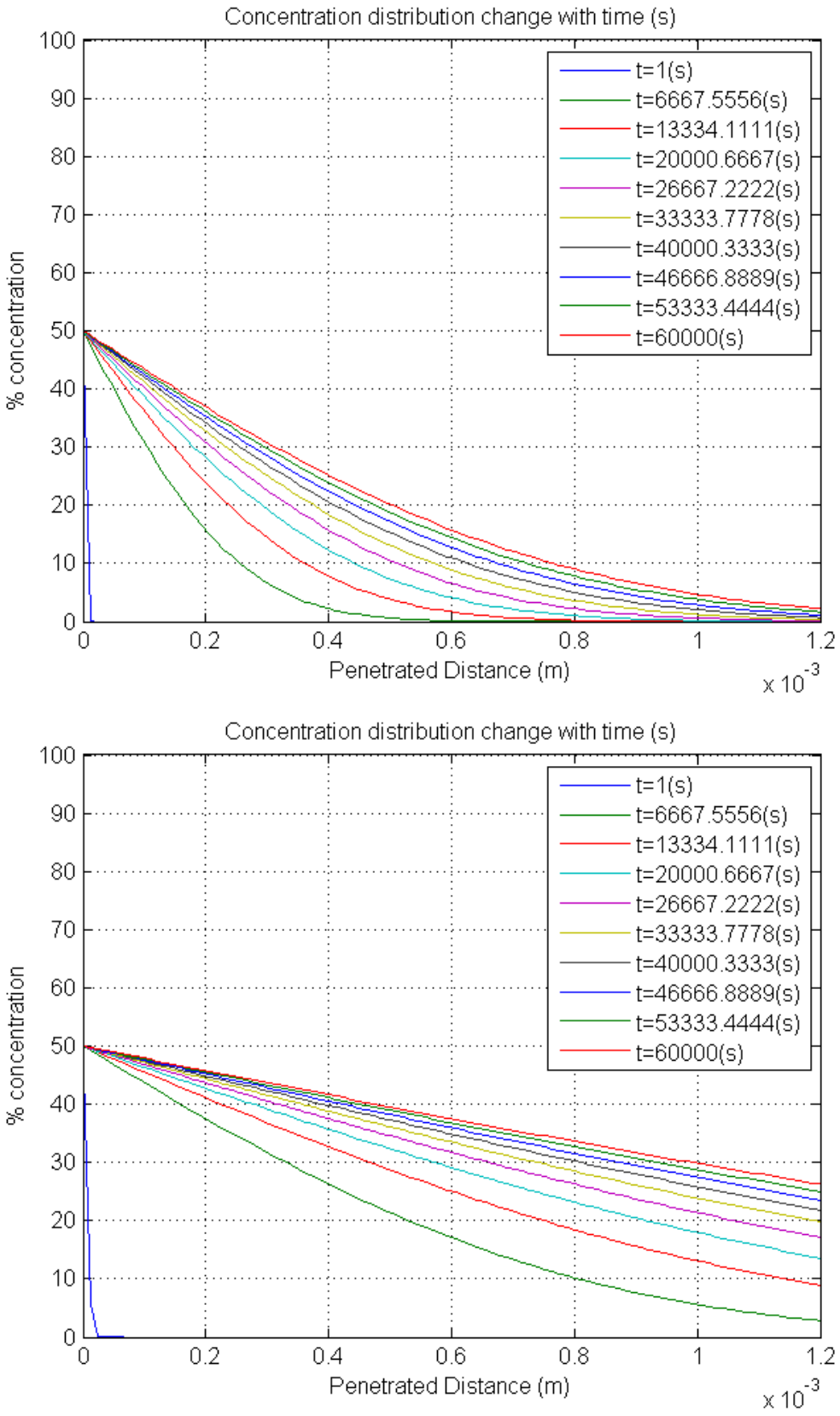

Figure 9.10: Top: water concentration distribution in the dead end pore as a function of time for micelles with a diameter of 200 nm. Bottom: water concentration distribution in the dead end pore as a function of time for micelles with a diameter of 20 nm.

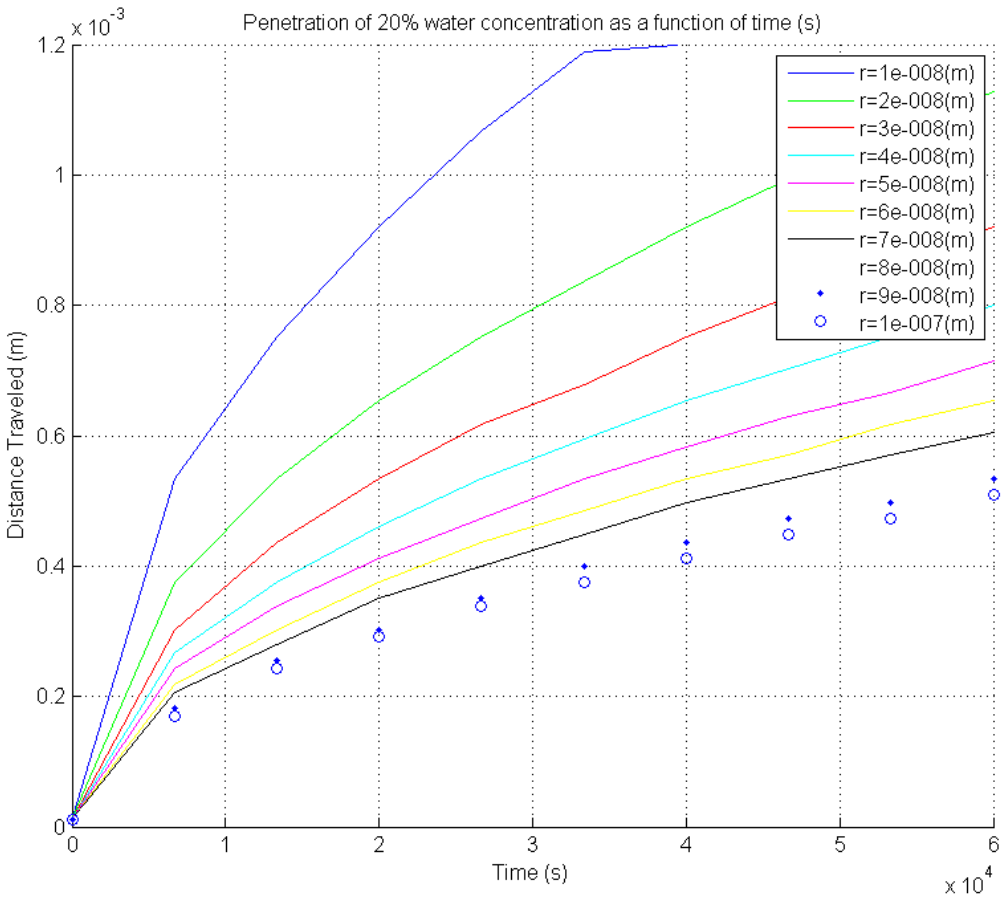

Figure 9.11: Penetration into the dead end pore of the 20% water concentration "front" as a function of time for 10 different micelle radii.

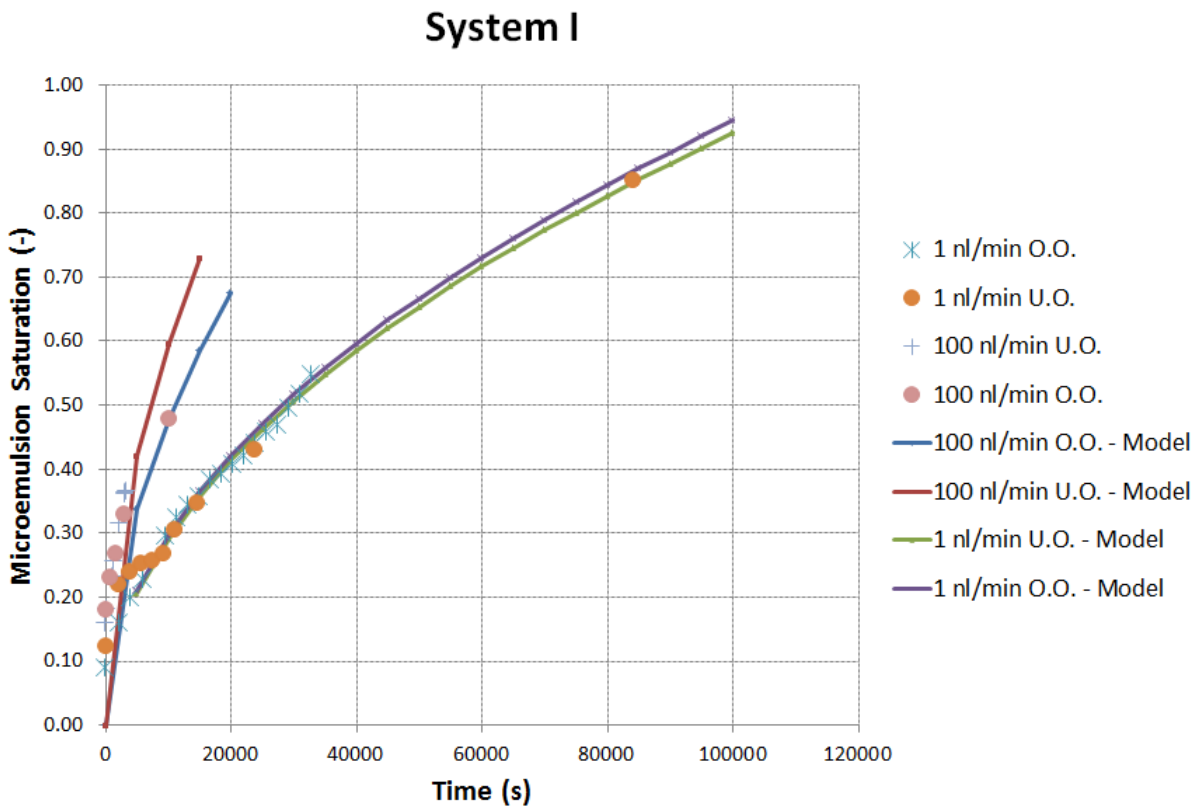

Figure 9.12: Penetration into the dead end pore of the 20% water concentration "front" as a function of time for 10 different micelle radii.

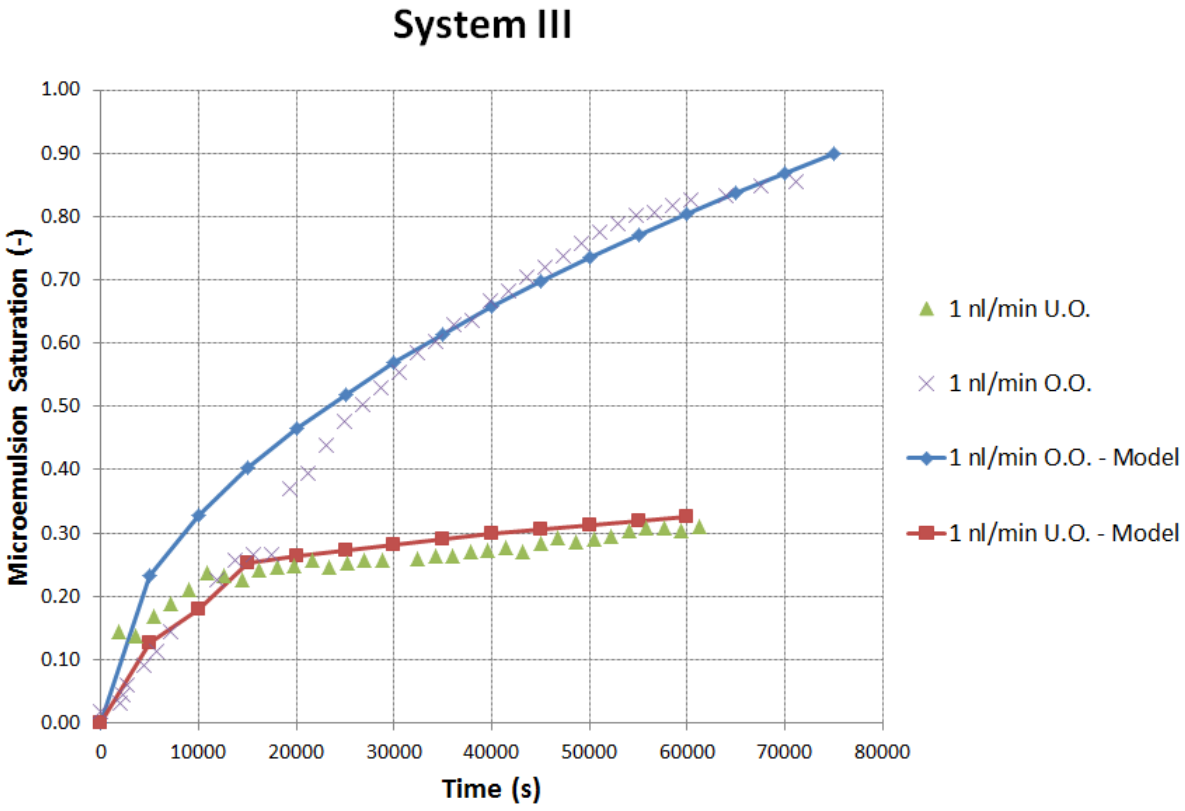

Figure 9.13: Penetration into the dead end pore of the 20% water concentration "front" as a function of time for 10 different micelle radii.

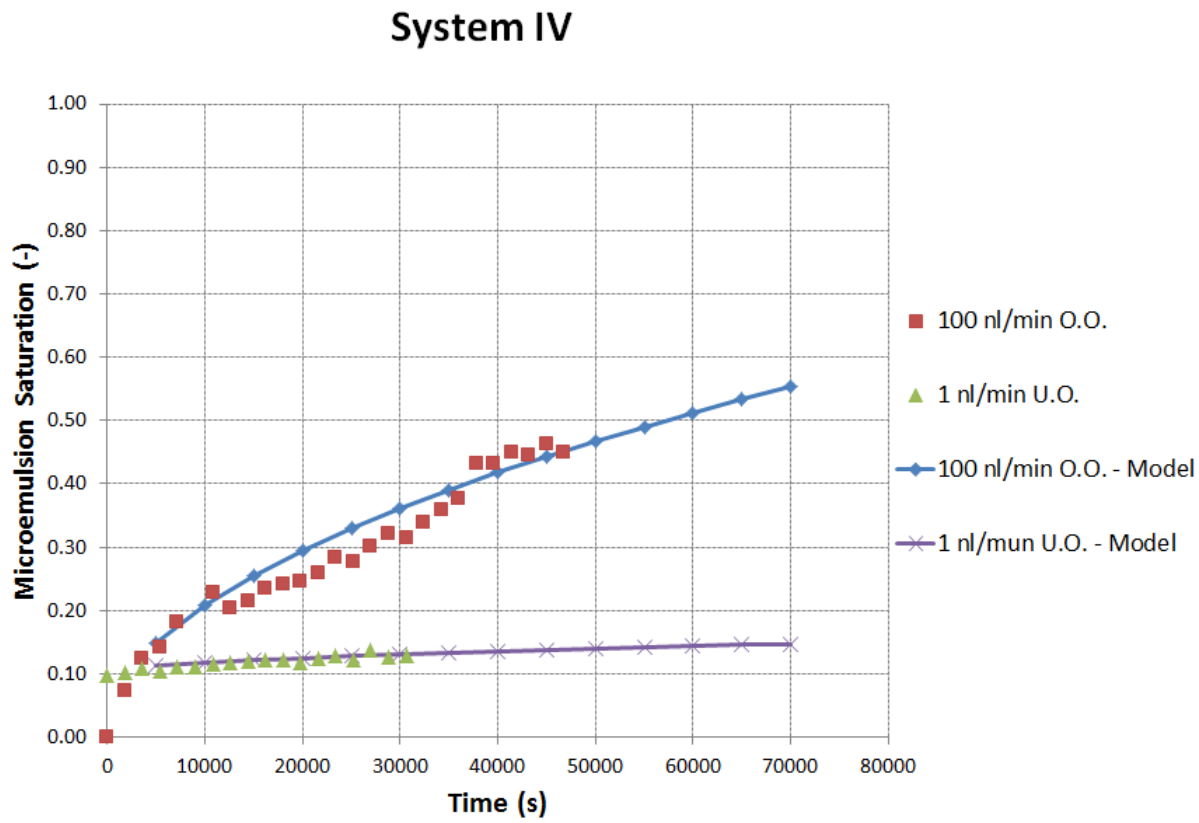

Figure 9.14: Penetration into the dead end pore of the 20% water concentration "front" as a function of time for 10 different micelle radii.

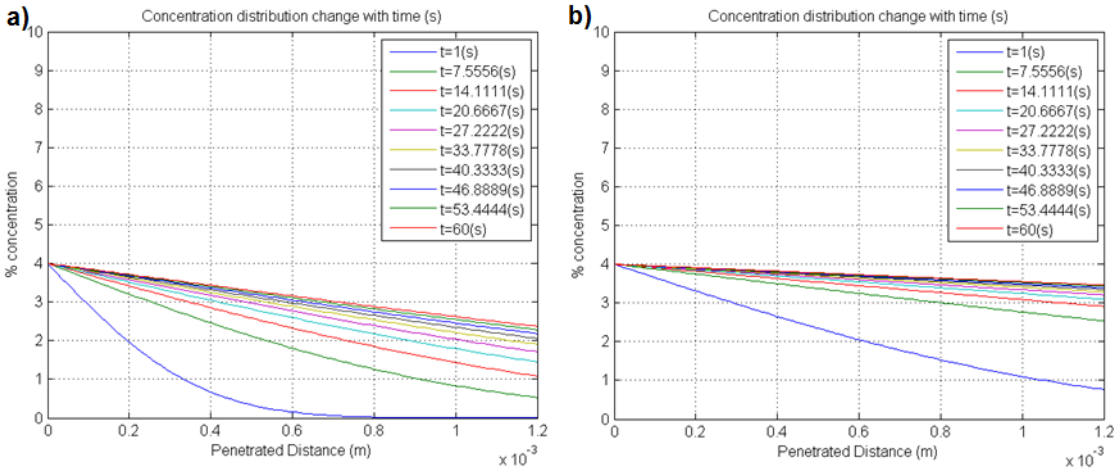

Figure 9.15: a) Evolution of the surfactant concentration distribution on the water film (1 nm) in the dead end pore over time b) Evolution of the surfactant concentration distribution on the water film (10 nm) in the dead end pore over time.

10

CONCLUSIONS

In situ formation of microemulsions of an EOR-surfactant with n-decane was studied at t-junctions and in dead end channels. The microemulsion was formed in situ by injecting the surfactant solution and the n-decane into capillaries which were etched into a water-wet microfludic chip. Using fluorescence microscopy direct visualization of the aqueous solution and the oil phase as well as the in situ emulsification was possible. Two different capillary configurations were used. A T-junction geometry was used to study the intial mixing and consequently microemulsion formation while both injected phases were mobile. This allowed us to study the time and length scale of microemulsion formation. The following observations were made:

- Microemulsion forms at the interface between the surfactant system and the oil as soon as they come into contact at the T-junction. An interface between the oil and the aqueous phase was always visible indicating that there was still an interfacial tension acting, however low it might be.
- At low injection rates and high surfactant concentrations where the viscosity of the aqueous phase was higher than the viscosity of the oil, snapping off of the oil phase occurred. This could indicate that the penetrating oil phase is more likely to snap off due to the shear forces from the aqueous phase (which is the wetting phase).
- The low flow rates allow snap offs to occur at this viscosity ratio. However at higher rates this was not the case and so a higher viscosity ratio is probably necessary for snap off to occur at these rates as well.
- At higher injection rates and lower surfactant concentrations there were no instabilities such as snap offs at the T-junction.
- The proposed model that was used to simulate the experiments did not capture the snapping off of the oil phase at high surfactant concentration and low flow rates. Because the model does not take account of the formation of microemulsion it is likely that the formation of the microemulsion at the interface further destabilizes the bulk of the oil in the experiments which in combination with the shear forces causes a snap off.

After the T-junction the phases continue into the downstream channel. In the experiments where snap offs took place the flow regime was sluggy where microemulsion and unsolubilized oil blobs traveled in the aqueous phase. Further down the channel, most of the oil and aqueous phase was then emulsified into microemulsion.

In the case of steady state parallel flow two types of emulsification were observed at the interface between the oil phase and the aqueous phase. The microemulsion can either form as a separate phase between the surfactant solution and the oil (higher capillary number regime, 7.3) or separate from the interface and form specks of microemulsion which are carried by the aqueous phase (lower capillary number regime, 7.9). All experiments were in the laminar flow regime so there was no turbulent mixing component. Because these experiments were steady state an emulsification rate could be quantified.

- The emulsification was driven by diffusion of oil, water and surfactant across the interface between the surfactant system and the oil.

- The emulsification rate that was measured was linear for short times (high flow rates) and showed $\sqrt{time}$ dependence at later times (lower flow rates) indicating a dispersive mixing component due to velocity gradients in the flow field perpendicular to the direction of flow. This was especially the case for the surfactant system with a higher viscosity due to the extra viscosity induced velocity gradient.
- The emulsification rate increases with increasing surfactant concentration and injection rate. The effect of the latter was less pronounced.
- The solubilization ratio of water and oil into a microemulsion may be different under dynamic conditions compared to static conditions. The proposed model for the downstream saturations indicated that the solubilization ratio of the microemulsion in the phase behavior tests is lower than that of the microemulsion observed in the dynamic experiments.
- The effect of the salinity on the interfacial tension or the water/oil solubilization ratio in the microemulsion under dynamic conditions was less pronounced than expected from phase behavior tests. Further research is adviseable.

In addition to the T-junction, a micromodel geometry that represents dead end pores was used. In this case the microfluidic model was initially saturated with the oil phase (n-decane) and only the aqueous phase was injected. The following observaions were made:

- Microemulsion forms at the pore throat of dead end pores during surfactant flooding. Assuming a continuous supply of water and surfactant, the microemulsion volume in the pore increases (increase in water and surfactant saturation in the pore) as oil is emulsified and transported out of the pore (decrease in oil saturation in the pore).
- The emulsification process shows $\sqrt{time}$ dependence which indicates that it is diffusion driven. A mechanism called spontaneous emulsification which is described in literature seems to describe what is observed in the experiments well.
- The emulsification rate is affected by concentration gradients of the surfactant, cosolvent and the salinity.
- The emulsification rate is affected by the injection rate of the surfactant system. This is because the injection rate controls the suply of water and surfactants to the microemulsion and therefore functions as a boundary condition for the emulsification process.
- At low cosolvent concentrations no third phase micro-emulsion necessarily forms.
- Surfactants are transported across the water film surrounding the oil in the dead end channel. This causes emulsion to form in the corners in the back of the pore initially. This process quickly equilibrates when emulsion has filled the corners and is not responsible for the emulsification of the bulk of the oil.

This study shows that static or dynamic studies alone do not cover the full range of physical phenomena which play a role in microemulsion formation in EOR. While the phase behavior tests indicate how the surfactants behave in their equlibrium state once they have reacted with the oil, the dynamic studies provide information on the transition to the equilibrium state. An integrated approach is necessary for designing effective Alkali-Surfactant-Polymer systems for a given reservoir.

11

RECOMMENDATIONS

Based on the work presented in this report the following recommendations are made for future research:

- The effect of salinity should be studied in more detail by varying the salinity with larger increments
- To confirm whether the snap offs are shear induced a series of microfluidic experiments with a larger viscosity ratio ($\frac{\mu_{aqueous}}{\mu_{oil}}$) at higher flow rates should be performed.
- The microfluidic experiments should be extended to pore network geometries to study the effect of connectivity on microemulsion formation. With such a configuration the oil recovery can also be studied.
- Differen EOR surfactants as well as different oils should be tested. If crude oil were to be used, a different imaging technique/dye may be necessary.
- It is known from phase behavior tests with polymers that they prefer to stay in the aqueous phase rather than solubilizing into the microemulsion. This could also have an effect on the formation of microemulsion under dynamic conditions. It is recommended to study the formation of microemulsions under dynamic conditions in combination with polymers.
- The solvatochromic fluorescent dye Nile red is known to show shifts in the emission spectrum depending on the solvent polarity. Whether the shifts in polarity that were observed are due to the structure of the microemulsion or the solubilization ratios of oil and water could not be confirmed. A more detailed study on the emission spectrum dependence of Nile red on microemulsion structure should be conducted.
- Measurments of the microemulsion structure sizes with a technique such as small angle neutron scattering would be useful to study the size and shape of the in situ formed microemulsions.
- The results of this work should be integrated into a coreflood study which similar surfactant systems and oil.

A

APPENDIX A

The model for the downstream saturations is shown in figure A.1. The following assumptions are made:

- Oil and surfactant solution meet at the t-junction
- The situation is steady state
- The surfactant solution hold a limited amount of surfactant based on the phase behavior tests
- No velocity gradients are taken into account
- No viscosity is taken into account (the two liquid phases take up equal fractions of the capillary)
- As the two liquids flow downstream microemulsion forms at the interface
- The emulsification rate is based on the values that were observed in the experiments (7.1)
- The microemulsion that forms has a water/oil/surfactant ratio based on the ratios observed in the phase behavior tests
- As soon as one of the components of the microemulsion runs out the emulsification stops

$$V_{i+1} = V_i + V_{me,prod} \tag{A.1}$$

$$V_{i+1} = V_i + \frac{R_{prod} u_x}{\Delta x} \tag{A.2}$$

In these quations, V represents the microemulsion volume in m^3, R_{prod} is the linear emulsification rate which was observed in the experiments, u_x is the flow velocity in the x-direction and Δx is the width of a grid cell.

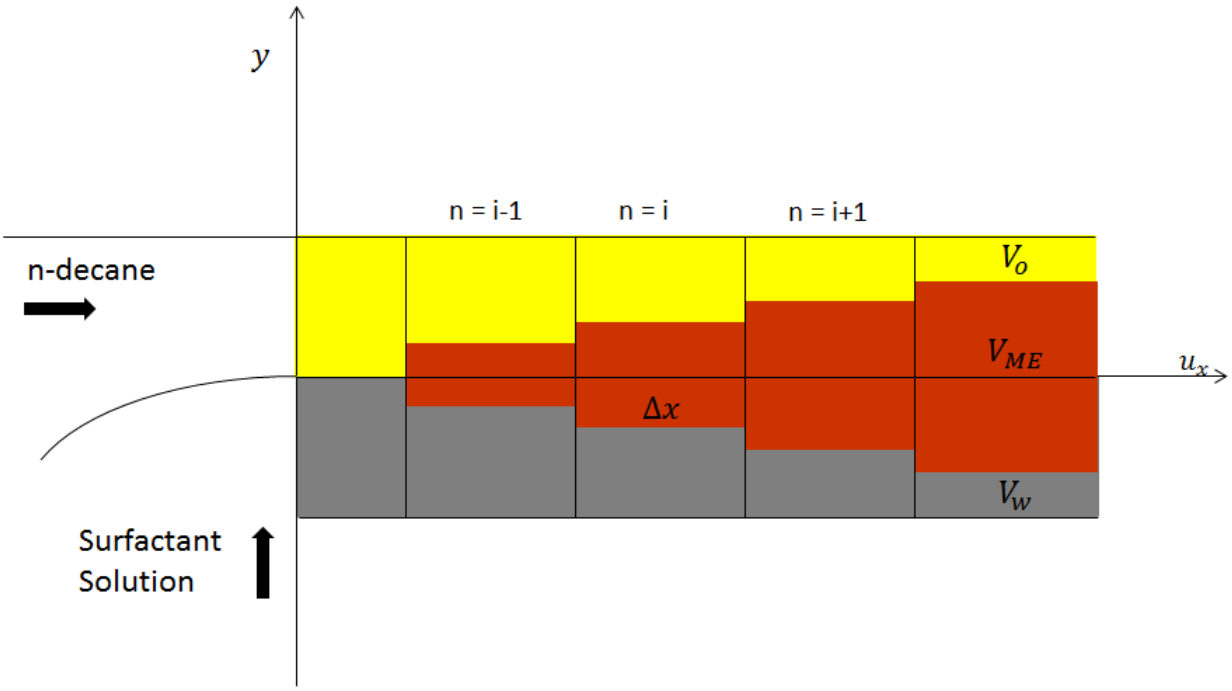

Figure A.1

B

APPENDIX B

A linear system is considered consisting of a thin liquid layer on a substrate. The surfactants can move over the interface of the liquid (water) with another liquid (oil). The liquid in the layer has a viscosity μ, the layer thickness is H_0 and its width is W. The surfactant concentration on the interface is $\Gamma(x)$ with x the distance in the propagation direction and the velocity of the liquid interface that contains the surfactants is v(x). Both Γ and v can vary with x. The schematic of figure B.1 shows the situation considered for making a surfactant balance. No convective transport is assumed here. The surfactant balance is given by:

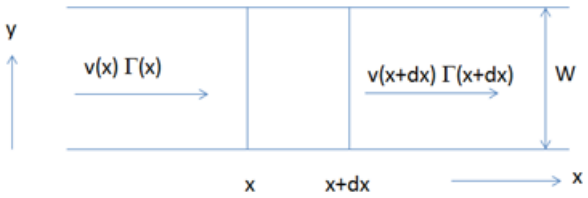

Figure B.1: Schematic for making the surfactant balance.

$$W[v(x+\Delta x)\Gamma(x+\Delta x) - v(x)\Gamma(x)]\Delta t = -W\frac{d\Gamma}{dt}\Delta t \tag{B.1}$$

which can be written as:

$$(v(x)+\frac{dv}{dx}\Delta x)(\Gamma(x)+\frac{d\Gamma}{dx}\Delta x) - v(x)\Gamma(x) = -\frac{d\Gamma}{dt}\Delta x \tag{B.2}$$

After neglecting second order terms the equation can be rewritten as:

$$v(x)\frac{d\Gamma}{dx} + \frac{dv}{dx}\Gamma(x) = -\frac{d\Gamma}{dt} \tag{B.3}$$

For an interface with a certain interfacial tension σ the interface has the tendency to contract with a force σW, if two interfaces with a difference in interfacial tension say $\sigma 1$ and $\sigma 2$, are adjacent then there is a unbalance of forces resulting in a contraction force of $(\sigma 2 - \sigma 1)$W. This force will move the uppermost layer containing the surfactants (film) but this motion will be counteracted by the viscous drag of liquid in the layer and a velocity profile as shown in fig B.2 will establish over the liquid layer. It is assumed that the other liquid (or air) forming the interface has negligible viscosity. The force required to move the interface with velocity v is given by:

$$F = W\frac{\mu}{H_0}v \tag{B.4}$$

This force when turned into a tension is balanced by the gradient in the interfacial tension giving:

$$\frac{\mu}{H_0}v = \frac{d\sigma}{dx} \tag{B.5}$$

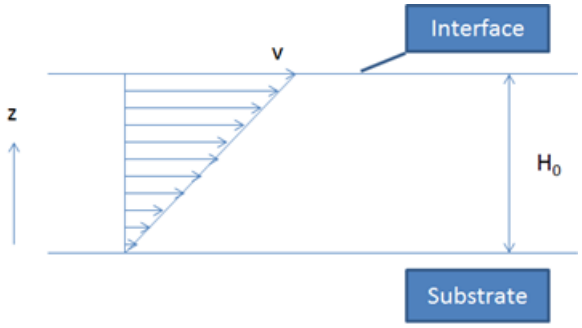

Figure B.2: Velocity distribution within the liquid layer, the surfactants reside on the interface.

or

$$v = \frac{H_0}{\mu}\frac{d\sigma}{dx} \tag{B.6}$$

For coupling the interfacial tension to the surfactant concentration at the interface a linear relation between interfacial tension and surfactant concentration is assumed (figure B.3). As σm is small in our applications it

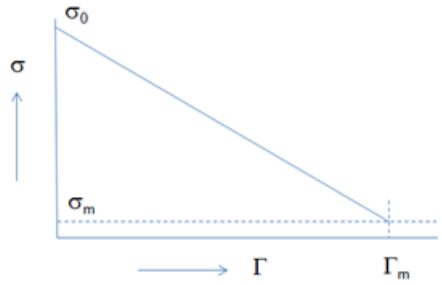

Figure B.3: Approximate relation between interfacial tension and surfactant concentration.

is assumed 0, which gives the equation:

$$\sigma = \sigma_0 - \beta\Gamma \tag{B.7}$$

with

$$\beta = \frac{\sigma_0}{\Gamma_m} \tag{B.8}$$

This gives:

$$\frac{d\sigma}{dx} = -\frac{\sigma_0}{\Gamma_m}\frac{d\Gamma}{dx} \tag{B.9}$$

and

$$v = -\frac{H_0}{\mu}\frac{\sigma_0}{\Gamma_m}\frac{d\Gamma}{dx} = -\frac{H_0}{\mu}\sigma_0\frac{d\Gamma^*}{dx} = -\alpha\frac{d\Gamma^*}{dx} \tag{B.10}$$

With

$$\Gamma^* = \frac{\Gamma}{\Gamma_m} \tag{B.11}$$

and

$$\alpha = \frac{H_0}{\mu}\sigma_0 \tag{B.12}$$

Substituting the expression for v in the surfactant balance equation gives:

$$\alpha[(\frac{d\Gamma^*}{dx})^2 + \Gamma^*\frac{d^2\Gamma^*}{dx^2}] = \frac{d\Gamma^*}{dt} \tag{B.13}$$

or alternatively written:

$$\alpha\frac{d}{dx}(\Gamma^*\frac{d\Gamma^*}{dx}) = \frac{d\Gamma^*}{dt} \tag{B.14}$$

This modified diffusion equation is very similar to the standard diffusion equation:

$$\alpha \frac{d^2\Gamma^*}{dx^2} = \frac{d\Gamma^*}{dt} \tag{B.15}$$

Thanks to John van Wunnink from Shell Global Sollutions for the derivation presented in this appendix.

C

APPENDIX C

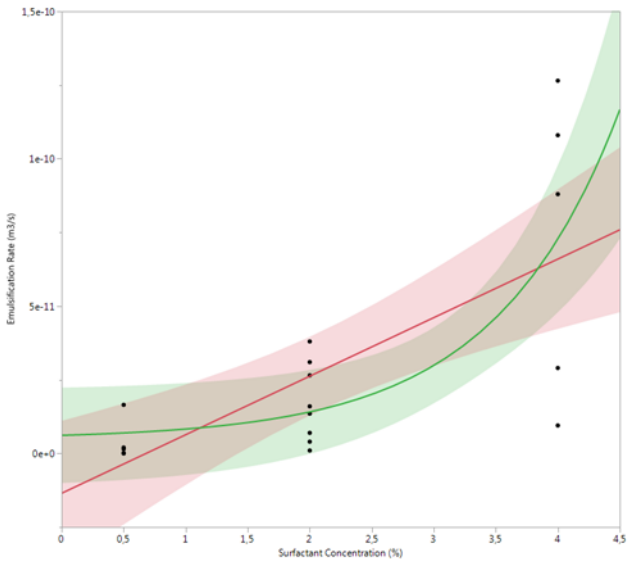

Figure C.1: effect of surfactant concentration on emulsification rate based on model fit

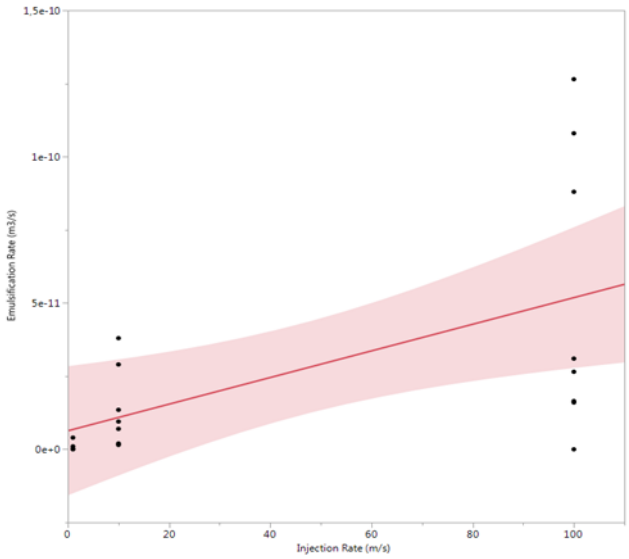

Figure C.2: effect of injection rate on emulsification rate based on model fit

D

APPENDIX D

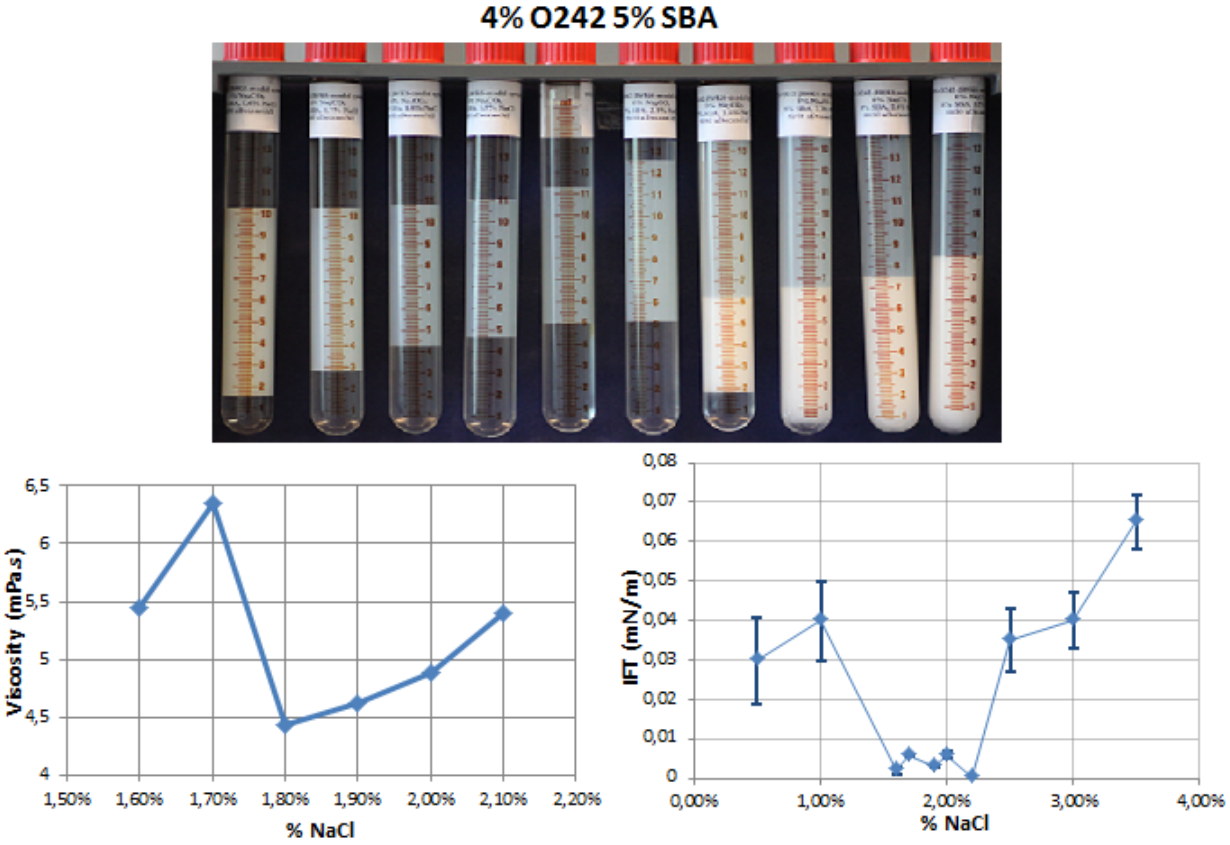

Figure D.1: a) Salinity scan for a 4% Shell Chemicals ENORDET O242, 5% 2-butanol surfactant system between 1.6% and 2.5 % NaCl. The salinity was varied with 0.1% increments. Each tube contains 7.5 mL surfactant solution and 7.5 mL n-decane. The test tubes show Winsor type III behaviour between 1.6% and 2.1% NaCl with an optimum salinity at 1.8% b) Viscosity of the middle phase measured by the shear rheometer as a function of salinity for the system. c) IFT between the microemulsion phase and the brine measured using the spinning drop method

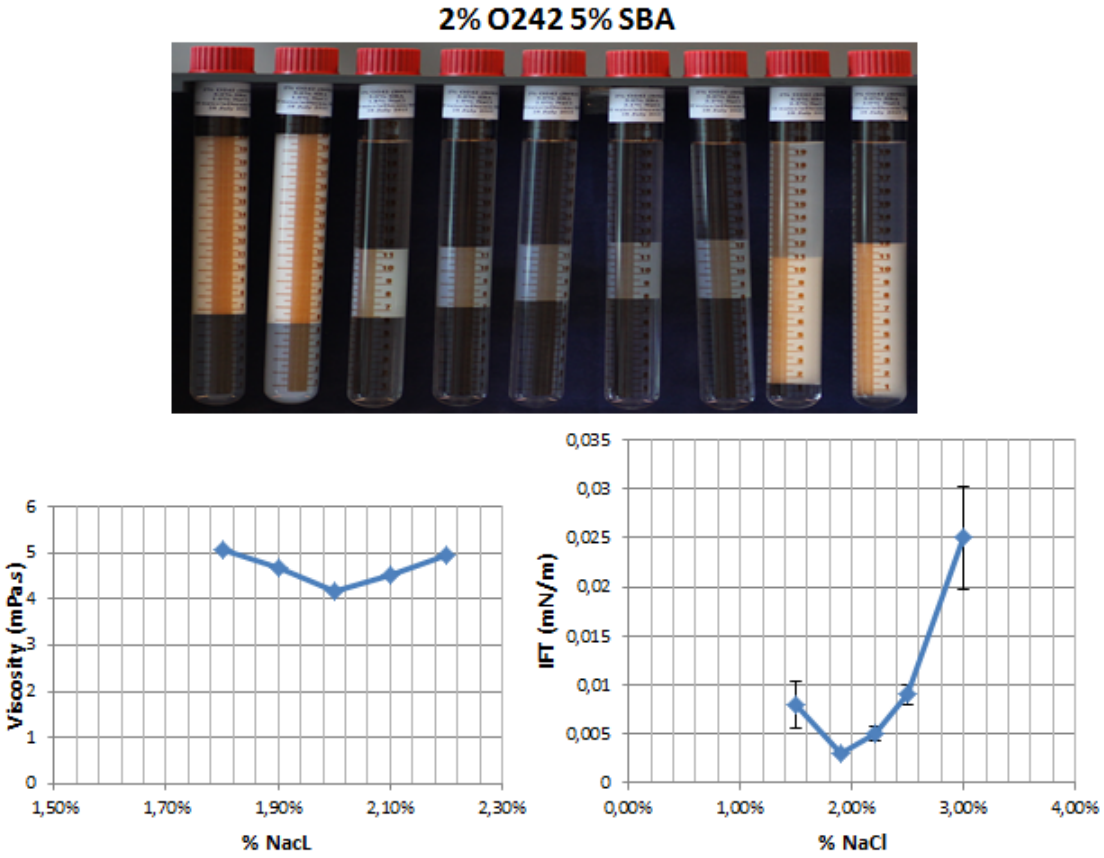

Figure D.2: a) Salinity scan for a 2% Shell Chemicals ENORDET O242, 5% 2-butanol surfactant system between 1.0% and 3.0 % NaCl. Each tube contains 10 mL surfactant solution and 10 mL n-decane. The test tubes show Winsor type III behavior between 1.8% NaCl and 2.2% NaCl. b) Viscosity of the middle phase measured by the shear rheometer as a function of salinity for the system. c) IFT between the microemulsion phase and the brine measured using the spinning drop method

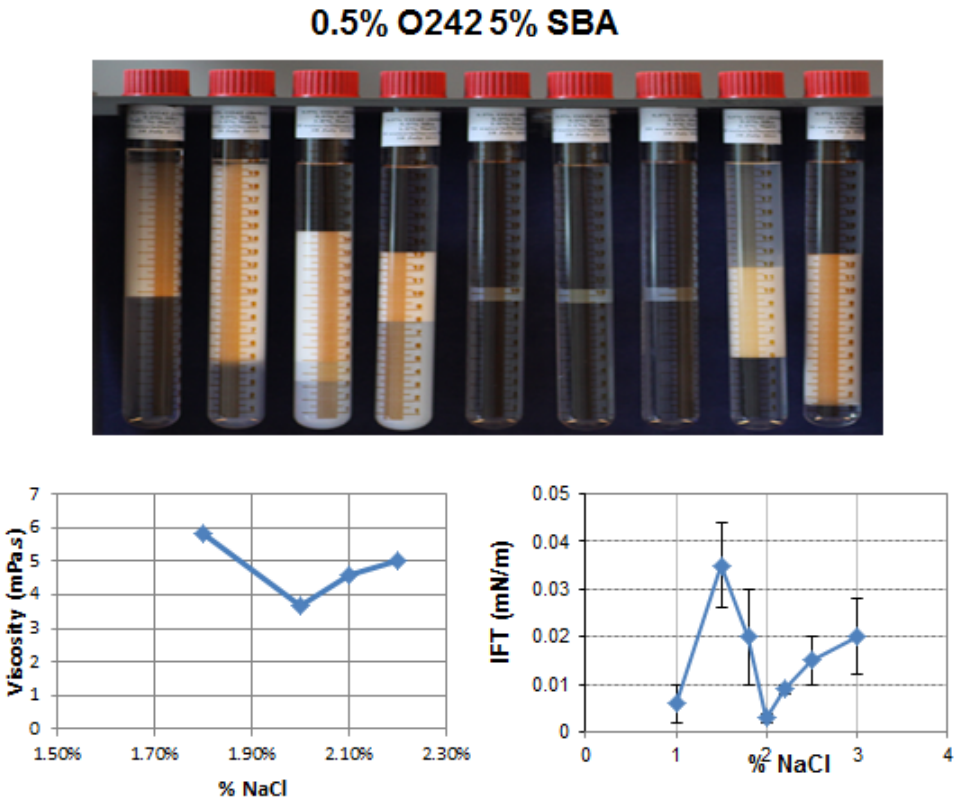

Figure D.3: a) Salinity scan for a 0.5% Shell Chemicals ENORDET O242, 5% 2-butanol surfactant system between 1.0% and 3.0 % NaCl. The tubes show Winsor type III behavior between 2.0% and 2.2% NaCl. Each tube contains 10 mL surfactant solution and 10 mL n-decane. b) Viscosity of the middle phase measured by the shear rheometer as a function of salinity for the system. c) IFT between the microemulsion phase and the brine measured using the spinning drop method

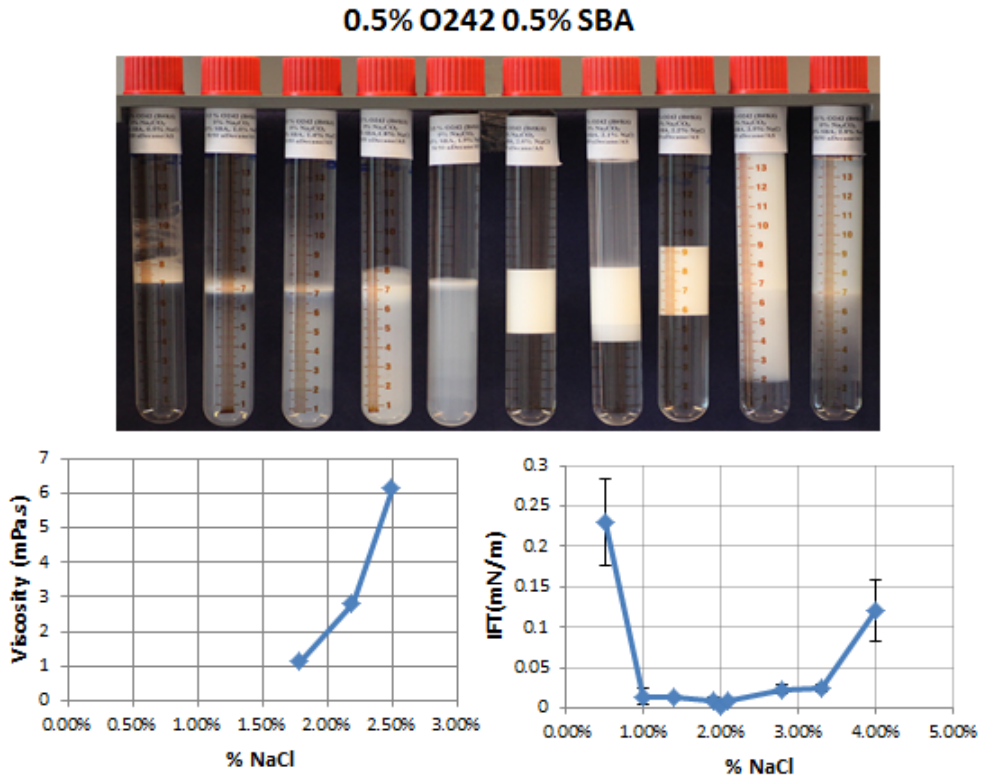

Figure D.4: a) Salinity scan for a 0.5% Shell Chemicals ENORDET O242, 0.5% 2-butanol surfactant system between 1.0% and 3.0 % NaCl. The tubes show Winsor type III behavior between 2.0% and 2.2% NaCl. Each tube contains 7.5 mL surfactant solution and 7.5 mL n-decane. b) Viscosity of the middle phase measured by the shear rheometer as a function of salinity for the system. c) IFT between the microemulsion phase and the brine measured using the spinning drop method

E

APPENDIX-E

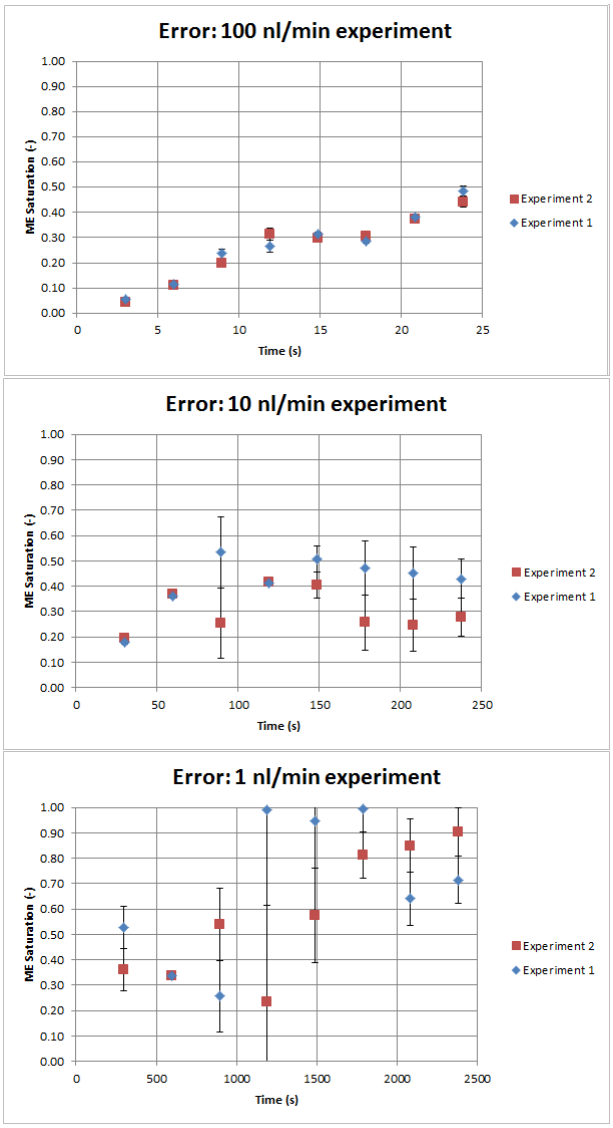

Figure E.1: Experimental error for the downstream saturations which were used to quantify the emulsification rates. The errors were measured by repeating the experiment and calculating the standard deviation between the results. This was done for experiments at three different injection rates.

BIBLIOGRAPHY

[1] IEA, *Key world energy statistics,* www.iea.org (2014).

[2] S. S. et al., *Enhanced oil recovery scoping study,* EPRI, www.energy.ca.gov (1999).

[3] V. Santanna, F. Curbelo, T. C. Dantas, A. D. Neto, H. Albuquerque, and A. Garnica, *Microemulsion flooding for enhanced oil recovery,* Journal of Petroleum Science and Engineering **66**, 117 (2009).

[4] G. Stegemeier, *Mechanisms of entrapment and mobilization of oil in porous media,* Improved Oil Recovery by Surfactant and Polymer Flooding , 55 (1977).

[5] L. W. Lake, *Enhanced oil recovery,* (1989).

[6] A. Bashiri, N. Kasiri, *et al.*, *Properly use effect of capillary number on residual oil saturation,* in *Nigeria Annual International Conference and Exhibition* (Society of Petroleum Engineers, 2011).

[7] J. Eastoe, *Surfactant chemistry: Microemulsions,* http://www.chm.bris.ac.uk/eastoe/SurfChem/ .

[8] S. Mehta and G. Kaur, *Microemulsions: thermodynamic and dynamic properties* (INTECH Open Access Publisher, 2011).

[9] R. Nagarajan and E. Ruckenstein, *Molecular theory of microemulsions,* Langmuir **16**, 6400 (2000).

[10] R. Healy, R. Reed, D. Stenmark, *et al.*, *Multiphase microemulsion systems,* Society Of Petroleum Engineers Journal **16**, 147 (1976).

[11] P. Winsor, Trans. Faraday Soc. (1948).

[12] R. N. Healy, R. L. Reed, *et al.*, *Immiscible microemulsion flooding,* Society Of Petroleum Engineers Journal **17**, 129 (1977).

[13] A. Putz, J. Chevalier, G. Stock, J. Philippot, *et al.*, *A field test of microemulsion flooding, chateaurenard field, france,* Journal of Petroleum Technology **33**, 710 (1981).

[14] J.-L. Salager, R. E. Antón, D. A. Sabatini, J. H. Harwell, E. J. Acosta, and L. I. Tolosa, *Enhancing solubilization in microemulsions—state of the art and current trends,* Journal of surfactants and detergents **8**, 3 (2005).

[15] W. Gogarty, W. Tosch, *et al.*, *Miscible-type waterflooding: oil recovery with micellar solutions,* Journal of Petroleum Technology **20**, 1 (1968).

[16] L. Holm, S. D. Robertson, *et al.*, *Improved micellar/polymer flooding with high-ph chemicals,* Journal of Petroleum Technology **33**, 161 (1981).

[17] C. Solans and H. Kunieda, *Industrial applications of microemulsions*, Vol. 66 (CRC Press, 1996).

[18] V. Jain and A. H. Demond, *Conductivity reduction due to emulsification during surfactant enhanced-aquifer remediation. 1. emulsion transport,* Environmental science & technology **36**, 5426 (2002).

[19] R. Martel, P. J. Gelinas, R. Lefebvre, A. Hébert, S. Foy, L. Saumure, A. Roy, and N. Roy, *Laboratory and field soil washing experiments with surfactant solutions,* in *Emerging Technologies in Hazardous Waste Management 8* (Springer, 2002) pp. 55–67.

[20] B. Ding, G. Zhang, J. Ge, and X. Liu, *Research on mechanisms of alkaline flooding for heavy oil,* Energy & Fuels **24**, 6346 (2010).

[21] M. Zagnoni, J. Anderson, and J. M. Cooper, *Hysteresis in multiphase microfluidics at a t-junction,* Langmuir **26**, 9416 (2010).

[22] E. Unsal, G. Mason, N. R. Morrow, and D. W. Ruth, *Bubble snap-off and capillary-back pressure during counter-current spontaneous imbibition into model pores,* Langmuir **25**, 3387 (2009).

[23] H. Pei, G. Zhang, J. Ge, M. Tang, and Y. Zheng, *Comparative effectiveness of alkaline flooding and alkaline–surfactant flooding for improved heavy-oil recovery,* Energy & Fuels **26**, 2911 (2012).

[24] L. Chen, Y. Tian, and T. Karayiannis, *The effect of tube diameter on vertical two-phase flow regimes in small tubes,* International Journal of Heat and Mass Transfer **49**, 4220 (2006).

[25] E. Rebrov, *Two-phase flow regimes in microchannels,* Theoretical foundations of chemical engineering **44**, 355 (2010).

[26] C. N. Baroud and H. Willaime, *Multiphase flows in microfluidics,* Comptes Rendus Physique **5**, 547 (2004).

[27] R. M. et H. van den Akker., *Fysische transport verschijnselen,* .

[28] H. A. Stone, A. D. Stroock, and A. Ajdari, *Engineering flows in small devices: microfluidics toward a lab-on-a-chip,* Annu. Rev. Fluid Mech. **36**, 381 (2004).

[29] A. Einstein, *Über die von der molekularkinetischen theorie der wärme geforderte bewegung von in ruhenden flüssigkeiten suspendierten teilchen,* Annalen der physik **4** (1905).

[30] M. Schwarze, T. Pogrzeba, I. Volovych, and R. Schomacker, *Microemulsion systems for catalytic reactions and processes,* Catal. Sci. Technol. **5**, 24 (2015).

[31] J. T. Davies, *Interfacial phenomena 2e* (Elsevier, 2012).

[32] C. A. Miller, *Spontaneous emulsification produced by diffusion—a review,* Colloids and Surfaces **29**, 89 (1988).

[33] K. J. Ruschak and C. A. Miller, *Spontaneous emulsification in ternary systems with mass transfer,* Industrial & Engineering Chemistry Fundamentals **11**, 534 (1972).

[34] J. R. Barnes, H. Dirkzwager, J. Smit, J. Smit, A. On, R. C. Navarrete, B. Ellison, M. A. Buijse, *et al.*, *Application of internal olefin sulfonates and other surfactants to eor. part 1: Structure-performance relationships for selection at different reservoir conditions,* in *SPE Improved Oil Recovery Symposium* (Society of Petroleum Engineers, 2010).

[35] S. Moulik and B. Paul, *Structure, dynamics and transport properties of microemulsions,* Advances in Colloid and Interface science **78**, 99 (1998).

[36] J. Brujić, C. Song, P. Wang, C. Briscoe, G. Marty, and H. A. Makse, *Measuring the coordination number and entropy of a 3d jammed emulsion packing by confocal microscopy,* Physical review letters **98**, 248001 (2007).

[37] P. Greenspan, E. P. Mayer, and S. D. Fowler, *Nile red: a selective fluorescent stain for intracellular lipid droplets.* The Journal of cell biology **100**, 965 (1985).

[38] A. Datta, D. Mandal, S. K. Pal, and K. Bhattacharyya, *Intramolecular charge transfer processes in confined systems. nile red in reverse micelles,* The Journal of Physical Chemistry B **101**, 10221 (1997).

[39] B. A. Cicciarelli, T. A. Hatton, and K. A. Smith, *Dynamic surface tension behavior in a photoresponsive surfactant system,* Langmuir **23**, 4753 (2007).

[40] R. Varghese and H.-A. Wagenknecht, *Non-covalent versus covalent control of self-assembly and chirality of nile red-modified nucleoside and dna,* Chemistry-A European Journal **16**, 9040 (2010).

[41] I. N. Kurniasih, H. Liang, P. C. Mohr, G. Khot, J. P. Rabe, and A. Mohr, *Nile red dye in aqueous surfactant and micellar solution,* Langmuir **31**, 2639 (2015).

[42] M. Oliveira, G. Hungerford, M. da G Miguel, and H. Burrows, *Solvatochromic fluorescent probes in bicontinuous microemulsions,* Journal of Molecular Structure **563**, 443 (2001).

[43] L. Capretto, W. Cheng, M. Hill, and X. Zhang, *Micromixing within microfluidic devices,* in *Microfluidics* (Springer, 2011) pp. 27–68.

[44] A. Gupta and R. Kumar, *Flow regime transition at high capillary numbers in a microfluidic t-junction: Viscosity contrast and geometry effect,* Physics of Fluids (1994-present) **22**, 122001 (2010).